MODELING AND ANALYSIS OF ANTHROPOGENIC IMPACTS AND SOIL PROPERTIES ON GLOBAL RIVER SEDIMENT DYNAMICS

by

NISHANI POORNA MORAGODA

SAGY COHEN, COMMITTEE CHAIR
LISA DAVIS
JOHN GARDNER
MUKESH KUMAR
NICHOLAS MAGLIOCCA

A DISSERTATION

Submitted in partial fulfillment of the requirements
for the degree of Doctor of Philosophy
in the Department of Geography
in the Graduate School of
The University of Alabama

TUSCALOOSA, ALABAMA

2023

ABSTRACT

Sediment transport by rivers plays a key role in ecosystem functioning, biogeochemical cycling and geomorphological processes of the Earth. Human activities including land use changes, water diversions, and damming have profoundly altered natural fluvial sediment transport processes. Accurately modeling sediment transport can be of great use in elucidating the effects of these stresses on global river fluxes.

To analyze the impact of anthropogenic modifications of the landscape and fluvial systems on global river sediment dynamics, three main research questions were investigated: (1) What is the sensitivity of fluvial sediment dynamics to soil properties (e.g. soil moisture) that govern soil resistance/erodibility? (2) What is the impact of sediment trapping behind dams on sediment dynamics in global rivers? (3) What are the individual and combined impacts of anthropogenic land use and damming on global fluvial sediment dynamics?

To address the first research question, an extensive literature review and meta-analysis were conducted in Chapter 2 to develop a relationship between soil moisture and soil erodibility. The second research question was addressed in Chapter 3, by quantifying sediment trapping behind dams across the Continental United States (CONUS) using a novel remote sensing sediment dataset. The resulting sediment trapping dataset was used to develop a new reservoir trapping efficiency (*Te*) model. In Chapter 4, the *Te* model was implemented within a new global sediment flux model. The development of this new sediment model (termed WBMsed-ELM) described in Chapter 4, is used to answer the third research question by comparing multiple simulation scenarios in which the investigated drivers are isolated.

The results of Chapter 2 show that soil in the dry state has the lowest resistance to erosion and thus has a high erodibility, and erosion resistance increases (erodibility decreases) with increasing antecedent moisture content until a certain threshold. In order to incorporate this relationship in models, we presented an exemplar relation that captures the variation in erosion resistance with soil moisture content. In chapter 3, we developed data-driven CONUS and global models to predict *Te* in large-scale hydro-geomorphic models. Contrary to the common assertion, our results in Chapter 3 revealed that large reservoirs can have a wide range of *Te* values. The WBMsed-ELM model predictions in Chapter 4 showed that croplands alone have increased average global river sediment fluxes by 63.4% between 1960 and 2014. In contrast, dams have reduced the global sediment load to the ocean from large rivers by 19.1%. Considering the combined effect of land use changes and sediment trapping behind dams, WBMsed-ELM estimates that there is a net global increase of 6.4% in sediment delivery to the ocean, compared to pristine conditions. This new WBMsed-ELM framework provides several capabilities to explicitly simulate major river sediment processes and better represent individual and combined effects of anthropogenic stresses on global river sediment dynamics.

Overall, this dissertation offers a global-scale perspective of key human drivers of changes in riverine processes, critical areas of sediment detachment, physical mechanisms of sediment transport in rivers, and provides a robust modeling framework for predicting and analyzing global-scale riverine sediment fluxes.

DEDICATION

To my loving family

ACKNOWLEDGEMENTS

I had a remarkable and fulfilling graduate journey and I have many people to thank for that. First, my sincere gratitude goes to my advisor Dr. Sagy Cohen for his guidance, advice, and unwavering support. I am fortunate to have had such an exceptional mentor, and I am grateful for his profound impact on my academic and personal growth. I would like to thank my dissertation committee members Dr. Lisa Davis, Dr. John Gardner, Dr. Mukesh Kumar, and Dr. Nicholas Magliocca for their support in making my research successful. To my colleagues, co-authors, and brilliant scientists whom I had the privilege to work with and learn a lot from throughout these years, I extend my appreciation.

I wish to thank the University of Alabama, the Department of Geography, Graduate School, the International Student and Scholar Services for providing me a nurturing and welcoming atmosphere, and for the funding that enabled me to carry out my research successfully. Being part of the Surface Dynamics Modeling Lab has been a joy and I am grateful to all my lab mates for making my days memorable.

My biggest source of strength has always been my family. I am eternally grateful to my dearest husband Dinuke, for always being there for me and encouraging me to reach greater heights, and my father, mother, brother, and sister-in-law who have been my biggest pillars of support. I am also thankful to my relatives, friends and teachers for helping me become a better version of myself. My heartfelt gratitude extends to Dr. Virginia Wimberley, John Wimberley, and Anuska Narayanan for being such amazing friends. Names mentioned or not, I dedicate my achievements to all the kind souls who brightened my path to success.

CONTENTS

LIST OF TABLES

LIST OF FIGURES

CHAPTER 1

INTRODUCTION

The world's large rivers are not only a source of water for millions of people, but also an essential resource provider, a source of livelihood, and a major regulator of the overall health of the planet (Best, 2019). The transportation of sediment by rivers has a direct impact on Earth's ecosystems, biogeochemical cycles, and geomorphological processes (Vörösmarty et al., 2003; Walling and Fang, 2003). It plays a crucial role in shaping landforms such as deltas and the morphology of river channels and floodplains (Bamunawala et al., 2018; Ibáñez et al., 2019). Changes in fluvial sediment delivery towards the coast can affect deltaic systems, as deltas depend on the continued supply of sediment to offset the impacts of rising sea levels and ground subsidence (Darby et al., 2016; Dunn et al., 2019; Syvitski et al., 2009). Sediment serves as a major water quality indicator and increases the risk of floods through excessive sediment deposition (Battista et al., 2020; Lamb et al., 2020). Sediment transports eroded soil from hillslopes to downstream areas that contain nutrients as well as agricultural/industrial pollutants, acting as an important mode of nutrient and pollutant transport (Boardman et al., 2019; Walling, 2009). The substantial role that particulate organic carbon plays in the Earth's terrestrial carbon budget is becoming increasingly evident. (Tan et al., 2017; Zhang et al., 2020). Changes in river sediment equilibrium can disrupt riverine, coastal, and marine ecosystem functioning, human water uses, and the stability of infrastructure (Battista et al., 2020; Vercruysse et al., 2017). Therefore, evaluating and predicting these changes in river sediment fluxes is essential to

understand the quality of available water resources on the planet and the functioning of the earth surface processes (Haddeland et al., 2014; Tsuruta et al., 2018).

Global fluvial sediment transport is vulnerable to a variety of stresses from human activities including land use changes, water diversions, and damming (Best, 2019; Lewis et al., 2013). Rivers respond to such stresses in numerous, profound, and complex ways which can lead to various environmental consequences (Li et al., 2020). The construction of dams and impoundments for hydropower, flood control, irrigation, and water supply is among the greatest stressors to the connectivity and functionality of rivers (Vörösmarty et al., 2003; Zarfl et al., 2015). Globally, there are now ~58,000 large dams (heights greater than 15 m) and ~3,700 dams that are planned or under construction (Best and Darby, 2020; Mulligan et al., 2020; Syvitski and Kettner, 2011). These impoundments collectively account for a cumulative storage capacity of ~8300 km^3, which is equal to around one-sixth of the total annual river discharge to the world's oceans (Lehner et al., 2011a; Wada et al., 2016). Through trapping a large amount of sediment behind them, dams modify downstream flow regimes affecting sediment carrying capacities, and exacerbate bank erosion and riverbed incision due to sediment starvation (Best, 2019; Kondolf et al., 2014). Research has revealed that nearly 26% of the global sediment flux is trapped behind large reservoirs (Syvitski and Milliman, 2007). Construction of dams without assessing their potential consequences has led to degraded floodplains and coastal environments around the world (Latrubesse et al., 2017). Moreover, the increasing demands posed by burgeoning population growth are driving land-use changes, such as deforestation of catchment hillslopes and floodplains, urbanization, and agriculture, that can modify the quantity of sediment entering rivers through soil and bank erosion (Best and Darby, 2020). These changes in sediment supply can cause changes in sediment concentrations in rivers, and thereby river water quality (Lewis et

al., 2013). In order to understand how these stressors influence changes in river systems, new and innovative methods and data are required.

Accurately modeling sediment transport can be of great use in elucidating the effects of these stresses on sediment dynamics. Although a general scientific understanding about the relationships between natural sediment transport processes and anthropogenic and human influences exists, including them in predictive modeling frameworks remains challenging (Cohen et al., 2014; Tsuruta et al., 2018). Such models are vital for understanding anthropogenic influences on riverine fluxes, studying the influence of individual stressors, simulating future or theoretical change scenarios, quantifying changes in ungagged locations, and predicting spatial and temporal dynamics across the river systems from local to global scales (Merritt et al., 2003). Although great advancements in simulating sediment fluxes at various scales have been reported over the past few decades (e.g. Hatono and Yoshimura, 2020; Li et al., 2022; Tsutura et al., 2018), existing models still have a long way to go in terms of explicitly and accurately representing anthropogenic and climatic drivers over large spatial scales (Fagundes et al., 2020).

The explicit representation of soil erosion in sediment models (e.g. Tan et al., 2018) is a step forward in this direction, however, it is itself a complex process involving a variety of interconnected, intrinsic, as well as dynamic properties of soil (Battista et al., 2020; Grissinger, 1966). The stability of soil against erosion is dependent on the balance between hydrodynamic forces that cause erosion and the forces within the soil that resist it (Bryan, 2000). Therefore, estimates of spatial and temporal soil losses by erosion not only depend on the prediction of runoff generation, which has been studied extensively, but also on an accurate representation of the resistance of soils to erosion (Knapen et al., 2007). Soil resistance is a highly important parameter in models for realistically simulating the spatial and temporal variability in soil

detachment/sediment transport processes. Therefore, it is important to consider the intrinsic soil properties as well as dynamic environmental factors that govern the soil's resistance to erosion, because the effects of climate and anthropogenic activities can also be manifested through their influence on the soil's erosion resistance/susceptibility parameter. Within this backdrop, it is clear that predicting the contemporary changes in global riverine sediment fluxes needs a robust predictive framework that can accurately represent the drivers of change as well as how they are manifested in different components of the earth system.

The overarching goal of this dissertation project is, therefore, to *elucidate anthropogenic impacts and soil properties on global river sediment dynamics*. In order to achieve this goal, three main research themes were explored; (1) Investigating the potential of improving sediment flux predictions by incorporating the influence of dynamic soil properties (e.g soil moisture) into the soil's resistance/susceptibility parameter; (2) development of conceptual understanding and parameterization of sediment trapping behind dams; (3) development of a more process-based sediment model to explicitly simulate sediment transport processes and analyze the anthropogenic influence on global fluvial sediment dynamics.

The corresponding three main research questions are:

Question 1: *What is the sensitivity of fluvial sediment dynamics to soil properties (e.g. soil moisture) that govern soil resistance/erodibility?*

This first phase of the project is focused on understanding the processes and mechanisms by which soil moisture affects erosion resistance of soils, and developing a generic equation that can be used to incorporate this relation in sediment yield assessment models.

Question 2: *What is the impact of sediment trapping behind dams on sediment dynamics in global rivers?*

In order to address this question, the second phase of the dissertation involves the development of conceptual understanding and parameterization of sediment trapping behind dams for modeling efforts. A novel reservoir trapping efficiency (*Te*) parameter was developed using a recent, high-resolution, and spatially explicit remote sensing dataset, informing more realistic trapping of sediment at dams.

Question 3: *What are the impacts of anthropogenic land use and damming on global fluvial sediment dynamics?*

A new global sediment transport model with more process-based representations of Earth surface processes was developed. This new sediment transport model includes (i) a hillslope soil erosion component to represent sediment supply to rivers, (ii) more explicit and improved representations of anthropogenic factors (i.e. dam trapping and land use changes) that affect fluvial sediment dynamics, and (iii) more process-based soil erosion and sediment transport representations in place of current empirical equations. It was then applied to investigate how global river sediment fluxes change in response to anthropogenic activities.

The above research questions form Chapter 2, 3, and 4 in this dissertation, respectively. Chapter 2 resulted in a journal paper titled "Representing the role of soil moisture on erosion resistance in sediment models: Challenges and opportunities" (Moragoda et al., 2022) published in Earth Science Reviews (Impact factor = 12.038). Chapter 3 led to a journal paper titled "Modeling and Analysis of Sediment Trapping Efficiency of Large Dams using Remote Sensing" (Moragoda et al., 2023) published in Water Resources Research (Impact factor = 6.159). A manuscript corresponding to Chapter 4 titled "Simulating Anthropogenic Influence on Fluvial Sediment Dynamics using a Global River Sediment Model" is currently in preparation. Overall, this dissertation offers a global-scale perspective of key human drivers of changes in

riverine processes, critical areas of sediment detachment, physical mechanisms of soil erosion and sediment transport in rivers, and provides a robust modeling framework for predicting and analyzing global-scale riverine sediment fluxes.

CHAPTER 2

REPRESENTING THE ROLE OF SOIL MOISTURE ON EROSION RESISTANCE IN SEDIMENT MODELS: CHALLENGES AND OPPORTUNITIES

Abstract

Soil's resistance to erosion or its susceptibility to resist detachment is a key parameter in the majority of soil erosion and sediment models. Although soil resistance is a function of both the intrinsic properties of soil and dynamic environmental variables (e.g., soil moisture), the influence of the latter is seldom explicitly incorporated in the definition of soil resistance. The significant and complex role of soil moisture content on erosion resistance is recognized by many studies, however, much of the emphasis regarding the role of soil moisture on sediment yield modeling has been on its impacts on runoff generation rather than on soil resistance. In this paper, we synthesize the existing state of knowledge on the processes and mechanisms by which moisture affects erosion resistance of soil, and highlight the challenges and opportunities associated with incorporating this relation in sediment yield assessment models. Through a detailed analysis of literature, we find that dry soil has the lowest resistance to erosion and thus has a high erodibility, and erosion resistance increases (erodibility decreases) with increasing antecedent moisture content until a certain threshold. After this threshold is reached, soil resistance decreases with further increase in moisture content, and soils become more susceptible to erosion. Next, the study identifies the candidate variables that may be used to quantitatively represent the soil's resistance to erosion vis-à-vis moisture, and discuss the challenges in incorporating this relation in modeling frameworks. As a way forward, through a meta-analysis

of published data, we develop an exemplar relation that could be used to represent the variation in erosion resistance with soil moisture content. We find that the parameters of such a relation vary significantly across soil types, thus raising the possibility for developing a soil-type based moisture-resistance relations. Overall, this review underscores the considerable impact of antecedent soil moisture on the erosion resistance of soils, and makes a case for integrating the influence of dynamic soil moisture content on erosion resistance into predictive modeling frameworks.

1. Introduction

In the recent past, a large number of soil erosion and sediment models with varying representations of erosion, deposition, and transport processes have been developed. Their differences and consequent impact on predictions is a subject of several reviews (e.g., Aksoy and Kavvas, 2005; De Vente et al., 2013; Merritt et al., 2003; Pandey et al., 2016; Papnicolaou et al., 2008) and model intercomparison studies (e.g., Bhuyan et al., 2002; Zi et al., 2019). Irrespective of the process representation used, the majority of the sediment models account for the role of soil's resistance to erosion on sediment yield and/or erosion processes. Soil resistance, often also conversely termed as the susceptibility of soil to erosion by water, is a key physical property of the soil that indicates its ability to resist detachment by water flow or raindrop impact. It is frequently the reason for differential rates of yield and erosion across regions with different soil types (Goudie, 2013). It is also used to explain the changes in sediment yield in time, especially due to changes in land use. Although measured at a diverse range of spatial scales, ranging from point to bench to hillslope to watershed scales, the resistance property captures the erosion rate per unit area for a given erosivity from water flow or raindrop impact. In models, this term is

often obtained through calibration using measured soil erosion and other variables (Knapen et al., 2007). Although it is widely accepted that soil resistance is both a function of intrinsic properties of soil and exogenous dynamic environmental variables (Bryan, 2000; Paaswell, 1973), the influence of the latter is seldom explicitly incorporated in the definition of soil resistance (Knapen et al., 2007). Soil moisture is one such exogenous environment property that has been known to impact soil's resistance to erosion (Allen et al., 1999; Fell et al., 2017).

An obvious and a widely studied effect of soil moisture on sediment yield is through runoff generation. Drier soils tend to generate less runoff (Chen et al., 2015) thus have less sediment transport capacity than a wet soil where more runoff is generated and more soil will be eroded (Flanagan et al., 1988; Wei et al., 2007). The influence of moisture content on soil erosion resistance and consequently on sediment yield, although relatively understudied, can also be significant (Luk and Hamilton, 1986; Knapen et al., 2007; Shainberg et al., 1996). For example, studies have discussed the importance of moisture on the development of cohesion forces in soil (e.g. Kemper et al., 1985; Panabokke and Quirk, 1957; Shainberg et al., 1996), and have reported a differential erosional response based on differences in antecedent moisture state owing to the resistance the soil develops against erosion (e.g. Govers and Loch, 1993; Parker et al., 1995; Poesen et al., 1999). Not only the spatial variation in soil moisture, but also the temporal variation in soil moisture at the beginning, during, and between individual rain events is vital for determining erosion resistance of soil. Despite its importance, a clear elucidation of the relationship between moisture and soil's resistance to erosion for a range of soils has not yet emerged. Not surprisingly, this has resulted in non-consideration of the explicit role of antecedent moisture on soil's resistance to erosion in most sediment models.

In this paper, we synthesize the existing state of knowledge on the role of moisture on erosion resistance of soil, and highlight the opportunities and challenges associated with incorporating such a relation in sediment yield assessment models. The focus here is on the fluctuation in soil resistance to erosion at as short as event time scale, as soil moisture dynamics may vary considerably at these scales (Katul et al., 2007; Rosenbaum et al., 2012). To this end, we, (i) review the literature on the influence of soil moisture content on erosion resistance and the processes and mechanisms associated with it, (ii) highlight the need to include the moisture-erosion resistance relationship in sediment models, (iii) detail the candidate variables that may be used to quantitatively represent the soil's resistance to erosion and its relation to moisture, (iv) underscore the challenges and opportunities in incorporating the effect of soil moisture content on erosion resistance in modeling frameworks and (v) discuss future research directions.

2. Influence of soil moisture content on erosion resistance: Contrasting variations and diverse physical controls

Soil moisture affects resistance of soils to erosion through several mechanisms. Below we highlight the reported disparate relations between soil moisture and soil erosion resistance, and discuss varied mechanisms responsible for them.

2.1. Increasing soil erosion resistance with increasing moisture content

A large number of the studies agree that a completely dry soil has low resistance to erosion, and the resistance generally increases with increasing moisture (e.g. Cernuda et al., 1954; Govers, 1991; Grissinger, 1966; Kemper and Rosenau 1984; Le Bissonnais and Singer, 1992; Lyles et al., 1974; Nachtergaele and Poesen, 2002; Shainberg et al., 1996). Below, we

review studies that report an increasing (a decreasing) trend in soil's resistance with moistness (dryness), and organize them based on the disparate mechanisms explaining the trend. Table 2.1 provides a summarization of the assumptions and key findings of many of these studies.

2.1.1. Slaking

Slaking is often defined as the aggregate breakdown by increase in the pressure exerted by the escaping entrapped air during the rapid wetting process (Bastos et al., 2002; Kemper et al., 1985). Although slaking itself is not erosion, it breaks down soil aggregates and makes the soil more erodible during intense rainfall or runoff events when the soil is wetted rapidly. It has been identified as a prominent cause for high erosion rates in dry soil (Auerswald, 1993; Lim, 2006; Shainberg et al., 1996). Panabokke and Quirk (1957) and Le Bissonnais et al. (1995) noted that in certain conditions, slaking can be more efficient at breaking down dry soils and increasing detachment capacity compared to raindrop impact. In clay soils, slaking caused by differential swelling was identified as responsible for the breakdown of aggregates (Kemper and Rosenau, 1984; Panabokke and Quirk, 1957). Le Bissonnais and Singer (1992) attributed the increased aggregate stability of pre-wetted soil, as opposed to an air-dry soil, to a decrease in slaking. Diminished slaking decreases aggregate breakdown and the generation of smaller easily movable particles, thus also reducing crust formation. Le Bissonnais and Singer (1992) showed (Fig. 2.1a) that pre-wetted soils with high initial moisture content experienced low erosion rates compared to air-dried soils in successive rainfall events, 24 hours and 7 days apart. For the pre-wetted soil, the amount of splashed material that remained was little throughout the three consecutive rainfall events, although runoff increased 10-fold. In Cernuda et al. (1954), for all fifteen soil types tested, slaking and ease of destruction with water drops decreased with increasing initial

moisture content. Lyles et al. (1974) also supported the claim that much less soil was detached from field-moist soil than from air-dried clods by raindrops when other variables were kept constant (Fig. 2.1b). By measuring water absorption and expansion of clods, it was discovered that due to their initial larger water saturation, field-moist aggregates absorbed extra water slowly and hence resisted erosion (Kemper and Rosenau, 1984). Slower rates of wetting due to high soil moisture contents prevents entrapment of air and lowers differences in swelling, allowing a greater portion of the particles to remain cohered in the aggregates. Lim (2006) showed that the intensity of slaking (slaking slope), measured by the slaking test, increased 3 to 5 orders of magnitude for a 30% reduction in the degree of saturation (Fig. 2.1c). Therefore, the rate of water absorption upon wetting has been suggested to be a good measure of soil erodibility, as it indicates the intensity of the disruption occurring due to wetting (Govers and Loch, 1993; Knapen et al., 2007). A few studies suggest that slaking maybe sufficient to breakdown even the highly cohesive clay soil (Kemper and Rosenau, 1984), and this effect is predominant over any softening or solution effect of water on aggregate breakdown (Cernuda et al., 1954). Overall, slaking causes more sediment to be broken down and become available for transport by runoff, while moist soils prevent slaking and limit the ability of the soil to be disaggregated (Legates et al., 2010).

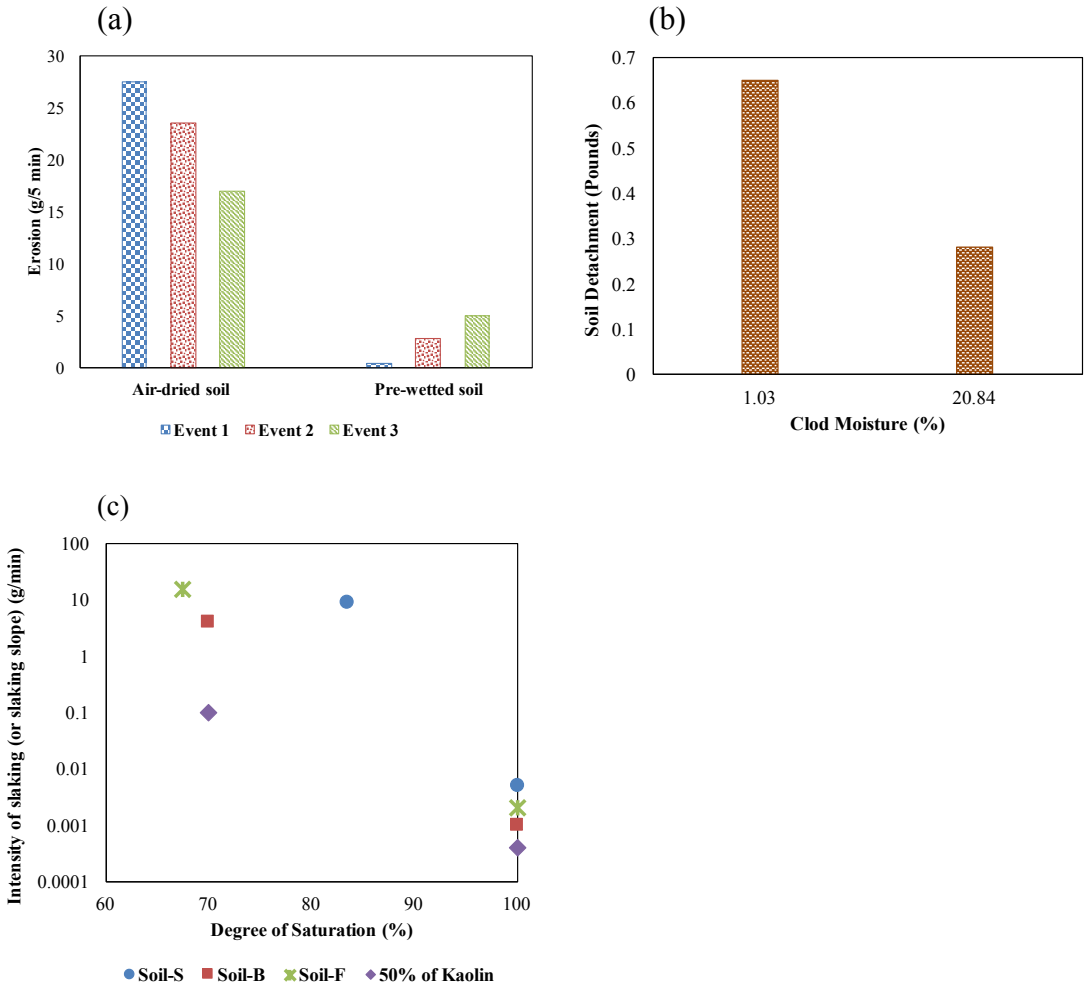

Figure 2.1. (a) The change in erosion between initially air-dry and pre-wetted Solono soil for three consecutive rainfall events 24 hours and 7 days apart as reported in Le Bissonnais and Singer (1992), (b) Effect of moisture on soil detachment based on Lyles et al. (1974), (c) Changes in the intensity of slaking with degree of saturation in non-dispersive soils, as reported in Lim (2006).

2.1.2. Microfissuration

Another mechanism for the lower erosion resistance in dry soils has been attributed to the microfissuration occurring during the rapid wetting of initially dry soil (Govers and Loch, 1993; Govers et al., 1990; Le Bissonnais et al., 1989; Poesen, 1999). Larinov et al. (2018) experimentally found that drying of soil samples increase their erodibility due to soil cracking that decreases the amount and strength of inter-aggregate bonds (see Fig. 1 of Larinov et al.,

2018). Poesen et al. (1999) reported that concentrated flow erosion rates were 20 - 65% less on initially wet topsoils compared to initially air-dry topsoils. Although air-dry soil had high infiltration rates and lower sediment concentrations in the initial phase of their flume experiment, high detachability due to slaking and microcracking of dry aggregates in the intermediate and final phases contributed to high erosion rates compared to initially wet soil.

2.1.3. Cohesion from surface tension

Lower erosion from moist soil has also been attributed to surface tension forces created by the water films that increase soil cohesion (Cernuda et al., 1954; Haines, 1925; Kemper and Rosenau, 1984; Kemper et al., 1985; Panabokke and Quirk, 1957). This cohesion provides a resistance against both the raindrop impact and shearing action of the flowing water. Govers and Loch (1993) conducted a field rill erosion experiment to determine the effect of the antecedent water content on the resistance of soil to erosion by overland flow in two clay soils. They found that variations in initial moisture content, which can contribute towards the development of inter-aggregate bonds, can be linked to major changes in soil erodibility. In fact, the soil strength (both shear and unconfined compressive strength) and erosion resistance were found to be higher for soils with high moisture content than air-dried soils. The effect of surface tension created by soil water on erosion resistance has been experimentally investigated in several other studies (Kemper and Rosenau, 1984; Cernuda et al., 1954; Panabokke and Quirk, 1957). Kemper and Rosenau (1984) found that cohesional forces created by water are sufficiently large to provide a significant portion of the cohesion measured in the silty loam soil they used, however, this was not true for the tested clay soil. Panabokke and Quirk (1957) tested the water stability of various soil aggregates over a range of moisture tension values and found that the aggregates were most

stable at lower moisture tension values pF 2-3, i.e., at higher moisture contents, due to the capillary water films created by low tensions.

The rate at which cohesion develops in disrupted soils is also slower in an air-dried soil than in a moist soil (Kemper and Rosenau, 1984; Kemper et al., 1985), and some studies have noted that moisture must be present for cohesion forces to re-form with time (Kemper et al., 1985; Shainberg et al., 1996). Kemper et al. (1985) suggested that highest rate of cohesion increase takes place when the soils are wet, but have enough tension in the water to bind the particles strongly together. The moisture content supporting the most rapid formation of bonds after disturbances was about 0.21 g/g for Portneuf silt loam soil aggregates (Kemper et al., 1985). Kemper et al. (1985) highlighted that after disruption of inter particle bonds through agricultural or construction activities, lack of time and optimal moisture content to retrieve soil's cohesion plays a key role in the greater erosion rates of the tilled or disrupted soil. Cohesion, generally, also decreases with rapid wetting, mainly owing to the loss of bonding between soil particles/aggregates caused by the action of water (Bastos et al., 2002).

2.1.4. Continuity of soil air in pore spaces

Parker et al. (1995) observed an increased erodibility of a soil composed of 87% sand, 4% silt, and 9% clay, with reducing initial soil water content between the moisture range 0.125 and 0.200 kg/kg (Fig. 2.2), and attributed this to the influence of continuity of soil air in pore spaces with decreasing soil water content triggering more erosion.

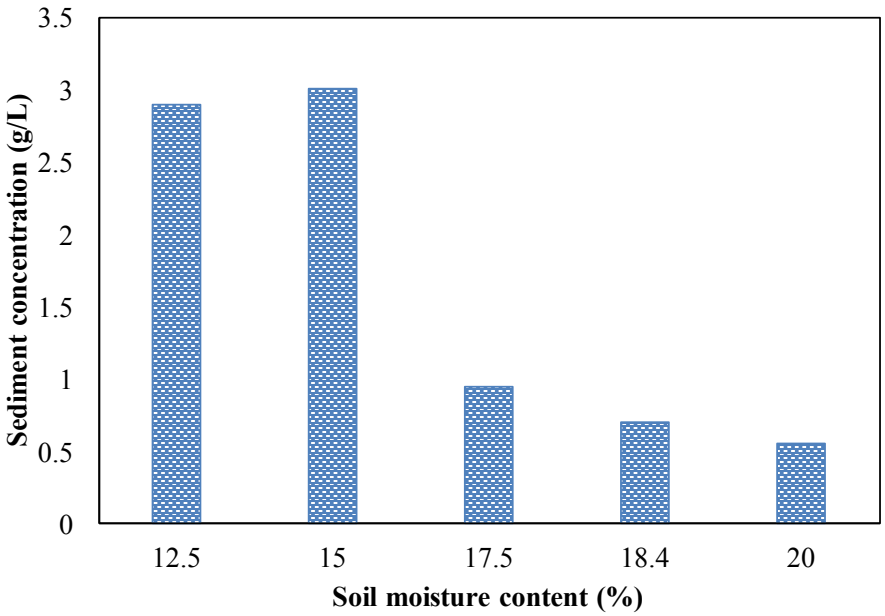

Figure 2.2. Sediment concentration measured in runoff at t=150 seconds for different initial soil moisture contents based on Parker et al. (1995).

2.1.5. Particle reorientation

An experimental study by Shainberg et al. (1996) revealed that in the clayey grumusol, increased soil water facilitates the movement and reorientation of clay particles. This improves clay-to-clay connections and cementing of soil particles into a cohesive, erosion resistant structure. Therefore, rill erodibility of this clay soil decreased with increasing antecedent soil water content. Larionov et al. (2014) also suggested that water acts as a lubricant that causes uniform distribution of aggregates in soil, promoting cohesion between aggregates in their loamy soil.

2.1.6. Runoff armoring

The formation of a runoff water layer, which reduces the impact of raindrops and runoff on detachment and transport of sediment, was identified by Auerswald (1993) as contributing to

reduction in soil loss. Also, moist soil conditions can lead to more ponding on the surface which acts as a protective water armor that reduces raindrop impact (Hairsine and Rose, 1992; Holz et al., 2015).

2.2. A decrease or an absence of any apparent trend in soil's resistance to erosion with increasing moisture content

In contrast to studies discussed in section 2.1, several studies have reported a decrease or absence of a defined relation in the variation of soil resistance with increasing moisture, or higher resistance in dry soil. Varied mechanisms have been noted to be responsible for it. Below we highlight these studies vis-à-vis the dominant controlling mechanism(s) in play. Table 2.2 provides a summary of the key findings of many of these studies.

2.2.1. Near-saturation effects

Cernuda et al. (1954) reported that soil aggregates are easily eroded when soil was completely saturated. The effect of hydraulic and surface tension forces created by water films on the stability of soil aggregates is lacking in completely saturated soils (Bastos et al., 2002; Christensen and Das, 1973; Hanson and Robinson, 1993). After soil disturbance, when the aggregates were close to saturation, inter-particle bonds did not reinforce with time (Kemper et al., 1985). Kemper and Rosenau (1984) mentioned that in order for moisture to cause cohesion in soils, air pressure should remain greater than the pressure of the soil water. Govers (1991), using their flume experiment with a loamy soil (17% sand, 69% silt and 14% clay), presented a parabolic equation to calculate runoff erosion resistance vis-à-vis initial moisture content for soils with 2-20% initial moisture contents. For moisture contents exceeding 20%, the erosion

resistance was not dependent on moisture. Several other studies also imply that the increase in erosion resistance with antecedent moisture content is more important when the soil is drier, but when the moisture contents are closer to saturation, cohesion between aggregates and particles diminish and aggregate strength decreases resulting in high erosion rates (Bryan, 2000).

Luk and Hamilton (1986) and Coote et al. (1988) are two of the few studies that claimed that soil loss increased and aggregate stability decreased with soil moisture. Coote et al. (1988) reported that aggregate stability was negatively correlated with soil moisture content from 16.5 to 47.5%. However, Luk and Hamilton (1986) acknowledged that this observation may be true only for the data in the wetter range of the moisture scale. In the drier range, antecedent moisture may lead to an increase in soil strength and thus soil loss may decline until the moisture content corresponding to the plastic limit is reached. The plastic limit represents the soil moisture content at which the soil becomes malleable and clay begins to crack, and this reduces the shear strength of the material which increases its susceptibility to detachment (Allen et al., 1999; Holz et al., 2015). Data in Luk and Hamilton (1986) did not cover the entire moisture range to be able to investigate this effect. Atterberg consistency limits, which empirically define soil behavior as a function of changing soil moisture content, could provide some guidance to determine the optimum soil moisture content that results in greatest erosion resistance (Bryan, 2000; Lyle and Smerdon, 1965), however, the utility of this measure alone for soil erodibility prediction has been questioned (Grabowski et al., 2011; Partheniades, 2007).

2.2.2. Crust formation

Kemper and Rosenau (1984) reported faster rate of wetting in drier soil resulted in more disruption of aggregates leading to interlocking of particles to make a structure that has greater

cohesion. Breakdown of aggregates from rapid wetting allows the resulting micro-aggregates and primary particles to later settle into tightly packed and well inter-leaved configurations, which would develop a greater soil strength when drying. This is also known as the surface sealing effect or crust formation. While soil crust formation could also be driven by several other biophysical and chemical mechanisms (Park et al., 2017; Williams et al., 2018), research has shown that aggregate break down and seal formation due to rapid wetting is faster in soils with < 30% moisture than soils with > 30% moisture (Holz et al., 2015; Le Bissonnais et. al. 1989). Therefore, dry soil has a higher predisposition for surface sealing and once the crust is formed, dried crusted soil is more resistant to erosion.

2.2.3. Entrapped air preventing water entry in dry soils

Panabokke and Quirk (1957) reported that soils drier than pF 5.5 had higher aggregation due to entrapped air preventing water from entering pore spaces.

2.2.4. Limited volume of fine pores

In coarse textured soil with limited volume of fine pores required for slaking, low moisture conditions may not cause disruptive slaking during rapid wetting, thus does not cause higher erosion rates when soil is dry (Cernuda et al., 1954).

2.2.5. Mineralogical influence upstaging moisture control

Allen et al. (1999) did not find a significant relationship between moisture content and erodibility in loamy or clay soils. They suggested that when the clay content is greater than 10% in a soil, natural cohesive properties of clay becomes dominant and hinder the effect of moisture

on soil cohesion. Higher soil resistance for drier soils (Billings clay soil from Colorado) was reported by Kemper and Rosenau (1984), who attributed this to the difference in the bonding mechanism of the tested clay soil that facilitates clay-to-clay bonding during drying. An increase in erodibility with increasing antecedent water was also reported for unoriented coarse kaolinitic-Greneda mixture (Grissinger, 1966). A negligible influence of soil moisture on erosion resistance was reported for dispersive soils (Lim, 2006), and loamy loess (Shainberg et al., 1996).

2.3. Moisture-erosion resistance relation shows contrasting trend beyond the optimum moisture content at which erosion resistance reaches a maximum

The two previous sections indicate that there could be an optimum moisture content beyond which the increasing trend in soil resistance with antecedent moisture may start decreasing (or at least do not show an increasing variation). Several studies have noted the existence of such an optimum moisture content (Grissinger, 1966; Larionov et al., 2014; Shainberg et al., 1996). In an experiment to test the effect of moisture content on the cohesion and erodibility of Chernozem soil samples, Larionov et al. (2014) found that the heavy loamy Chernozem samples (loess like loams) containing 22-24% water had the lowest erosion rate, and thus lowest erodibility (Figure 2.3). The erosion rate increased with both increasing and decreasing antecedent water content. In Grissinger (1966), erosion rates of different types of clay soils were evaluated by subjecting molded samples of various soil mixtures to a uniform erosive force in a small flume. Erodibility decreased with increased antecedent water for the Grenada silt loam, illitic-Greneda mixture, montmorillonitic-Greneda mixture, and oriented coarse kaolinitic-Greneda mixture samples up to approximately 25% antecedent water content. After this point,

erodibility increased with further increasing antecedent water (see Figs. 2 to 7 of Grissinger, 1966).

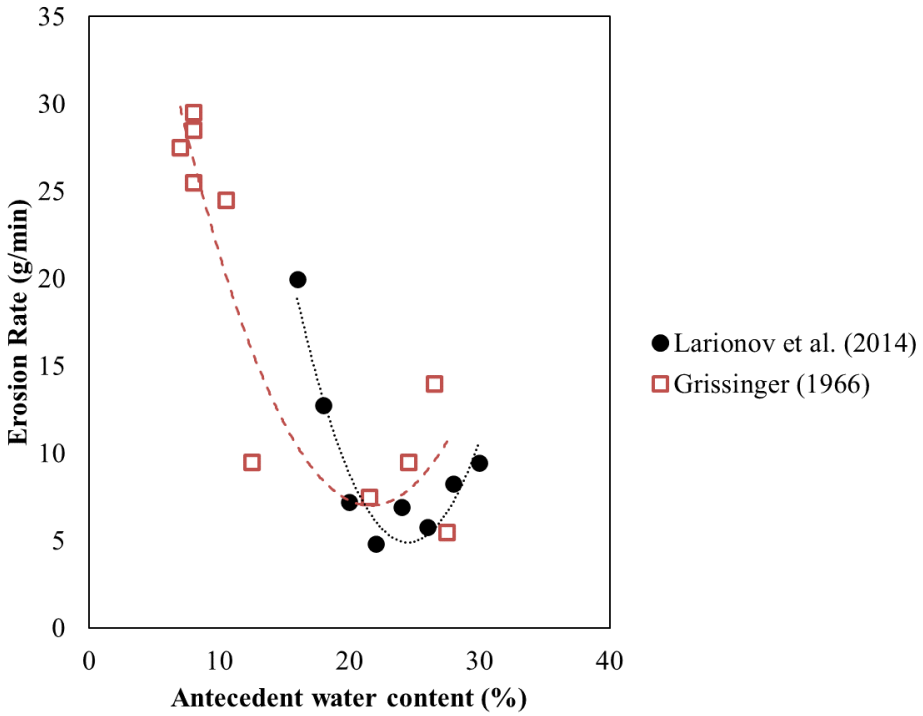

Figure 2.3. Erosion rate of the soil sample as a function of water content as reported in Larionov et al., 2014 and Grissinger (1966).

Varied reasons for the existence of optimum moisture content have been noted. Grissinger, (1966), Larionov et al., (2014), and Shainberg et al., (1996) attributed it to nonlinear variations in cohesion. Development of cohesive forces is absent in air-dry soils. Also, when the soil water content is close to saturation, the rate of cohesive force development is slow and the soils are also more susceptible to erosion. Between these, there is an optimum water content that yield the highest erosion resistance. Studies also noted that a minimum moisture content is needed for the development of interparticle forces, which are strong enough to resist rill erodibility (Shainberg et al., 1996; Luk and Hamilton, 1986). In the loamy loess soil that

Shainberg et al. (1996) used, the low-water-content treatment (246 g/kg) after 15 min of curing provided adequate water to support fast development of cohesive forces between soil particles that lead to low rill erodibility (see Fig. 2 of Shainberg et al., 1996). In contrast, the low-water-content treatment in the clayey grumusol (322 g/kg) was lower than the critical water content required for the fast formation of cohesion forces. Consequently, the rill erodibility was still relatively high after 15 min in the grumusol.

Overall, preceding studies highlight the existence of optimum moisture content at which soil's resistance to erosion (soil erodibility) is maximum (minimum), with resistance decreasing with both increase or decrease in antecedent moisture. Notably, the optimum moisture content appears to be different for different soils. Larionov et al. (2014) and Grissinger (1966) both suggested that the influence of antecedent water content on erodibility varied among soils, depending upon the clay minerals in the mixture, clay particle orientation, bulk density of the sample, and particle size. In addition, aggregation characteristics such as aggregate size and shape which influence pore space geometry were also suggested to determine moisture-erodibility relationship (Bryan, 2000).

2.4. Ancillary dynamic factors that influence the moisture-erosion resistance relation

Aforementioned studies highlight the role of soil moisture content on soil resistance to erosion. However, several studies have noted that in addition to the magnitude of the antecedent moisture in the soil, moisture-erosion resistance relation is also influenced by factors such as (i) the curing or aging time, and (ii) moisture at the time of compaction. Curing, also known as aging of soil, refers to the time for which the soil is left undisturbed, during which stable linkages develop. Kemper and Rosenau (1984) found that cohesive strength increases due to curing, after reaching a desired water content. Shainberg et al. (1996) found that aging of soil

samples reduced rill erodibility due to the development of cohesion forces with time, and that soil must be wet for these cohesion forces to develop. The rill erodibility values obtained by Shainberg et al. (1996) after 24 hours of curing were similar at all moisture contents. Thus, after reaching a critical moisture content, the effect of aging time on rill erodibility was more pronounced than that of soil water content.

Moisture content at the time of compaction also has an effect on erosion resistance of soil. Compaction may be experienced during anthropogenic interventions related to agricultural and engineering activities. The erosion resistance increases as the compaction moisture content increases with the exception when soil is saturated (Christensen and Das, 1973; Hanson and Robinson, 1993; Wan and Fell, 2004). This increase in resistance was attributed to the influence of moisture on smoothening of the surface of the clay (Christensen and Das, 1973), reduced swelling during compaction (Hanson and Robinson, 1993), and an overall facilitation of the orientation of clay particles to a high cohesion low energy state (Grissinger, 1966).

2.5. Soil moisture's influence on erosion resistance at field or larger scales

Beyond the laboratory scale experiments where studies have demonstrated a strong control of soil moisture on soil erosion resistance (see previous subsections for numerous examples), field scale studies have also noted the differences in sediment yield from wet and dry soils. Antecedent soil moisture at the start of a rain event is shown to be particularly important for soil erosion in field settings, due to its influence on soil's resistance (Govers et al., 1990; Grissinger, 1966; Rauws and Auzet, 1989). The effect of initial moisture content alone can cause a few orders of magnitude change in runoff erosion resistance of loamy soils (Govers, 1991). Moderate to high intensity rainfall events occurring on dry, bare soil can lead to greater erosion,

whereas initially moist soil can be relatively hard to break down by the impact of raindrops or overland flow. This can lead to a range of sediment concentrations at the outlet for the same runoff/discharge values depending on high and low initial soil moisture conditions (Battista et al. 2020). Nachtergaele and Poesen (2002) showed that morphological differences in gullies formed in winter and summer under similar erosive power were due to different initial soil moisture contents. Wide and shallow gullies in the summer were attributed to intense rain that hit an air-dry top soil, whereas small winter gullies were formed when soil is at or near field capacity. In contrast to decreasing the runoff erosion resistance of soils, low initial moisture contents are also known to increase the infiltration capacity of the soil and decrease runoff generation, which can lead to a reduction in erosion (Sun et al., 2018). In an attempt to assess the relative significance of these two countering factors, Govers et al. (1990) found that a given rainfall event may lead to more erosion and sediment when the soil is initially dry, regardless of their higher infiltration capacity. The greater sediment yields in arid and semiarid zones (Collins and Bras, 2008; Istanbulluoglu and Bras, 2006) may also be because of the higher runoff detachability of dry soil, in addition to the reduced contribution of vegetation cover to provide protection against erosion (Govers et al., 1990). In arid and semiarid areas, the likelihood of precipitation events occurring on a dry soil is greater than in temperate or tropical settings (Pilgrim et al., 1988). Overall, reductions in soil erosion/sediment generation due to enhanced infiltration capacity and reduced runoff in dry soil can be potentially offset by high erosion rates of dry soil due to their low erosion resistance specially during intense rainfall events (Figure 2.4). Therefore, the influence of initial soil moisture content on erosion resistance may provide an explanation to the runoff-sediment relationships observed at continental and global scales (Govers et al., 1990).

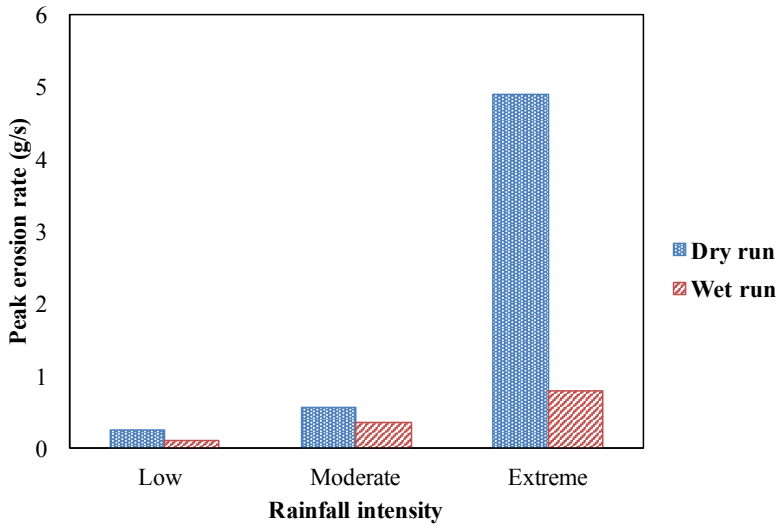

Figure 2.4. Peak erosion rate under rainfalls of low intensity long duration, moderate intensity and duration, and extreme intensity short duration, for soils in dry state (blue) and wet state (red), based on Ran et al. (2012).

3. A need to define moisture-erosion resistance relationship in sediment modeling

Aforementioned studies (discussed in section 2) emphasize that soil erosion models, especially those that perform predictions at seasonal, event, or finer temporal resolutions, should incorporate the effects of antecedent soil moisture content on soil loss predictions not only via runoff generation but also soil's resistance (Luk and Hamilton, 1986; Poesen et al., 1999). It is also important to recognize and incorporate the spatial and temporal dimensions of this relation as well (Nachtergaele and Poesen, 2002). Spatially, local rainfall patterns and the fraction of runoff occurring on initially wet soil need to be considered when simulating soil loss (Govers and Loch, 1993), because the relative contribution of the amount of sediment produced in various areas of a catchment may highly depend on the spatial distribution of antecedent moisture content of the soil (Kim et al., 2016; Zi et al., 2019). Given the fact that antecedent

moisture can cause several orders of magnitude change in erosion (Govers, 1991), accounting for its spatial distribution may help reduce errors in sediment simulations. Temporally, the variation in moisture content on sediment response during a single rainfall event as well as a series of events needs to be considered. When a series of rainfall events occur after a dry period, sediment production may be largest in the first storm, and erosion resistance will increase in subsequent events due to soil becoming moist and also due to surface sealing effect (Govers, 1991). As one of the few studies that considered the time series of soil loss, Luk and Hamilton (1986) recognized the complexity that is added to the erosion resistance-soil moisture relationship by the variation in soil moisture content over time during a single rainfall event. During a single event, for dry soil, the variability in sediment concentration can be higher, and peak sediment concentration can occur toward the beginning of the event as more dry, easily removable materials are available (Figure 3 of Ran et al., 2012), whereas on moist soil, sediment concentrations can be largely constant in time (Govers, 1991). Although antecedent soil moisture content during and between individual storm events is most vital for determining erosional response, erodibility is also influenced by soil moisture regime over longer time periods (Bryan, 2000). Many studies have shown that recurring wetting–drying cycles can result in a decline of aggregate stability (Bryan, 2000; Shiel et al. 1988), while there can be complex responses with both increased and decreased stability considering disturbed and undisturbed soils (Utomo and Dexter, 1982). At longer time scales (e.g., annual to interdecadal) as well, changes in moisture regimes due to variations or changes in climate may result in variations in soil erosion resistance. In summary, spatially and temporally dynamic relationships of soil resistance needs to be incorporated in sediment models for both short- and long-term predictions.

All the evidence presented here suggest that the use of a single value for erodibility can cause serious errors in trends and magnitudes of predicted erosion, especially for event scale simulations. It is important that the variation in soil erosion resistance through time and space vis-à-vis the influence of initial soil moisture contents be considered in erosion resistance variables (Nachtergaele and Poesen, 2002).

4. Candidate variables for quantifying the soil's resistance to erosion vis-à-vis antecedent moisture

To account for the role of moisture on soil erosion resistance, several candidate variables exist. These include soil cohesion (Haines, 1925; Kemper and Rosenau, 1984), aggregate stability (Cernuda et al., 1954; Kemper and Rosenau, 1984; Panabokke and Quirk, 1957), erodibility (Allen et al., 1999; Grissinger, 1966; Larionov et al., 2014; Parker et al., 1995; Shainberg et al., 1996), soil loss/rate of erosion (Govers et al., 1990; Le Bissonnais and Singer, 1992; Lim, 2006; Luk and Hamilton, 1986; Lyles et al., 1974), intensity of slaking (Lim, 2006), critical shear stress (Allen et al., 1999; Gilley et al., 1993; Nachtergaele and Poesen, 2002), and shear strength (Govers and Loch, 1993; Yokoi, 1968). More details regarding each variable vis-à-vis the soil resistance property they encapsulate are listed below.

4.1. Erodibility

Erodibility is a widely used lumped parameter that captures the average annual soil erosion from a standard plot. It is used in a range of models, including the Universal Soil Loss Equation (USLE, Wischmeier and Smith, 1978) and modified USLE, ANSWERS (Beasley et al., 1980), GUESS (Carroll et al., 1986), and SWAT (Arnold et al., 2012). Erodibility (or *K-factor*)

is used to indicate the resistance that soils have against the effect of raindrops on the soil surface and the shearing action of runoff between soil clods (FAO, 2019). It is quantified as the average rate of soil loss per unit rainfall erosivity from a cultivated continuous fallow plot with 9% slope and 22.1 m length. Since direct measurement of the *K-factor* for each soil configuration is implausible, data from long-term erosion measurements at standard field plots has been used to generate a soil erodibility nomograph, which relates erodibility to inherent properties of the soil. Specifically, a soil erodibility nomograph relates the *K-factor* to soil parameters such as percentage of silt, percentage of sand, percentage of organic matter, and structure and permeability classes (Wischmeier et al., 1971). Since it was first developed, the nomograph has formed the basis for soil erosion prediction in many parts of the world. Later, a sixth variable, namely rock fragment cover, was added by Wischmeier and Smith (1978). In summary, erodibility is often parameterized as a constant value for a given soil type (Bryan, 2000; Nachtergaele and Poesen, 2002).

Notably, erodibility does not explicitly account for the impact of soil moisture on soil resistance. Given that standard erosion plots with identical soils in two different hydroclimatological settings can yield different sediment amounts, erodibility estimate is after all not agnostic of local hydroclimatology (and associated hydrologic states such as the soil moisture regime) at the measurement plot (Coote et al., 1988; Govers and Loch, 1993; Grissinger, 1966). Hence, its estimate based on data from experimental plots may be affected by moisture regime of the setting where the observations were made (Bryan, 2000). This limitation is being increasingly recognized and attempts are being made to address this concern. For example, Dangler and El-Swaify (1976) calculated *K* values for wet and dry soil conditions, and Hosoyamada (1986) calculated cold and warm *K* values. Seasonal effects on the USLE *K*,

intended to capture the effect of freezing and thawing processes and other factors influencing the temporal variations in soil erodibility including antecedent soil water (Alewell et al., 2019; Mutchler and Carter, 1983), are also being considered. However, these do not and are not intended to exclusively represent the full effects of the soil moisture content on erosion resistance. Govers et al. (1990) conducted experiments in a 20 m flume to evaluate the changes in the erosion resistance of a loamy soil due to compaction and initial moisture content. The constant k_1 (measured in kg/(m h $(m^3/h)^{5/3}$), which is proportional to the total soil loss, was found to be reasonably well predicted using a parabolic equation with percent initial gravimetric moisture content (GMC_i) being one of the independent variables:

$$k_1 = 2005.63 - 157.47GMC_i + 3.23\ GMC_i^2 \quad (1)$$

Allen et al. (1999) conducted field experiments using a submerged jet apparatus to calculate the erodibility coefficients in alluvial soils along stream channels. Increasing moisture contents yielded lower erodibility coefficients for moisture content range ~ 6 to 21% for sand/silt textured alluvial soil along stream channels. Using multiple regression analysis on different soil parameters, erodibility coefficient, K, (measured in cm/hr/Pa) was derived for soils with less than 10% clay,

$$Jet\ Index = -0.0272 + 0.000459Sand - 0.0004752Moisture \quad (2)$$

$$K = 0.003e^{385Jet\ Index} \quad (3)$$

This equation indicates that, for soils with less than 10% clay, antecedent moisture content is important in determining soil erodibility measured by the submerged jet test, and the

erodibility increases with decreasing moisture content. Preetha and Al-Hamdan (2019) developed a method to dynamically predict the modified USLE erodibility factor or K factor for a selected watershed and identified it to be affected by five variables one of which is soil moisture content. The robust correlation between the *K* value (measured in ton ha hr/ha MJ mm) estimated from the multiple linear regression model and the measured *K* indicated that the using soil moisture content as a predictor variable ($R^2 = 0.84$, $p < 0.05$) provides a better estimate of soil erodibility in areas with notable temporal variability in land cover. Two regression equations were developed,

$$K = -0.059 + 0.161AWC + 0.134BD - 0.000062P; \qquad R^2 = 0.898 \tag{4}$$

$$K = -0.064 + 0.173AWC + 0.122BD - 0.000044P + 7.699LS + 0.0081C; \qquad R^2 = 0.903 \tag{5}$$

where, AWC is antecedent soil moisture content (%), BD is bulk density (g/cm^3), P is soil permeability (mm/h), LS is USLE slope length and steepness (m), and C is USLE crop management factor. Studies such as these are promising. However, a relation defining the variation in erodibility with moisture for a range of soil types still remains unidentified.

4.2. Soil cohesion

Soil cohesion is another variable that is used to represent the resistance of soils to erosion. Kemper and Rosenau (1984) presented equations to calculate the cohesion forces due to hydraulic pressure and surface tension. Using the results of their study, they suggested that pressure difference between air and water i.e., $(P_a - P_w)$, and the soil volume occupied by water,

θ, (m^3 m^{-3}) could provide an estimate of the cohesion in bulk soils due to hydraulic pressure, F_{hs}, (N/m^2) as follows:

$$F_{hs} = \theta(P_a - P_w) \tag{6}$$

The cohesion associated with surface tension forces was calculated by assuming spherical pores with an air water interface around their perimeter that applies a surface tension. Therefore, a given pore of radius r_i, produces a cohesion of, $2\sigma\pi r_i$ in the soil. σ is the surface tension of the air-water interface measured in N/m. The cohesional force due to surface tension in the soil, F_{ss}, was estimated using

$$F_{ss} = \sum_{i=1}^{n} \frac{\theta_i}{\pi r_i^2} 2\pi r_i \sigma = 2\sigma \sum_{i=1}^{n} \frac{\theta_i}{r_i} \tag{7}$$

The summation of cohesional forces created by water phase hydraulic pressure and surface tension were sufficient to explain the measured soil cohesion for these soils. In spite of these quantitative theoretical developments, a review performed by Jain and Kothyari (2009) showed that quantitative relations between the effect of cohesion and erosion/sediment transport processes have not been established yet.

A few efforts have been made to incorporate the influence of soil moisture conditions on cohesion. Zi et al. (2016) incorporated the dependency of soil cohesion on soil moisture in the spatially-explicit, sediment erosion, deposition and transport module they developed for the GEOtop distributed hydrological model. They used soil cohesion to represent the soil's resistance to erosion and calculate rainfall splash detachment D_R (kg m^{-2} s^{-1}) using

$$D_R = \left(0.1033\frac{K_e}{\zeta}e^{-1.48h} + 3.58\right) * I \quad (8)$$

where ζ is soil cohesion (kPa), K_e is rainfall kinetic energy (J/m^2 mm), h is depth of overland flow (m), and I is the precipitation intensity (mm/h). This cohesion term is a combination of the effect of soil moisture and root tensile strength on cohesion (ζ).

$$\zeta_s = \left(\frac{\theta}{\theta_s}\right)^2 \zeta_{ss} \quad (9)$$

$$\zeta = \zeta_{add} + \zeta_s \quad (10)$$

where $\zeta_s, \zeta_{ss}, \zeta_{add}$ are bare soil cohesion, saturated bare soil cohesion and cohesion added by roots respectively, θ and θ_s are the moisture content and the saturated moisture content of the soil respectively.

Although cohesion seems to be the right parameter to represent the resistive forces of soils against water erosion, its magnitude as measured by a torvane under saturated conditions, is not very appropriate for studying the spatial and temporal variability in soil erosion resistance (Govers et al., 1990; Knapen et al., 2007). This is because, all the soil and environmental properties affecting the soil's erosion resistance (e.g. tillage effects, roots, rock fragments etc.) cannot be represented by variations in cohesion. Notably, even if a nomograph connecting the easily observable soil properties to cohesion under saturated conditions were available, a need to incorporate the influence of soil moisture conditions on cohesion for a wide range of soils still remain.

4.3. Aggregate stability

Aggregate stability is another variable used to define soil resistance to erosion. Grissinger (1966) related erosion contribution from aggregate instability to the rate of sample wetting. This empirical relationship is given by (Paaswell, 1973),

$$ER = b * p(\frac{\Delta \text{water}}{\text{time}}) \tag{11}$$

where, ER is erosion rate, b is regression constant, and p is sample porosity. Auerswald (1993) presented the following equation that explained 81% of the variation in soil loss (SL) in t/ha using only two variables; antecedent soil moisture (ASM) in % wt., and time since tillage (TsT) in days. They attributed the increased stabilization of soil against erosion with increasing moisture between 10-31%, to two processes that reduced aggregate breakdown; reduced slaking, and the development of a protective water mulch that reduced splash.

$$SL = \frac{1}{-0.027 + 0.0022 * ASM + 0.006 * ASM * TsT} \tag{12}$$

Le Bissonnais (1996) proposed a unified framework to measure aggregate stability that can be used to effectively measure soil's susceptibility to erosion. However, Le Bissonnais (1996) and Le Bissonnais and Singer (1992) both noted that aggregate stability tests will not provide a comprehensive assessment of crusting and erodibility. A quantitative relation between aggregate stability and soil moisture remains undetermined.

4.4. Flow shear stress and soil shear strength parameters

Flow shear stress and soil shear strength parameters have also often been used to evaluate erosion-related soil properties (Briaud et al., 2001; Nearing and West, 1988; Nearing et al., 1988; Shainberg et al 1996). Nachtergaele and Poesen (2002) demonstrated that detachment rate (D_r) in kg m^{-2} s^{-1} for a given loamy soil horizon, could be predicted using only flow shear stress and initial gravimetric moisture content:

$$D_r = \left(nw_g^2 - mw_g + p\right)\tau + b \tag{13}$$

where, w_g is initial gravimetric soil moisture content (kg kg^{-1}), τ is flow shear stress (Pa) and n, m, p and b are constants. They derived these coefficients as well as the lower and the upper limit of the initial gravimetric moisture content that is applicable. Values of τ which represents the force of the moving water flow against the soil bed was calculated using water density, acceleration due to gravity, width of the experimental channel, flow velocity, flow discharge, and slope gradient. Detachment calculated using this equation resulted in a R^2 of 0.83 for the top soil layer with observed values. However, some researchers have reported little or no correlation between critical flow shear stress and soil erodibility (Knapen et al., 2007; Laflen et al., 1991; Mamo and Bubenzer, 2001), and erodibility and soil shear strength (Ansari et al., 2003; Knapen et al., 2007; Parker et al., 1995). They reported that factors or processes that affect critical flow shear stress or shear strength of soils do not necessarily affect erodibility and vice versa.

The above review indicates that while some promising advances have been made in regards to quantifying the soil's resistance to erosion and estimating the influence of soil

moisture content, they have mostly been performed for specific catchments, soil categories, and resistance variables. Challenges associated with measuring or estimating resistance variables across a range of soil types and properties remain.

5. Synthesis

Based on the review presented above, next we discuss the potential challenges and opportunities in incorporating the effect of soil moisture content on erosion resistance.

5.1. Challenges

A multitude of challenges exist towards representing the influence of soil moisture on soil erosion resistance. These include:

i) There are a number of parameters used to represent the soil's resistance to erosion. Each parameter, be it erodibility, cohesion, shear stress, or aggregate stability, includes various erosional processes and any single parameter does not capture all the processes involved in erosion or all the factors that influence soil erosion resistance. Also, the way these variables are measured are different, and many a times the same variable is measured differently. Most importantly, the implementation of these parameters lacks explicit representation of the dynamic nature of soil and environmental factors that govern erosion resistance. This poses a major challenge in incorporating the relationship between soil moisture content and erosion resistance in soil erosion and sediment models.

ii) Studies report various factors affecting the control of soil moisture on erosion resistance, including the type and percentage of clay minerals in the mixture (Grissinger, 1966; Larionov et al., 2014), clay particle orientation (Grissinger, 1966), curing/aging time

(Kemper and Rosenau, 1984; Kemper et al., 1985; Le Bissonnais and Singer, 1992; Shainberg et al., 1996), bulk density of the sample (Grissinger, 1966), organic matter content (Cernuda et al., 1954), soil type (Shainberg et al., 1996), and texture/particle size (Allen et al., 1999; Grissinger, 1966; Kemper and Rosenau, 1984; Larionov et al., 2014). In general, there are no clear guidelines as to how prominent soil moisture influence will be on soil erosion resistance under a certain combination of soil physical conditions. Moreover, contradictory results are often reported for some parameters. For example, when the influence of texture is concerned, Allen et al. (1999) found that antecedent moisture content is important in determining soil erodibility for soils with less than 10% clay, but no significant relationship when clay content is higher. However, in many other studies, discussed above, water content in soils of diverse textural classes, including fine grained soils, has been found to have an influence on erosion resistance and this effect also shows conflicting results for some soil types (Kemper and Rosenau, 1984). No standardized relations have been derived (for different soils) that can help parameterize models easily.

iii) Most of the studies have been conducted under controlled settings. Notably, the standard laboratory tests often use small disturbed samples (Holz et al., 2015). Although these data are useful to assess the behavior of agricultural soils, most of the time they neglect the natural structure and macroporosity of the soil. In the context of fluvial geomorphology and hydrology, it is essential to consider the behavior of soil in natural undisturbed settings. Unfortunately, our understanding of the behavior of natural soils, especially in complex topographic or forested conditions, where structural characteristics of soil are usually different from agricultural soils (Chaer et al., 2009), is greatly lacking. Therefore,

more appropriate tests that use much larger blocks that mimic natural soil conditions or soil in natural state are needed in order to understand the effect of dynamic soil properties on erosion resistance (Bryan, 2000).

iv) It is clear that soil resistance variables such as erodibility are not a single constant value for a given soil type, but they are strongly influenced by spatially and temporally dynamic intrinsic soil properties and extrinsic environmental conditions. The USLE erodibility or K-factor is purely a lumped, empirical parameter and intended to provide a practical tool to aid in agricultural decision making. It is not intended to apply for complex soils and topographical conditions which are typically of interest in sediment modelling. Also, it was designed to capture long-term response patterns and was not envisioned to provide the spatial and temporal variability necessary for event-based predictive modelling. In the long term, researchers propose that a standardized erosion resistance parameter that can integrate dynamic properties such as soil moisture need to be introduced, for use in dynamic sediment modeling (Bryan, 2000; Knapen et al., 2007).

5.2. Opportunities

Equations provided by various studies that are discussed in section 4 provide the basis for incorporating moisture's influence on soil erosion resistance in sediment yield predictions. Specially equations proposed by Preetha and Al-Hamdan (2019) and Zi et al. (2016) can be important starting points. However, generic equations that can be easily parameterized based on soil properties, as is done using nomographs for soil erodibility (Wischmeier et al., 1971), will likely be more useful for future soil erosion and sediment modeling efforts.

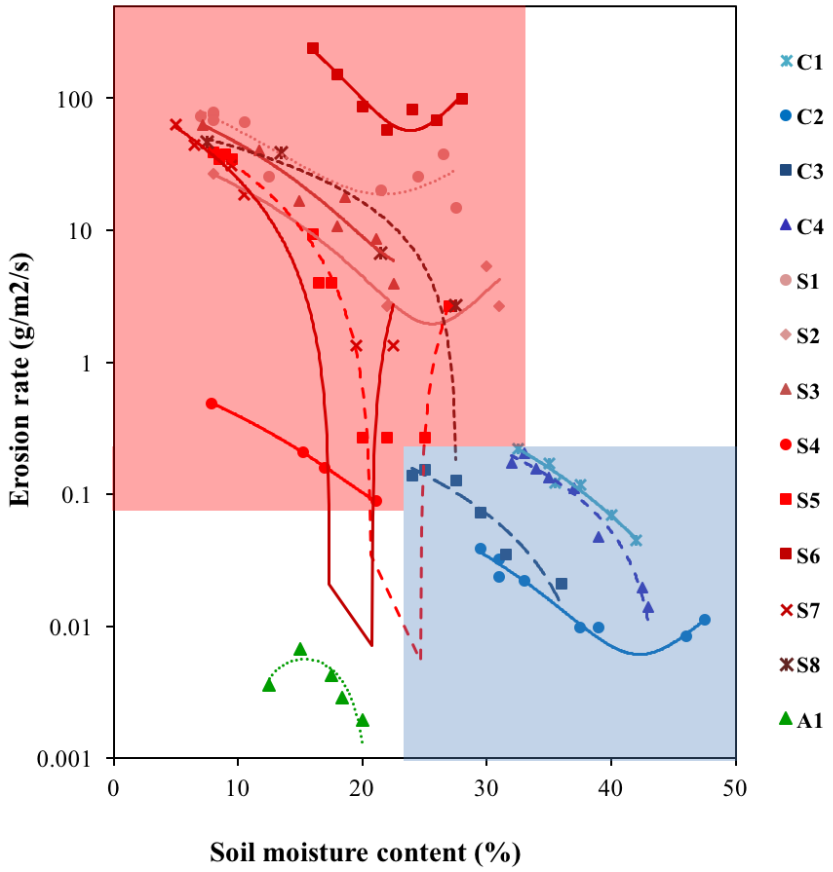

Figure 2.5. Variation of soil moisture content and soil erosion rates presented by various studies. Blue, red, and green colors indicate clay, loamy, and sandy soils, respectively. Soil types and their data sources corresponding to the legend entries are provided in Table 2.3. The unit erosion rate (calculated in $g/m^2/s$) is log-stretched to aid visualization.

Given the fact that there is some coherence in the relation between soil resistance to erosion vis-a-vis soil moisture reported in literature, we compared the experimental observations reported for 13 soil samples from 6 different studies after transforming the reported erosion values into erosion rates per unit surface area (Figure 2.5). These studies report experimentally determined soil erosion values for different antecedent soil moisture contents. All studies that reported soil moisture data along with soil erosion values that were either in (or could be converted to) erosion rate per unit surface area, were included in this meta-analysis. It is to be

noted that these studies have significant differences in methodologies as well as experimental conditions. These differences are in the definition of erosion, choice of erosion measurement device, slope, soil compaction, rainfall duration and characteristics etc. Despite these differences, and the fact that erosion rates span over several orders of magnitude, all the relationships presented here show a fairly consistent trend where erosion rate decreases as initial moisture content increases, and for some, beyond a threshold moisture content, erosion rate starts increasing again. Overall, these variations can be represented by a generic quadratic equation of the form,

$$Ln\left(\frac{E}{E_d}\right) = \sigma\theta^2 - b\theta \tag{14}$$

where, E is the erosion rate per unit area of the soil (g/s/m^2) at a given moisture content, E_d is dry soil erosion rate (erosion rate at 8% moisture), θ is soil moisture content (%), and σ and b are constants. Equation 14 was fitted to the data obtained from meta-analysis of literature. Derived parameter values of this relation for each soil type are summarized in Table 2.3. Table 2.3 and Fig. 2.5 highlight that parameters (in equation 14) for silt/loam, clay, and sand are quite distinct. If E_d can be measured for a given soil, equations such as this may allow for the estimation of E at a particular soil moisture content. Although here the relation has been derived between $(\frac{E}{E_d})$ and θ, ratio of other soil resistance variables can be considered in place of $(\frac{E}{E_d})$. The 'optimum moisture content' at which moisture vs. cohesion relation changes trend, in other words the moisture content at which the erosion resistance is maximum, appears to be in the range of 19%-26% soil moisture depending on the soil type, given that they are cured for at least 4 hours. This range was derived based on seven soil types including sandy, silty and clayey soils

as reported by 5 studies reviewed in this paper (Govers, 1991; Grissinger, 1966; Larinov et al., 2014; Nachtergaele and Poesen, 2002; Shainberg et al., 1996). However, this range may differ for other soil configurations depending on the types and fraction of clay minerals present, organic matter content, and other soil conditions. More confidence in the model structure and the magnitude of optimum moisture content may be established by collecting data from a large number of soil samples with different soil types and configurations.

Table 2.3. Parameters of equation 14 for each soil type, as derived in figure 2.5.

Soil type	Soil name	Regression coefficients		R^2	Reference
		σ	b		
			Silt/loam		
S1	10% Natural silt - Grenada silt loam	0.2838	12.287	0.853	Grissinger (1966)
S2	10% Illite - Grenada silt loam	0.0795	4.0714	0.985	Grissinger (1966)
S3	Caen silt loam with 8.5% sand, 76.2% silt and 15.3% clay	0.1948	9.4951	0.962	Govers et al. (1990)
S4	Loamy soil with 17% sand, 69% silt and 14% clay	0.0014	0.0709	0.999	Govers (1991)
S5	5% Ca montmorillonite - Grenada silt loam	0.1891	8.5869	0.989	Grissinger (1966)
S6	Heavy loamy Chernozem samples	2.8119	134.22	0.959	Larionov et al. (2014)
S7	Grenada silt loam with 20% clay, 74% silt, 6% fine sand	0.3075	11.732	0.984	Grissinger (1966)
S8	5% Illite - Grenada silt loam	0.0238	3.2816	0.939	Grissinger (1966)
			Clay		
C1	Kaolinite-sand mixture	0.0010	0.0902	0.958	Christinsen and Das (1973)
C2	Grundite clay	0.0002	0.0156	0.945	Christinsen and Das (1973)
C3	Grundite-sand mixture	0.0004	0.0361	0.908	Christinsen and Das (1973)
C4	Kaolinite clay	0.0004	0.0438	0.949	Christinsen and Das (1973)
			Sandy		
A1	Loamy sand soil with 87% sand, 4% silt, and 9% clay	-0.0002	0.0062	0.775	Parker et al. (1995)

6. Future research directions

Deriving robust quantitative relations that capture the influence of antecedent soil moisture on erosion resistance of soils, and methods (preferably resembling a nomograph) for easy parameterization of such relations, remain a high priority for fluvial geomorphology research. Based on the above review, several short-term and long-term future research needs can be identified.

Future short-term research need to be directed towards a better understanding of how antecedent moisture content in soils affect erosion resistance under rainfall events of different intensities and soil types. This should include experiments designed to understand the role of rain intermittency and duration. Much of the work, so far, has been conducted under controlled laboratory conditions involving a limited number of samples. Transferring small lab-scale experimental results to large-scale systems could face challenges associated with representativeness of the samples and transferability of derived relations. Field research in natural settings and laboratory experiments involving large undisturbed soil blocks can be useful in this regard, as it can provide a more comprehensive picture for realistic settings and thus potentially broaden the applicability of results.

As noted in this study, soil moisture's impact on soil's resistance to erosion is generally contradictory to its effects on runoff generation and consequent sediment erosion. For example, higher soil moisture generally increases the soil's erosion resistance, but leads to higher runoff. It is important to conduct research to understand how and when these countering factors overwhelm the other under different soil, environmental, and rainfall conditions.

One potential strategy to isolate the influence of moisture content on soil resistance to erosion is to study the sediment yield variations between events with identical runoff, and then

evaluating these relations over a range of runoff magnitudes. The derived relations using data from training-years may then be used in test-years to assess the improvement in explainability of sediment dynamics, when moisture's influence on soil resistance is explicitly accounted for. To limit the challenges posted by heterogeneity of soil types, initial explorations may focus on hillslopes or watersheds with homogeneous soil distribution. Follow-up studies may assess the applicability of these relations across different soils, and over larger settings with significant soil moisture heterogeneity arising from spatial variations in topography, soil types, and other physiographic attributes (Wilson et al., 2004).

Although factors such as type and percentage of clay minerals, clay particle orientation, curing/aging time, bulk density of the sample, organic matter content, soil type, and texture/particle size have been identified to have an influence on moisture vs. erosion resistance relation, no clear understanding exists as to how prominent this effect might be or how to quantitatively incorporate the influence of these factors. Data of sediment yield from diverse sources over the landscape, which can be aided by methods such as sediment fingerprinting (Smith and Blake, 2014), and from multiple, well-instrumented watersheds such as the critical zone networks (Anderson et al., 2008) may serve useful. Overall, the aforementioned proposed explorations will likely lead to improvement in the understanding and prediction of soil erosion resistance dynamics over large spatial and temporal scales, and will especially help capture the impacts of extreme events on sediment yield better as the system transition from dry to wet conditions.

In the long-term, in agreement with Bryan (2000) and Knapen et al. (2007), we propose that soil erosion and sediment prediction research needs to define a standardized erosion resistance parameter that can integrate dynamic controls such as soil moisture. In addition, as

discussed in the previous sections of this study, the resistance property being measured for quantification of this parameter should be standardized as well. Differences in measurement method and the resistance property across applications pose a major challenge for incorporating the dynamic influence of moisture on erosion resistance. Future research focused on evaluation of this dynamic resistance parameter and its ability to capture sediment yield dynamics, over a manifold of soil composition, hydroclimatic conditions, and moisture conditions, could allow for benchmarking and intercomparison with existing parameter representations.

7. Conclusion

In this study, we performed a comprehensive review of the influence of antecedent soil moisture content on erosion resistance of soils. The goals were to assess the influence of soil moisture on soil's erosion resistance, identify the various mechanisms in play, pinpoint the challenges associated with representing the influence of moisture on soil erosion resistance in sediment models, and finally to come up with a few recommendations towards developing a general parameterization that can be used in soil erosion and sediment models. We found that while several studies have highlighted a significant role of antecedent moisture content on soil erosion resistance, reported covariation of the two variables were very distinct depending on the antecedent wetness of the soil. Dry soils exhibited the lowest resistance to erosion, and thereby showed high erodibility, compared to their moist counterparts. This is mainly attributed to a range of factors including slaking caused by increase in the pressure and expansion of the entrapped air due to rapid wetting, microfissuration, lack of cohesional forces provided by soil moisture, increased continuity of soil air in pore spaces, restricted soil particle reorientation to a position with low energy and high cohesion, and lack of armoring provided by the runoff water

film. Soil's resistance to erosion generally increases with increasing moisture. However, after the moisture content exceeds a threshold, soil resistance was observed to decrease with further increasing soil moisture content, and soils become more susceptible to erosion. This optimum water content that yields the highest erosion resistance is highly dependent on soil type.

Soil erosion and sediment yield models, especially event-based and seasonal, should incorporate the effects of antecedent soil moisture content on soil loss prediction via not only runoff generation but also soil's resistance. The use of a single soil resistance value in this regard, say in form of a constant erodibility variable, may lead to considerable biases in trends and magnitudes of predicted erosion. Consideration of dynamic influence of initial soil moisture content will therefore result in more robust predictions. However, development of a unifying equation to predict erosion resistance based on dynamic sediment properties such as soil moisture remains challenging due to (i) disparate definitions of soil's resistance to erosion (e.g. erodibility, cohesion, shear stress, aggregate stability, etc.), and the differences in measurement methods, (ii) use of a single constant value for soil erosion resistance that does not allow to consider spatially and temporally dynamic soil properties and environmental conditions, (iii) lack of a comprehensive understanding and quantification of the factors on which the moisture-erosion resistance relationship depends on e.g. type and percentage of clay minerals, clay particle orientation, curing/aging time, bulk density, organic matter content, soil type and texture/particle size, and (iv) lack of understanding about the behavior of soil in natural undisturbed settings. Despite these challenges, synthesis of erstwhile studies point to latent opportunities towards developing a moisture-explicit erosion resistance relation arising from (i) the coherent trend in the relation between soil resistance to erosion vis-a-vis soil moisture reported in literature, (ii) equations developed by various studies to quantify the relationship, and (iii) observed trends in

watershed, continental and global scales that show dry, bare soil may lead to greater erosion during intense rainfall events, whereas initially moist soil produce less sediment. Data from previous studies indicate a quadratic relation between the logarithm of normalized soil resistance variable vs. soil saturation. Notably, parameters for such a relation were observed to be significantly different for silt/loam, clay, and sand. Thus a general parameter set for each of these soil types may be used. However, robust parametarization of moisture-driven soil resistance, still needs to be derived for each soil type/composition. Development of such a relation across soil types could be facilitated by standardization of the definition of soil resistance term and its measurement methodology. Irrespective of the functional form used to capture the moisture-erosion resistance relation, it is high time to start considering the influence of moisture on soil erosion resistance in sediment models, especially in light of climate change that is anticipated to affect soil moisture regimes and hence soil erosion trends.

Table 2.1. Summary of studies that found an increase in soil resistance to erosion with increasing moisture

Reference	**Indicator of erosion resistance**	**Test method**	**Soil type**	**Assumptions/conditions/dependencies**	**Key findings**
Allen et al. (1999)	Erodibility coefficient K	Submerged jet test	Alluvial soil with < 10% clay		For soils tested with < 10% clay, antecedent moisture content is important in determining soil erodibility and erodibility increases with decreasing moisture content.
Auerswald (1993)	Soil loss	Filed erosion experiment using a rainfall simulator with plot size 1.8 m by 4.7 m.	Loessial Dystric Eutrochrept top horizon (24% clay 61% silt, 4% very fine sand and 15% sand)	Rainfall over a period of 10 days, 1 h first run, and a 0.5 h second run after a break of 0.5 h. Average rain intensity 55 mm/h with a kinetic energy of 19 J/(m^2 mm).	81% of the variation in soil loss explained by only moisture and time since tillage. Increased stabilization of soil against erosion with increasing moisture between 10-31%, owing to reduced aggregate breakdown due to reduced slaking, and the development of a water mulch that reduced splash.

Bastos et al. (2002)	Erodibility by Inderbitzen test, shear stress represented by cohesion	Inderbitzen test, conventional and suction-controlled direct shear tests	B (lateritic) and C (saprolitic) horizons of four residual soils found in Southern Brazil		Soils where total cohesion decreased significantly with rapid moisture increase (due to the action of superficial flow) were those more susceptible to erosion. Rapid wetting causes a significant decrease in soil shear strength related to pore pressure, the destruction of bonding between soil particles/aggregates triggered by the force of erosion flow, and slaking.
Cernuda et al. (1954)	Aggregate stability	Slaking and resistance to falling water drops	15 types of soils from Puerto Rico		Low tensions created by capillary water films can increase the stability of soil aggregates. Slaking and the ease of destruction was greatest for dry soil.
Govers and Loch (1993)	Sediment concentration	Field erosion experiment	Irving clay soil (66% clay 18% silt and 12% fine sand) and Moola clay soil (44% clay 18% silt 32% fine sand and 6% coarse sand) of Queensland	Sites with wet soils were kept for 4-5 days after wetting. Discharges of 0.15, 0.4, and 1.2 l/s.	Erosion resistance was greater for soils with initially high water content than air dried soil due to the development of inter-aggregate bonds and disruption of the soil aggregates by slaking and microfissuration during rapid wetting of initially dry soil.
Govers et al. (1990)	Sediment concentration and soil loss.	Flume study on a 20 m long flume with a 0.07 slope using a rainfall simulator	Caen silt loam with 8.5% sand, 76.2% silt and 15.3% clay.	For wet runs, moisture was regulated for at least 24 h before the experiment. Experiment duration was 1 h 30 m and rainfall intensity was 100mm/h.	Runoff erosion by high- intensity events of medium duration may lead to more erosion and sediment when the soil is initially dry, regardless of their higher infiltration capacity. Micro-cracking caused by differential expansion of the swelling clay components of soil contribute to soil shear strength reduction.
Govers (1991)	Sediment concentration	Flume experiment	Loamy soil (17% sand, 69% silt and 14% clay)		Variations in the initial soil moisture content is an important factor in explaining spatial and temporal variations in sediment yield. The relationship between moisture and soil resistance can be expressed by a simple parabolic equation. Erosion resistance increases with increasing initial moisture content.
Grissinger (1966)	Rate of erosion	Flume test	Grenada silt loam mixtures with various clay minerals	Erosion resistance-moisture relationship depends on the type and amount of clay minerals in the mixture, clay mineral orientation, bulk density, aging time after pre-wetting, water temperature, particle size.	Erodibility decreased with increased antecedent water up to 25% antecedent water content.
Kemper and Rosenau (1984)	Cohesion measured by aggregate stability and moduli of rupture	Wet sieving (aggregate stability) and soil cylinders (moduli of rupture)	Portneuf silty loam from Idaho (wind deposited over 60% silt and < 20% clay) and Billings clay soil from		The rate of cohesion increase after disruption was slower in an air-dry soil than a moist soil. Slower wetting allows more particles to remain coherent in the aggregates, due to reduced slaking. A substantial portion of the cohesion in Portneuf soil is

			Colorado (alluvial)		created by water phase tension and surface tension related to the air-water interface.
Larionov et al. (2014)	Erodibility calculated as $k = \frac{W}{\rho_0 u^3}$ Where k is soil erodibility, W is erosion rate, ρ_0 is the water density, u is jet velocity.	Vertical jet test	Heavy loamy Chernozem soil samples	Soil samples of density 1.4 g/cm^3, at a constant jet velocity of 1.42–1.43 m/s. After wetting, the samples were exposed in weighing cups for 10–12 h.	Maximum erosion stability was achieved at 22% initial water content, due to gaining the maximum cohesion between aggregates. The erosion rate increases with both increasing and decreasing initial water content. Water acts as a lubricant that causes uniform distribution of aggregates in soil, promoting cohesion between aggregates.
Larionov et al. (2018)	Erosion rate and erodibility calculated as Larionov et al. (2014)	Flume experiment	Light-clay leached chernozem (Luvic Cherno-zem (Pachic))	Water temperature of 18–20°C, a mean flow velocity of 0.98–1.03 m/s, and a flow depth of 1 cm.	Minimum erodibility detected at a moisture content of 30%. Under drying, the soil begins to crack, inter-aggregate bonds diminish, and the erodibility increases for soil water content from 30 to 9%.
Le Bissonnais and Singer (1992)	Sediment production rate	Plot experiment with simulated rainfall	Capay silty clay loam (fine, montmorillonitic , thermic Typic Chromoxerert) and Solano silt loam (fine-loamy, mixed, thermic Typic Natrixeralf)	Soil was packed to a depth of 10 cm over a 10 cm layer of sand at a bulk density of 1.2 mg/m^3. Slope 9%. rainfall rate 40 mm/h.	Higher initial soil water content decreases aggregate breakdown and crust formation, thereby reducing erosion due to decreased runoff and detachment. Erosion remained considerably lower in all the three rainfall events in pre-wetted soil than air dried soil.
Le Bissonnais et al. (1989)	Aggregate breakdown	Plot experiment with simulated rainfall	Orthic luvisol (a cultivated silty soil) from France (19.6 clay, 72.6 silt, 7.8 sand).	Aggregates were pre-wetted under vacuum, so no air-trapping (and hence slaking) in pre-wetted aggregates.	Aggregate breakdown is determined by the way of wetting and initial soil water content. Air-dry aggregates experience micro-cracking during wetting, whereas pre-wetted aggregates do not and hence aggregate breakdown is very slow.
Lim (2006)	Shear stress (critical and threshold), Erosion rate, Slaking intesity (slaking slope)/slaking rate	Rotating cylinder test, the hole erosion test, and the slaking test	Non-dispersive soils consisting of 4 natural clays and 3 commercial clay mixtures (30%, 50% and 70% kaolin mixed with fine sand)		The degree of saturation is important determining the erosion behavior of non-dispersive unsaturated soils. The intensity of slaking increased 3 to 5 times for a 30% reduction in saturation. Lower erodibility with increasing saturation. A little change in the erosion rate for clay soils of >90% saturation.
Lyles et al. (1974)	Soil detachment by weight	Raintower wind tunnel	Silty clay loam (sand 8.8%, silt 60%, clay 31.2%)	Bulk density of 1.45 g/cm^3, test clods 12.7 to 38.0 mm in diameter, mulch-covered soil clods exposed for 45 min to wind-driven rainfall with an intensity of 1.76 in/hr.	Substantially less soil was removed from field-moist clods than from air-dry clods by raindrops due to slower absorption of additional water owing to the initial degree of saturation. Field-moist aggregates lose their resistance to breakdown well in advance to becoming air-dry.
Nachtergae le and Poesen (2002)	Soil detachment rate	Flume experiment	Loess-derived soils in Belgium		Spatial and temporal variability in soil erosion is affected by soil moisture. From the range of gravimetric soil moisture contents, spatial and temporal variations in detachability over an area can be estimated using the relationships

					developed. Erodibility decreases with increasing soil moisture.
Panabokke and Quirk (1957)	Water stability of soil aggregates	Wet sieving and shaking end-over-end in a cylinder of water	Soil from South Australia Urrbrae loam (red brown earth) A and B horizons – cultivated and uncultivated Riverina clay (Grey soil of heavy texture) Black clay (Hydromorphic black earth)		The aggregate stability had a major effect from the tension of the soil water. A decrease in stability with decreasing water content, was associated with rapid wetting of the aggregates and the diminishing of cohesion. In clay soils, slaking caused by differential swelling is identified as responsible for the breakdown of aggregates.
Parker et al. (1995)	Sediment concentration	Flume test	A silty sand soil composed of 87% sand, 4% silt, and 9% clay	Bulk density of 1.52 Mg/m^3 flow rate of 0.38 $m^3/(m\ min)$, flow depth 15 mm, flume slope 0.005 m/m.	Erodibility increased with decreasing initial water content between moisture contents of 0.200 and 0.125 kg/kg, due to continuity of soil air in pore spaces with decreasing soil water content triggering more erosion.
Poesen et al. (1999)	Sediment concentration	Flume experiment	Silt loam from central Belgium containing 2% sand, 81% silt, 17% clay and 1.3% OM		Concentrated flow erosion rates were 20 - 65% less on initially wet topsoils compared to initially air-dry topsoils, depending on rock fragment cover. Rock fragment cover is less efficient in decreasing erosion rates when it is air-dry at the beginning than when it is moist. Dry soils are more detachable due to slaking and microcracking.
Shainberg et al. (1996)	Rill erodibility	Small hydraulic flume	Grumusol clay soil (Typic Chromoxerert)	0.5-m-long, 0.046-m-wide, and 0.12-m- deep flume placed at a 5% slope, under flow rates of 0.04, 0.08, 0.12, 0.16, 0.2, 0.24, 0.28, and 0.32 L/min.	Rill erodibility decreases with increasing water content. No cohesive force development when the soil is air-dry. The rate of cohesive force development increases with water content above a critical water content. The formed forces are sufficiently strong to resist rill erodibility. The critical water content depends on soil type. The effect of soil moisture content greater than a critical level on rill erodibility was less pronounced after 24 h of aging.

Table 2.2. Summary of studies that found a decrease (or no significant change) in soil erosion resistance with increasing moisture

Reference	Indicator of erosion resistance	Test method	Soil type	Assumptions/conditions/dependencies	Key findings
Allen et al. (1999)	Erodibility coefficient K	Submerged jet test	Alluvial soils with >10% clay (loamy and clay soils).		There is no significant relationship between moisture content and erodibility in loamy or clay soils. When clay content is > 10% in a soil, natural cohesive properties of clay becomes dominant and hinder the effect of moisture on soil cohesion.
Bastos et al. (2002)	Erodibility by Inderbitzen test, shear stress represented by cohesion	Inderbitzen test, conventional and suction-controlled direct shear tests	B (lateritic) and C (saprolitic) horizons of four residual soils found in Southern Brazil		Hydraulic and surface tension forces created by water films on the stability of soil aggregates is lacking in completely saturated soils.
Cernuda et al. (1954)	Aggregate stability	Slaking and resistance to falling water drops	15 types of soils from Puerto Rico		Slaking was not completely destructive when fine pores were limited/absent. Completely saturated soil lacks the stability associated with hydraulic and surface tension forces.
Christinsen and Das (1973)	Hydraulic tractive force (shear stress)	Maintaining a steady water flow through clay linings inside a brass tube	kaolinite and grundite as basic clay minerals and Ottawa sand as an additive	Water temperature 13-14°C, Shear stress of the flow 0.00496-0.00571 gm/cm^2	A sharp decrease in erosion with increasing compaction moisture content, with the exception when soil is saturated. Moisture influences a decrease in surface roughness that reduces erosion.
Coote et al. (1988)	Aggregate stabilty, shear strength	Water-stable aggregates by wet sieving, vane shear strength using a hand-held torvane.	Guelph Sandy Loam, Colwood Silt Loam, Fox Silt Loam, Haldimand Silt Clay, Fox Sand	Seasonal variation and freeze thaw conditions	Aggregate stability and shear strength are negatively correlated with soil water content from 16.5 to 47.5%.
Govers (1991)	Sediment concentration	Flume experiment	Loamy soil (17% sand, 69% silt and 14% clay)		For soil moisture contents exceeding 20%, the erosion resistance was not dependent on moisture.
Grissinger (1966)	Rate of erosion	Flume test	Grenada silt loam mixtures with various clay minerals	Erosion resistance-moisture relationship depends on the type and amount of clay minerals in the mixture, clay mineral orientation, bulk density, aging time after pre-wetting, water temperature, particle size.	Erodibility increased with increased antecedent water for unoriented coarse kaolinitic-Greneda mixture.

Hanson and Robinson (1993)	Erodibility using a jet index	Submerged jet test		Water supply under a constant head of 0.91 m with a nozzle velocity of 4.2 m/s.	The erosion resistance increases as the compaction moisture content increases. Resistance decreased for the saturated sample.
Kemper and Rosenau (1984)	Cohesion measured by aggregate stability and moduli of rupture	Wet sieving (aggregate stability) and soil cylinders (moduli of rupture)	Portneuf silty loam from Idaho (wind deposited over 60% silt and < 20% clay) and Billings clay soil from Colorado (alluvial)		Disintegration of the aggregates with rapid wetting allows crust formation with greater cohesion, when drying. The more cohesive Billings soil had higher cohesion at low moisture, due to the influence of other factors. If air pressure is less than the pressure of the soil water, moisture does not cause cohesion in soils.
Le Bissonnais and Singer (1992)	Sediment production rate	Plot experiment with simulated rainfall	Capay silty clay loam (fine, montmorillonitic, thermic Typic Chromoxerert) and Solano silt loam (fine-loamy, mixed, thermic Typic Natrixeralf)	Soil packed to a depth of 10 cm over a 10 cm layer of sand at a bulk density of 1.2 mg/m^3. Slope 9%. Rainfall rate 40 mm/h.	Soil detachability decreased for the initially air-dried soil, during the three consecutive rain falls due to crust formation.
Le Bissonnais et al. (1989)	Aggregate breakdown	Plot experiment with simulated rainfall	Orthic luvisol (a cultivated silty soil) from France (19.6 clay, 72.6 silt, 7.8 sand).	Aggregates were pre-wetted under vacuum, so no air-trapping (and hence slaking) in pre-wetted aggregates.	Aggregate break down and seal formation due to rapid wetting is faster in an air-dry soils than prewetted soils.
Lim (2006)	Shear stress (critical and threshold), Erosion rate, Slaking intesity (slaking slope)/slaking rate	Rotating cylinder test, the hole erosion test, and the slaking test	Dispersive clays consisting of 4 natural clays and 2 commercial clay mixtures (30% and 50% bentonite mixed with fine sand)		The variations in saturation had negligible influence on the erosion behavior of dispersive soils.
Luk and Hamilton (1986)	Soil loss, Soil shear strength	Field plot experiment with artificial rainfall using a hand-held picton torvane (field) and mechanized torvane (lab)	Two Gray-Brown Luvisol soils in southern Ontario, the Font loam and the Guelph silt loam	Artificial rainfall at 50 mm/h. Experimental plots of 7.8 m^2	Soil loss is mainly associated with moisture content. If the full range of soil moisture is considered, soil loss may vary by as much as 800 times. Soil loss increased and aggregate stability decreased with soil moisture.
Panabokke and Quirk (1957)	Water stability of soil aggregates	Wet sieving and shaking end-over-end in a cylinder of water	Soil from South Australia Urrbrae loam (red brown earth) A and B horizons – cultivated and uncultivated Riverina clay (Grey soil of heavy texture)		For soils drier than pF 5.5, had higher aggregation due to entrapped air preventing water from entering pore spaces.

			Black clay (Hydromorphic black earth)		
Shainberg et al. (1996)	Rill erodibility	Small hydraulic flume	A loamy loess (Calcic Haploxeralf), and a loamy sand hamra (Typic Rhodoxeralf)	0.5-m-long, 0.046-m-wide, and 0.12-m- deep flume placed at a 5% slope, under flow rates of 0.04, 0.08, 0.12, 0.16, 0.2, 0.24, 0.28, and 0.32 L/min	In the loamy sand hamra, an increase in water content increases rill erodibility of the soil. Negligible influence of water content on rill erodibility in the loamy loess. erodibility was less pronounced after 24 h of aging.
Wan and Fell (2004)	Rate of erosion, critical shear stress	Slot erosion test and the hole erosion test	13 soil types		The erosion resistance of a soil is strongly determined by the saturation at soil compaction. Saturated soils do not have an influence on erosion resistance.

8. References for chapter 2

Aksoy, H., & Kavvas, M. L. (2005). A review of hillslope and watershed scale erosion and sediment transport models. Catena, 64(2-3), 247-271.

Alewell, C., Borrelli, P., Meusburger, K. and Panagos, P. (2019). Using the USLE: Chances, challenges and limitations of soil erosion modelling. International soil and water conservation research, 7(3), pp.203-225.

Allen, P.M., Arnold, J. and Jakubowski, E. (1999). Prediction of stream channel erosion potential. Environmental & Engineering Geoscience, (3), pp.339-351.

Anderson, S.P., Bales, R.C. and Duffy, C.J. (2008). Critical Zone Observatories: Building a network to advance interdisciplinary study of Earth surface processes. *Mineralogical Magazine*, *72*(1), pp.7-10.

Ansari, S. A., Kothyari, U. C., & Ranga Raju, K. G. (2003). Influence of cohesion on scour under submerged circular vertical jets. Journal of Hydraulic Engineering, 129(12), 1014–1019. https://doi.org/10.1061/(ASCE)0733-9429(2003)129:12(1014)

Arnold, J.G., Moriasi, D.N., Gassman, P.W., Abbaspour, K.C., White, M.J., Srinivasan, R., Santhi, C., Harmel, R.D., Van Griensven, A., Van Liew, M.W. and Kannan, N. (2012). SWAT: Model use, calibration, and validation. Transactions of the ASABE, 55(4), pp.1491-1508.

Auerswald, K. (1993). Influence of initial moisture and time since tillage on surface structure breakdown and erosion of s loessial soil. Catena Supplement, 24, pp.93-93.

Bastos, C.A.B., The relationship between erodibility and geomechanical properties of unsaturated resdual soils, in Jucá, J.F.T., De Campos, T.M. and Marinho, F.A. eds. (2002). Unsaturated Soils: Proceedings of the Third International Conference on Unsaturated Soils, UNSAT 2002, 10-13 March 2002, Recife, Brazil (Vol. 2). CRC Press.

Battista, G., Molnar, P. and Burlando, P., 2020. Modelling impacts of spatially variable erosion drivers on suspended sediment dynamics. Earth Surface Dynamics, 8(3), pp.619-635.

Beasley, D.B., Huggins, L.F. and Monke, A. (1980). ANSWERS: A model for watershed planning. Transactions of the ASAE, 23(4), pp.938-0944.

Bhuyan, S. J., Kalita, P. K., Janssen, K. A., & Barnes, P. L. (2002). Soil loss predictions with three erosion simulation models. Environmental Modelling & Software, 17(2), 135-144.

Briaud, J., Ting, F. C. K., Chen, H. C., Cao, Y., Han, S. W., & Kwak, K. W. (2001). EROSION FUNCTION APPARATUS FOR SCOUR RATE PREDICTIONS. 5(February), 105–113.

Bryan, R.B. (2000). Soil erodibility and processes of water erosion on hillslope. Geomorphology, 32(3-4), pp.385-415.

Carroll, C., Rose, C.W., and Crawford, S.J. (1986). GUESS-Theory Manual. Report for National Soil Conservation Project, School of Environemental Studies, Griffith Univ., Brisbane.

Cerda, A. (2009). Fire effects on soils and restoration strategies (Vol. 5). CRC Press.

Cernuda, C.F., Smith, R.M. and Vicente-Chandler, J. (1954). Influence of initial soil moisture condition on resistance of macroaggregates to slaking and to water-drop impact. Soil Science, 77(1), pp.19-28.

Chaer, G., Fernandes, M., Myrold, D. and Bottomley, P. (2009). Comparative resistance and resilience of soil microbial communities and enzyme activities in adjacent native forest and agricultural soils. *Microbial ecology*, *58*(2), pp.414-424.

Chen, X., Kumar, M. and McGlynn, B.L. (2015). Variations in streamflow response to large hurricane-season storms in a southeastern US watershed. Journal of Hydrometeorology, 16(1), pp.55-69.

Christensen, R.W., Das, B. M. (1973). Hydraulic erosion of remolded cohesive soils. Highway Research Board Special Report, (135).

Collins, D.B.G. and Bras, R.L. (2008). Climatic control of sediment yield in dry lands following climate and land cover change. Water Resources Research, 44(10).

Coote, D.R., Malcolm-McGovern, C.A., Wall, G.J., Dickinson, W.T. and Rudra, R.P. (1988). Seasonal variation of erodibility indices based on shear strength and aggregate stability in some Ontario soils. Canadian journal of soil science, 68(2), pp.405-416.

Dangler, E.W. and El-Swaify, S.A. (1976). Erosion of selected Hawaii soils by simulated rainfall. Soil Science Society of America Journal, 40(5), pp.769-773.

De Vente, J., Poesen, J., Verstraeten, G., Govers, G., Vanmaercke, M., Van Rompaey, A., Arabkhedri, M. and Boix-Fayos, C. (2013). Predicting soil erosion and sediment yield at regional scales: where do we stand?. Earth-Science Reviews, 127, pp.16-29.

FAO, (2019). Soil Erodibility. Retrieved from http://www.fao.org/3/t1765e/t1765e0f.htm (11/28/2019).

Fell, R., Hanson, G. J., Herrier, G., Marot, D., & Wahl, T. (2017). Relationship between the erosion properties of soils and other parameters.

Flanagan, D.C., Foster, G.R. and Moldenhauer, W.C. (1988). Storm pattern effect on infiltration, runoff, and erosion. Transactions of the ASAE, 31(2), pp.414-0420.

Gilley, J.E., Elliot, W.J., Laflen, J.M. and Simanton, J.R. (1993). Critical shear stress and critical flow rates for initiation of rilling. Journal of Hydrology, 142(1-4), pp.251-271.

Goudie, A. (2013). Encyclopedia of geomorphology. Routledge.

Govers, G., & Loch, R. J. (1993). Effects of initial water content and soil mechanical strength on the runoff erosion resistance of clay soils. Australian Journal of Soil Research, 31(5), 549–566. https://doi.org/10.1071/SR9930549.

Govers, G. (1991). Time-dependency of runoff velocity and erosion the effect of the initial soil moisture profile. Earth Surface Processes and Landforms, 16(8), pp.713-729.

Govers, G., Everaert, W., Poesen, J., Rauws, G., De Ploey, J., & Lautridou, J. P. (1990). A long flume study of the dynamic factors affecting the resistance of a loamy soil to concentrated flow erosion. Earth Surface Processes and Landforms, 15(4), 313–328. https://doi.org/10.1002/esp.3290150403

Grabowski, R. C., Droppo, I. G., & Wharton, G. (2011). Erodibility of cohesive sediment: The importance of sediment properties. Earth-Science Reviews, 105(3–4), 101–120. https://doi.org/10.1016/j.earscirev.2011.01.008

Grissinger, E. H. (1966). Resistance of selected clay systems to erosion by water. Water Resources Research, 2(1), 131–138. https://doi.org/10.1029/WR002i001p00131

Haines, W.B. (1925). Studies in the physical properties of soils: II. A note on the cohesion developed by capillary forces in an ideal soil. The Journal of Agricultural Science, 15(4), pp.529-535.

Hairsine, P.B. and Rose, C.W. (1992). Modeling water erosion due to overland flow using physical principles: 1. Sheet flow. Water resources research, 28(1), pp.237-243.

Hanson, G.J. and Robinson, K.M. (1993). The influence of soil moisture and compaction on spillway erosion. Transactions of the ASAE, 36(5), pp.1349-1352.

Holz, D.J., Williard, K.W., Edwards, P.J. and Schoonover, J.E. (2015). Soil erosion in humid regions: a review. Journal of Contemporary Water Research & Education, 154(1), pp.48-59.

Hosoyamada, K. (1986). The effects of rainfall and soil properties on farmland conservation. Journal of irrigation engineering and rural planning, 1986(9), pp.5-14.

Istanbulluoglu, E. and Bras, R.L. (2006). On the dynamics of soil moisture, vegetation, and erosion: Implications of climate variability and change. Water Resources Research, 42(6).

Jain, R.K. and Kothyari, U.C. (2009). Cohesion influences on erosion and bed load transport. Water resources research, 45(6).

Katul, G.G., Porporato, A., Daly, E., Oishi, A.C., Kim, H.S., Stoy, P.C., Juang, J.Y. and Siqueira, M.B. (2007). On the spectrum of soil moisture from hourly to interannual scales. *Water Resources Research*, *43*(5).

Kemper, W. D., & Rosenau, R. C. (1984). Soil Cohesion as Affected by Time and Water Content. Soil Science Society of America Journal, 48(5), 1001–1006. https://doi.org/10.2136/sssaj1988.03615995005200030031x

Kemper, W. D., Trout, T. J., Brown, M. J., & Rosenau, R. C. (1985). Furrow Erosion and Water and Soil Management. Transactions of the American Society of Agricultural Engineers, 28(5), 1564–1572. https://doi.org/10.13031/2013.32478

Kim, J., Dwelle, M. C., Kampf, S. K., Fatichi, S., & Ivanov, V. Y. (2016). On the non-uniqueness of the hydro-geomorphic responses in a zero-order catchment with respect to soil moisture. *Advances in Water Resources*, *92*, 73-89.

Knapen, A., Poesen, J., Govers, G., Gyssels, G., & Nachtergaele, J. (2007). Resistance of soils to concentrated flow erosion: A review. Earth-Science Reviews, 80(1–2), 75–109. https://doi.org/10.1016/j.earscirev.2006.08.001.

Laflen, J.M., Elliot, W.J., Simanton, J.R., Holzhey, C.S. and Kohl, K.D. (1991). WEPP: Soil erodibility experiments for rangeland and cropland soils. Journal of Soil and Water Conservation, 46(1), pp.39-44.

Larionov, G. A., Bushueva, O. G., Dobrovolskaya, N. G., Kiryukhina, Z. P., Krasnov, S. F., & Litvin, L. F. (2014). Effect of the water temperature and soil moisture on the erodibility of chernozem samples: A model experiment. Eurasian Soil Science, 47(7), 734–739. https://doi.org/10.1134/S1064229314070096

Larionov, G.A., Bushueva, O.G., Gorobets, A.V., Dobrovolskaya, N.G., Kiryukhina, Z.P., Krasnov, S.F., Litvin, L.F., Maksimova, I.A. and Sudnitsyn, I.I. (2018). Experimental study of factors affecting soil erodibility. Eurasian soil science, 51(3), pp.336-344.

Le Bissonnais, Y. (1996). Aggregate stability and assessment of soil crustability and erodibility: I. Theory and methodology. European Journal of Soil Science, 47(4), 425–437. https://doi.org/10.1111/ejss.4_12311.

Le Bissonnais, Y., Bruand, A. and Jamagne, M. (1989). Laboratory experimental study of soil crusting: Relation between aggregate breakdown mechanisms and crust structure. Catena, 16(4-5), pp.377-392.

Le Bissonnais, Y., Renaux, B., & Delouche, H. (1995). Interactions between soil properties and moisture content in crust formation, runoff and interrill erosion from tilled loess

soils. *Catena*, *25*(1-4), 33-46.Le Bissonnais, Y.L. and Singer, M.J., 1992. Crusting, runoff, and erosion response to soil water content and successive rainfalls. Soil Science Society of America Journal, 56(6), pp.1898-1903.

Legates, D.R., Mahmood, R., Levia, D.F., DeLiberty, T.L., Quiring, S.M., Houser, C. and Nelson, F.E. (2011). Soil moisture: A central and unifying theme in physical geography. *Progress in Physical Geography*, *35*(1), pp.65-86.Lim, S. S., 2006. Experimental investigation of erosion in variably saturated clay soils. PhD Thesis, University of New South Wales.

Luk, S.H. and Hamilton, H. (1986). Experimental effects of antecedent moisture and soil strength on rainwash erosion of two luvisols, Ontario. Geoderma, 37(1), pp.29-43.

Lyle, W.M. and Smerdon, E.T. (1965). Relation of compaction and other soil properties to erosion resistance of soils. Transactions of the ASAE, 8(3), pp.419-0422.

Lyles, L., Dickerson, J. D., & Schmeidler, N. F. (1974). Soil Detachment From Clods By Rainfall: Effects of Wind, Mulch Cover, and Initial Soil Moisture. Transactions of the American Society of Agricultural Engineers, 17(4), 697–700.

Mamo, M. and Bubenzer, G.D. (2001). Detachment rate, soil erodibility, and soil strength as influenced by living plant roots part II: Field study. Transactions of the ASAE, 44(5), p.1175.

Merritt, W. S., Letcher, R. A., & Jakeman, A. J. (2003). A review of erosion and sediment transport models. Environmental Modelling & Software, 18(8-9), 761-799.

Mutchler, C.K. and Carter, C.E. (1983). Soil erodibility variation during the year. Transactions of the ASAE, 26(4), pp.1102-1104.

Nachtergaele, J. and Poesen, J. (2002). Spatial and temporal variations in resistance of loess-derived soils to ephemeral gully erosion. European Journal of Soil Science, 53(3), pp.449-463.

Nearing, M.A. and West, L.T. (1988). Soil strength indices as indicators of consolidation. Transactions of the ASAE, 31(2), pp.471-0476.

Nearing, M.A., West, L.T. and Brown, L.C. (1988). A consolidation model for estimating changes in rill erodibility. Transactions of the ASAE, 31(3), pp.696-0700.

Paaswell, R.E. (1973). Causes and mechanisms of cohesive soil erosion: The state of the art. Special report, 135, pp.52-74.

Panabokke, C.R. and Quirk, J.P. (1957). Effect of initial water content on stability of soil aggregates in water. Soil Science, 83(3), pp.185-196.

Pandey, A., Himanshu, S.K., Mishra, S.K. and Singh, V.P. (2016). Physically based soil erosion and sediment yield models revisited. Catena, 147, pp.595-620.

Papanicolaou, A. T. N., Elhakeem, M., Krallis, G., Prakash, S., & Edinger, J. (2008). Sediment transport modeling review—current and future developments. Journal of hydraulic engineering, 134(1), 1-14.

Park, C.H., Li, X.R., Jia, R.L. and Hur, J.S. (2017). Combined application of cyanobacteria with soil fixing chemicals for rapid induction of biological soil crust formation. *Arid Land Research and Management*, *31*(1), pp.81-93.

Parker, D. B., Michel, T. G., & Smith, J. L. (1995). Compaction and water velocity effects on soil erosion in shallow flow. Journal of Irrigation and Drainage Engineering, 121(2), 170–178. https://doi.org/10.1061/(ASCE)0733-9437(1995)121:2(170)

Partheniades, E. (2007). Engineering Properties and Hydraulic Behavior of Cohesive Sediments. CRC, Boca Raton. 338pp.

Pilgrim, D.H., Chapman, T.G. and Doran, D.G. (1988). Problems of rainfall-runoff modelling in arid and semiarid regions. Hydrological Sciences Journal, 33(4), pp.379-400.

Poesen, J., De Luna, E., Franca, A., Nachtergaele, J. and Govers, G. (1999). Concentrated flow erosion rates as affected by rock fragment cover and initial soil moisture content. catena, 36(4), pp.315-329.

Preetha, P.P. and Al-Hamdan, A.Z. (2019). Multi-level pedotransfer modification functions of the USLE-K factor for annual soil erodibility estimation of mixed landscapes. Modeling Earth Systems and Environment, 5(3), pp.767-779.

Ran, Q., Su, D., Li, P. and He, Z. (2012). Experimental study of the impact of rainfall characteristics on runoff generation and soil erosion. Journal of Hydrology, 424, pp.99-111.

Rauws, G. and Auzet, A.V. (1989). Laboratory experiments on the effects of simulated tractor wheelings on linear soil erosion. Soil and Tillage Research, 13(1), pp.75-81.

Renard, K.G. (1997). Predicting soil erosion by water: a guide to conservation planning with the Revised Universal Soil Loss Equation (RUSLE). United States Government Printing.

Rosenbaum, U., Bogena, H.R., Herbst, M., Huisman, J.A., Peterson, T.J., Weuthen, A., Western, A.W. and Vereecken, H. (2012). Seasonal and event dynamics of spatial soil moisture patterns at the small catchment scale. *Water Resources Research*, *48*(10).

Shainberg, I., Goldstein, D. and Levy, G.J. (1996). Rill erosion dependence on soil water content, aging, and temperature. Soil Science Society of America Journal, 60(3), pp.916-922.

Shiel, R.S., Adey, M.A. and Lodder, M. (1988). The effect of successive wet/dry cycles on aggregate size distribution in a clay texture soil. Journal of Soil Science, 39(1), pp.71-80.

Smith, H.G. and Blake, W.H. (2014). Sediment fingerprinting in agricultural catchments: a critical re-examination of source discrimination and data corrections. *Geomorphology*, *204*, pp.177-191.

Sun, D., Yang, H., Guan, D., Yang, M., Wu, J., Yuan, F., Jin, C., Wang, A. and Zhang, Y. (2018). The effects of land use change on soil infiltration capacity in China: A meta-analysis. Science of the Total Environment, 626, pp.1394-1401.

Utomo, W.H. and Dexter, A.R. (1982). Changes in soil aggregate water stability induced by wetting and drying cycles in non-saturated soil. Journal of Soil Science, 33(4), pp.623-637.

Wan, C.F. and Fell, R. (2004). Investigation of rate of erosion of soils in embankment dams. Journal of geotechnical and geoenvironmental engineering, 130(4), pp.373-380.

Wei, L., Zhang, B. and Wang, M. (2007). Effects of antecedent soil moisture on runoff and soil erosion in alley cropping systems. Agricultural water management, 94(1-3), pp.54-62.

Williams, A.J., Pagliai, M. and Stoops, G. (2018). Physical and biological surface crusts and seals. In *Interpretation of Micromorphological Features of Soils and Regoliths* (pp. 539-574). Elsevier.

Wilson, D.J., Western, A.W. and Grayson, R.B. (2004). Identifying and quantifying sources of variability in temporal and spatial soil moisture observations. *Water Resources Research*, *40*(2).

Wischmeier, W. H., Johnson, C. B., and Cross, B. V. (1971). A Soil Erodibility Nomograph for Farmland and Construction Sites. Jour. Soils and Water Cons., Vol. 26, pp. 189-193.

Wischmeier, W.H. and Smith, D.D. (1978). Predicting rainfall erosion losses: a guide to conservation planning (No. 537). Department of Agriculture, Science and Education Administration.

Yokoi, H. (1968). Relationship between soil cohesion and shear strength. Soil Science and Plant Nutrition, 14(3), pp.89-93.

Zi, T., Kumar, M., & Albertson, J. (2019). Intercomparing varied erosion, deposition and transport process representations for simulating sediment yield. Scientific reports, 9(1), 1-13.

Zi, T., Kumar, M., Kiely, G., Lewis, C. and Albertson, J. (2016). Simulating the spatio-temporal dynamics of soil erosion, deposition, and yield using a coupled sediment dynamics and 3D distributed hydrologic model. Environmental Modelling & Software, 83, pp.310-325

CHAPTER 3

MODELING AND ANALYSIS OF SEDIMENT TRAPPING EFFICIENCY OF LARGE DAMS USING REMOTE SENSING

Abstract

Quantifying the role of sediment trapping by dams is important due to its control on fluvial and coastal geomorphology, aquatic ecology, water quality, and human water uses. Sediment trapping behind dams is a major source of bias in large-scale hydro-geomorphic models, hindering robust analyses of anthropogenic influences on sediment fluxes in freshwater and coastal systems. This study focuses on developing a new reservoir trapping efficiency (*Te*) parameter to account for the impacts of dams in hydrological models. This goal was achieved by harnessing a novel remote sensing data product which offers high-resolution and spatially continuous maps of suspended sediment concentration across the Contiguous United States (CONUS). Validation of remote sensing-derived surface sediment fluxes against USGS depth-averaged sediment fluxes showed that this remote sensing dataset can be used to calculate *Te* with high accuracy ($R^2 = 0.98$). *Te* calculated for 222 dams across the CONUS, using incoming and outgoing sediment fluxes from their reservoirs, range from 0.13% to 98.3% with a mean of 45.8%. Contrary to the previous understanding that large reservoirs have larger *Te*, remote sensing data shows that large reservoirs can have a wide range of *Te* values. A suite of 22 explanatory variables were used to develop an empirical *Te* model. The strongest model predicts *Te* using four variables: incoming sediment flux, outgoing water discharge, reservoir length, and

reservoir storage. A global model was also developed using explanatory variables obtained from a global dam database.

1. Introduction

The construction of dams and impoundments for hydropower generation, flood control, irrigation, and water supply is among the greatest stressors to the connectivity and functionality of world's rivers (Grill et al., 2019; Verstraeten and Poesen, 2000; Vörösmarty et al., 2003; Zarfl et al., 2015). Currently, ~58,000 large dams (heights greater than 15 m) exist in the world with an additional ~3,700 dams that are either planned or under construction (Best and Darby, 2020; Mulligan et al., 2020). Apart from retaining a large amount of sediment, dams alter downstream flow regimes affecting sediment carrying capacities which can increase bank erosion and riverbed incision driven by sediment starvation (Best, 2019; Kondolf et al., 2014b; Schmidt and Wilcock, 2008; Williams and Wolman, 1984). These alterations also lead to coarsening of the substrate, changes in channel planform, and reductions in sediment-associated nutrients in downstream areas which could result in collapsed ecosystem functioning and impacts on the fisheries industry (Brandt, 2000; Syvitski, 2003; Wohl and Rathburn, 2003). Construction of dams without assessing their potential consequences has led to degraded floodplain and coastal environments worldwide (Latrubesse et al., 2017). In addition, reservoir sedimentation which affects the utility and sustainability of reservoirs, is mainly governed by the trapping efficiency of the dam impoundment (Jothiprakash and Vaibhav, 2008).

Dams have caused a major reduction in the sediment loads in many of the world's rivers (Haddeland et al., 2014; Wei et al., 2021; Wu et al., 2020). The Huang He River in China, which once had the highest river sediment flux in the world, now transport only ~50% of its natural

sediment flux to the coast, in large part due to the numerous small and large dams constructed throughout its watercourse (Wu et al., 2020). The construction of the Hoover dam caused a large reduction of sediment flux in the Colorado River from about 125 MT/y to 3 MT/y (Williams and Wolman, 1984). Another widely cited example is the Aswan High Dam on the Nile River which reduced sediment load from about 100 MT/y to nearly zero, causing a rapid shrinking of the Nile River Delta (Chakrapani, 2005; Walling, 2012). It has been estimated that approximately 25% of the global sediment flux is trapped in large reservoirs (Syvitski and Milliman, 2007, Syvitski et al., 2005; Syvitski et al., 2022; Vörösmarty et al., 2003).

Accurate estimation of reservoir sediment trapping is vital for a variety of applications such as, predicting river sediment transport (Cohen et al., 2014), quantifying the global sediment delivery into the ocean (Syvitski and Milliman, 2007), analysis of coastal/marine and deltaic environments (Syvitski et al., 2005), understanding anthropogenic influences on riverine fluxes (Wu et al., 2020), simulating future or theoretical change scenarios (Dunn et al., 2019), evaluating ecological impacts (Kummu & Varis, 2007), and informing dam operations (Espinosa-Villegas and Schnoor, 2009). Representation of sediment trapping by dams is currently a major source of bias in continental- and global-scale hydro-geomorphic modeling frameworks (e.g., WBMsed model; Cohen et al., 2013).

Several methods have been developed over the years to estimate reservoir trapping efficiency (e.g., Borland, 1971; Brown, 1943; Brune, 1953; Chen, 1975; Churchill, 1948; Heinemann, 1984; Verstraeten and Poesen, 2000; Vörösmarty et al., 2003). Likely the most widely used is Brune (1953) method where reservoir capacity to inflow ratio is considered. The Brune method was developed using 40 normally ponded (i.e., conventional reservoirs entirely filled with water and have their outlet at the top of the embankment) and 4 other types of

reservoirs. It was later modified by USDA-SCS (1983) to include particle size information. The Churchill (1948) approach calculates a 'sedimentation index' for a reservoir using water residence time and flow velocity. It is applicable for reservoir types such as desilting and semi-dry which are different from normally ponded reservoirs. The Chen (1975) method predicts trapping for different particle size classes using flow velocity and particle size data. Rausch and Heinemann (1975) developed an equation that predicts reservoir trapping using reservoir detention time, peak inflow rate (in place of inflow sediment particle size), storm runoff volume, sediment yield from storm, reservoir storage capacity, and drainage area. Their regression equation was developed using data from only three reservoirs in the Missouri River for individual storms and was not recommended for reservoirs with different characteristics.

Many large-scale sediment transport models currently rely on the approach of Vörösmarty et al. (2003) to calculate trapping as a function of local residence time change, an approximation of the Brune (1953) method (e.g. BQART: Syvitski and Milliman, 2007; WBMsed: Cohen et al., 2013; MOSART-sediment: Li et al., 2022; HydroTrend v3.0: Kettner and Syvitski, 2008; Grill et al., 2019). This method is convenient to use in large-scale models due to its simplicity and low input data requirement. These simplifications, however, can lead to increased bias and uncertainty. These methods were shown to significantly overestimated or underestimated trapping efficiency in reservoirs (e.g., Espinosa-Villegas and Schnoor, 2009; Lewis et al., 2013). However, to our knowledge, no large-scale comparison between measured and estimated sediment trapping efficiencies in individual reservoirs and dams has been reported in the literature. Calculation of trapping efficiency using in situ measurements requires long-term observations of sediment fluxes both upstream and downstream of a reservoir. Gauging stations

for calculating sediment trapping are typically located far upstream and/or downstream of dams, which can introduce considerable errors to the trapping efficiency calculations (Brune, 1953).

Emerging remote sensing methodologies and datasets of fluvial sediment (Dethier et al., 2020; Gardner et al., 2023; Overeem et al., 2017; Yang et al., 2022) provide a unique opportunity to quantify, analyze, and model sediment trapping and its downstream impacts at continental and global scales. Remote sensing can also provide temporal dynamics, which is important as sediment trapping and its downstream impacts can vary over time (Rausch and Heinemann, 1975). Longitudinal sediment profiles developed using remote sensing data also provide opportunities to study spatial and temporal recovery patterns of the river system downstream of a dam. Although remote sensing sediment data can have uncertainties associated with atmospheric corrections, algorithm development, etc., their greater spatial and temporal coverage offer an unparalleled opportunity to be used in large-scale applications (Dethier et al., 2020).

This paper is focused on the development of conceptual understanding and parameterization of sediment trapping efficiency of large dams and its impacts on sediment dynamics downstream of dams. A novel reservoir trapping efficiency empirical model is developed using a new remote sensing dataset (Gardner et al., 2022, 2023) that offers high-resolution and spatially continuous suspended sediment concentration (SSC) data across the Contiguous United States (CONUS). This is the first dataset of its kind that enables the observation and modeling of fluvial suspended sediment dynamics at a continental scale, a transformative capability considering the scarcity in sediment gauging. Suspended sediment loads entering the reservoir and leaving its dam are used to calculate sediment trapping in 222 reservoirs. These reservoir trapping data are used to develop a new reservoir trapping efficiency empirical model using widely available fluvial, environmental, and dam attributes. This analysis

provides insights into the factors controlling the magnitude of suspended sediment trapping by dams at large spatial scales. In order to develop these quantitative relations, we employ statistical approaches such as multiple regression as well as machine learning techniques. We developed an additional model based on a global dataset of dams to extend our estimation of sediment trapping globally, providing a unique attribute for future analyses and modeling efforts. We also discuss the changes in suspended sediment loads along rivers using longitudinal sediment profiles extracted from the remote sensing dataset.

2. Methodology

2.1 Dam selection and trapping efficiency calculation

The remote sensing sediment dataset used in this study was developed by Gardner et al. (2022, 2023), using Landsat 5, 7, and 8 processed in Google Earth Engine (GEE) and Machine Learning to convert surface reflectance into SSC, generating spatially continuous maps of SSC along 108,000 kilometers of large rivers across the CONUS. This approach provides SSC (mg/L) data linked to the National Hydrography Dataset (NHDplusV2) river network (McKay et al., 2015). The machine learning algorithm was trained using >21,000 coincident field and remote sensing observations and validated using >2,000 observations (Ross et al., 2019). While the algorithm has equal or higher accuracy (Root Mean Square Error (RMSE) of 29 mg/L, Mean Absolute Error (MAE) of 12 mg/L) than previous local Landsat-based models, there are many limitations of remotely sensed SSC such as only representing surface SSC down to one optical depth. In addition, these remote sensing data are spatially averaged to approximately 2 km river lengths unlike point measurements at river gauges. The SSC algorithm tends to overestimate low concentrations (0 to 10 mg/L) and underestimate very high concentrations (>3,000 mg/L). For

this study, 32% of the river reaches used to calculate *Te* were < 10 mg/L (smallest value 3.34 mg/L) and none had SSC values >3,000 mg/L. Given the consistent long-term record of spatially continuous SSC observations across US rivers, this dataset provides an unprecedented opportunity to calculate and understand *Te*. For more information about this data product and its validation, readers are referred to Gardner et al. (2022) and Gardner et al. (2023).

For this study, we calculated long-term averaged suspended sediment flux (kg/s) for each NHDPlus river reach by multiplying its remote sensing-derived long-term mean (1984-2018) SSC (mg/L) and NHDplus mean annual discharge (m^3/s). We used suspended sediment flux to calculate trapping efficiency instead of SSC to mitigate issues of water extraction and loss in reservoirs due to irrigation and evaporation, which can skew the calculation. For example, low sediment loads can be indicated as high sediment concentrations if a significant amount of water is extracted and removed from the system. Therefore, it is important to use flux values when calculating reservoir trapping even if it introduces an additional source of bias from the NHDplus discharge estimates.

We conducted a validation of the calculated suspended sediment flux values, and the NHDplus discharge values used to calculate them, against USGS gauge sediment flux and water discharge data, respectively. The main objective of the validation was to find how well suspended sediment flux calculated by remote sensing-derived surface SSC represents the total, depth-integrated, suspended sediment load of the river. The validation was conducted for 36 USGS gauge sites where daily suspended sediment discharge measurements were available over the same period of time, and for sites located on the river network for which remote sensing data were available (Supplementary Table S3.1). However, it should be noted that the temporally-averaged USGS sediment flux values for some gauging stations do not match the entire period of

the remote sensing data, due to missing values or discontinuation of the gauging station. Since we compared long-term average sediment values, it was reasonable to use these stations. Based on this validation of suspended sediment flux, we introduced a simple adjustment factor to match the remote sensing-calculated surface suspended sediment fluxes to depth-averaged suspended sediment fluxes.

For the CONUS-scale analysis, we used the National Inventory of Dams (NID) dataset, published by the U.S. Army Corps of Engineers (https://nid.sec.usace.army.mil/ords/). The NID consists of more than 91,000 dams with attributes such as dam storage, dam height, dam length, drainage area, surface area of the impoundment, dam history, inspection, and hazard potential. However, this dataset includes many dams such as dikes, saddle dams, dams on small ponds located outside the river network, dams that do not form impoundments, and sometimes multiple dams per reservoir (Renwick et al., 2005). Therefore, we had to carefully choose the main dam located on the river network, that releases water and sediment to the river from its reservoir. We first conducted an initial filtering to extract the dams located close to the river network for which remote sensing sediment data were available, and have valid (non-zero) values for reservoir storage, drainage area, dam height, and dam length. Then through a meticulous manual procedure involving ArcGIS base maps, Google Earth, USA detailed water bodies layer package (ESRI, 2021), Global Reservoir and Dam (GRanD) Database (Lehner et al., 2011), and NHDWaterbody layer, the locations of dams and reservoirs that correspond to the river network with remote sensing data were extracted. Reservoirs with storage capacities < 0.01 km^3 and dams that that do not form visible impoundments were removed. This resulted in 317 dams in total that are distributed across the CONUS.

Sediment trapping efficiency (*Te*; %) for individual dams was calculated as:

$$Te = \frac{Q_{s\_in} - Q_{s\_out}}{Q_{s\_in}} * 100 \quad (1)$$

where, Q_{s_in} is the suspended sediment flux entering the reservoir (kg/s), and Q_{s_out} is the suspended sediment flux immediately downstream of the dam. As demonstrated in Figure 3.1, reservoirs typically drain multiple streams in addition to the main stem of the river. Fluxes from these streams and rivers needs to be included in the calculation of Q_{s_in} (Condé et al., 2019). We found that if Q_{s_in} does not account for sediment loads from all the incoming river reaches, it can lead to significant underestimates of the total sediment load entering a reservoir. Ziegler and Nisbet (1995) also calculated sediment trapping efficiencies using sediment loads from both the main stem and tributaries. According to their estimates, 32.7% of the inflow sediment load in the Watts Bar reservoir on the Tennessee river was from other tributaries. In addition, Liu et al. (2022) found that sediment from smaller tributaries in the Three Gorges Reservoir carried approximately 10.8% of the total incoming sediment. For most reservoirs, however, remotely sensed suspended sediment data were not available for all draining streams given their small size (Figure 3.1). We estimated the sediment flux contribution of these reaches to each reservoir by multiplying their total discharge (from NHDplus) by the average SSC of the river reaches entering the reservoir with remote sensing data. This assumes similarity in average SSC among contributing reaches to each reservoir. We have found that *Te* calculation was not very sensitive to other scaling approaches given the dominance of the river main stem sediment flux on the calculation.

A potential problem associated with calculating *Te* using remotely sensed upstream and downstream sediment loads is that Q_{s_out} may capture erosion taking place in reaches immediately downstream of the dam (Kummu et al., 2010; Williams and Wolman, 1984). The river reaches of the modified NHDplus network are several kilometers long (Figure 3.1). Along this length, sediment replenishment through riverbed and bank erosion, small tributary input and deposition can impact sediment concentration (Brandt, 2000). Using the NHDplus reach immediately downstream of a dam to capture its discharged sediment flux is therefore prone to overestimation, leading to underestimation of the calculated *Te.* To mitigate this issue, we used the sediment load from the river reach immediately upstream of the dam (the most downstream of the reservoir) to get Q_{s_out}, assuming that the sediment load of this reach is representative of the amount released by the dam. This is further illustrated by the longitudinal sediment profiles of rivers in section 3.2. which shows the pattern of gradual sediment deposition within the reservoir. According to these profiles, the sediment load of the most downstream reach within the reservoir is better representative of the sediment load retained by the reservoir. From our experimentation with Q_{s_out} estimation we found that this approach yields *Te* values that better correspond to published estimates.

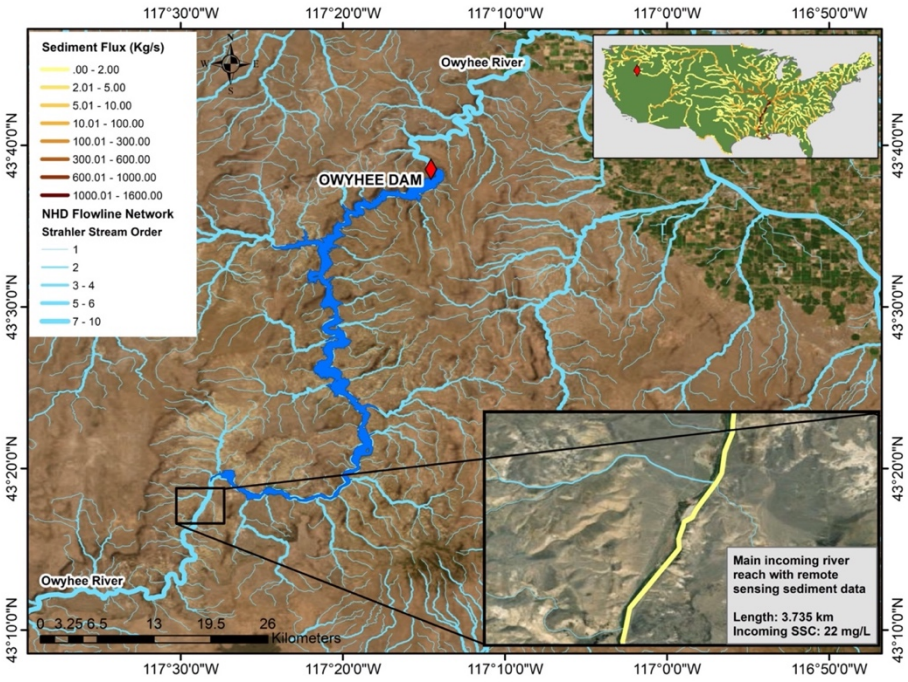

Figure 3.1. Figure illustrating the incoming river reaches into the reservoir.

Out of the 317 dams for which *Te* was calculated using Eq. 1, 75 yielded *Te* <0% indicating that these dams do not trap any sediment. This is possible for dams where no sediment is retained in the impoundment (Espinosa-Villegas and Schnoor, 2009). Other possible reasons for a <0% *Te* may include (i) underestimation of sediment load in incoming river reaches that does not have remote sensing sediment data, (ii) bias in remote sensing sediment data specially for low SSC values, and (iii) in a few instances, the NHDplus river reach used to get Q_{s_out} captures areas downstream of the dam.

Further investigation into the 75 dams that yielded *Te* <0% revealed that many of these dams have a primary purpose of navigation and hydropower generation. Conversely, dams built with the main purpose of irrigation, water supply, or flood risk reduction had only a few dams with zero *Te* values. It should be noted that many dams have multiple uses. These results are

reasonable as navigational dams or lock and dam structures are usually designed to release water, and thus sediment, downstream (Peteuil, 2012). Dams built for hydroelectricity, particularly run-of-river hydroelectric dams have little or no water storage and thus natural seasonal river flows are less obstructed (Brismar, 2002). Taking this distinction into consideration, all the Lock and Dams in the dataset were considered as having zero *Te*. However, no information was available in the NID dataset to distinguish run-of-river hydroelectric dams from conventional hydropower dams with impoundments. Therefore, all the hydropower dams with positive *Te* values were included in the dataset. After removing dams with a <0% *Te* and navigational dams, 222 dams were available for use in the analysis (Figure 3.2).

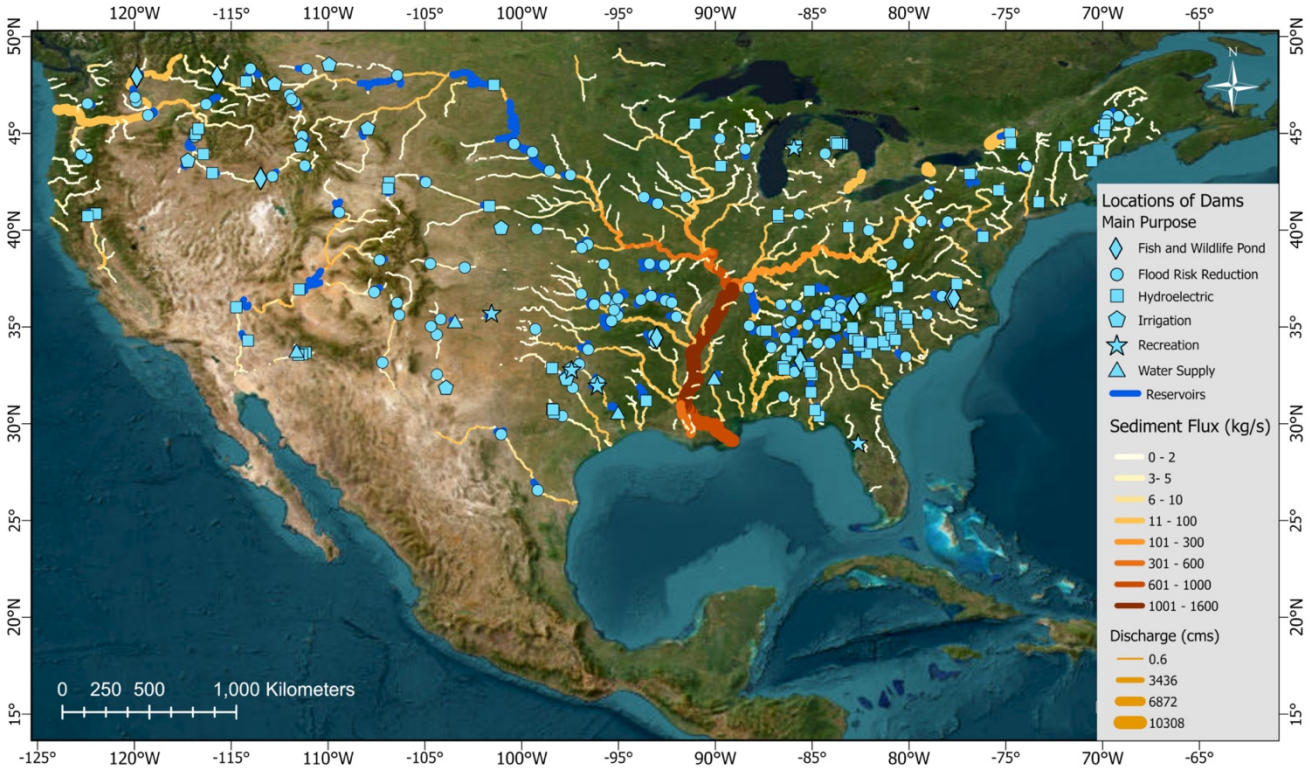

Figure 3.2. Map of the locations of 222 dams and reservoirs used in the analysis along with the river sediment fluxes calculated using the remote sensing data.

2.2 CONUS Te Model Development

Several, widely available, environmental, fluvial, and dam-related variables were collected to develop a CONUS-wide empirical *Te* model (Table 3.1). Reservoir length along its longest part was calculated along the NHDplus river network, using the NHDplus reservoir polygons. The relationship between these variables and *Te* was analyzed using multiple regression and machine learning. We used machine learning techniques, such as Random Forest Regression and Artificial Neural Network (e.g., Multi-layer Perceptron) models, with an 80% and 20% split of data for training and validation, respectively. Sensitivity and variable selection analyses (e.g., Variance Inflation Factor) were conducted to identify the key attributes that contain the largest variance of the data.

Table 3.1. Explanatory variables tested for developing the Te parameter

Variable	Symbols	Data type	Data source
Incoming sediment flux	*Qs_in*	Line	Gardner et al. (2022)
Incoming discharge	*Q_in*	Line	NHDplus V21
Outgoing discharge	*Q_out*	Line (NHDplus), point (GRanD)	NHDplus V21, GRanD
Dam length	*D_Length*	Point	NID, GRanD
Dam height	*H*	Point	NID, GRanD
Reservoir storage	*S*	Point	NID, GRanD
Reservoir surface area	*SA*	Point	NID, GRanD
Drainage area	*D*	Point	NID, GRanD
Slope	*Slp*	Line	Lin et al. (2020)
Elevation	*Elev*	Line (Lin), point (GRanD)	Lin et al. (2020), GRanD
% Sand	*Snd*	Line	Lin et al. (2020)
% Silt	*Slt*	Line	Lin et al. (2020)
% Clay	*Cly*	Line	Lin et al. (2020)
Sinuosity	*Sin*	Line	Lin et al. (2020)
Aridity Index	*AI*	Raster (~1 km)	Lin et al. (2020), Trabucco and Zomer (2019)
Leaf Area Index	*LAI*	Line	Lin et al. (2020)
Sum of soil erosion from within the river reach catchment	*E*	Line	Grill et al. (2019)

2-yr return period flood	*Q2*	Line	Lin et al. (2020)
Dam age	*A*	Point	NID, GRanD
Lake length	*L*	Line	Grill et al. (2019)
Reservoir Depth	*Depth*	Point	GRanD
Water temperature	*T*	Line	Syvitski et al. (2019)

2.3 Calculation and Analysis of a Global Te Dataset

A global empirical *Te* model was developed using dam attributes from the GRanD database (Lehner et al., 2011). A dataset of 264 observed *Te* values was used to develop the global *Te* model. The dataset includes the 222 CONUS dams, observed *Te* calculated for 4 dams in the Amazon Basin using a similar remote sensing dataset (Narayanan, 2022), literature-reported *Te* for 36 dams in China (Hu et al., 2009; Tan et al., 2019), the Bhakra Dam in India (Jothiprakash and Vaibhav, 2008; Sharma et al., 2018), and the Aswan High Dam in Egypt (Biswas and Tortajada, 2012). Some of the missing explanatory variable data for these 264 dams in GRanD were substituted with data from the NID dataset, the GeoDAR global reservoir and dam dataset (Wang et al., 2021), and World Register of Dams (WRD) maintained by the International Commission on Large Dams (ICOLD; https://www.icold-cigb.org). Reservoir lengths were calculated using an automated process using the Grill et al. (2019) river network and GRanD reservoir polygons. The developed global *Te* model was then applied for the GRanD dataset, with a total of 6823 dams which included all the needed attributes. This dataset is envisioned to provide a *Te* parameter for large-scale hydrological and geomorphic modeling frameworks.

3. Results and Discussion

3.1 Evaluation of the Remote Sensing Sediment Data

A limitation of remote sensing of sediment is that it only captures sediment concentration for the top layer of the river water column (Condé et al., 2019). Existing theoretical methods to obtain depth-averaged sediment concentration profiles such as the Rouse profile require data on water depth, sediment settling velocity, shear velocity at different water depths, and other coefficients (Laguionie et al., 2007) which are not readily available. Blanchard et al. (2011) reported that suspended sediment concentration varied at different depths among different sites they measured. A universal method to estimate sediment concentration profiles using surface sediment fluxes has not been proposed. We conducted a comparison between in situ measured and remote sensing-calculated sediment fluxes for 36 USGS gauging stations. It is important to note that the USGS measurements of discharge and suspended sediment are point measurements at gauging stations, whereas NHDplus discharge and remote sensing sediment data are average values over several kilometers of river length. The results show that the remote sensing sediment flux is consistently underestimated (Figure 3.3b).

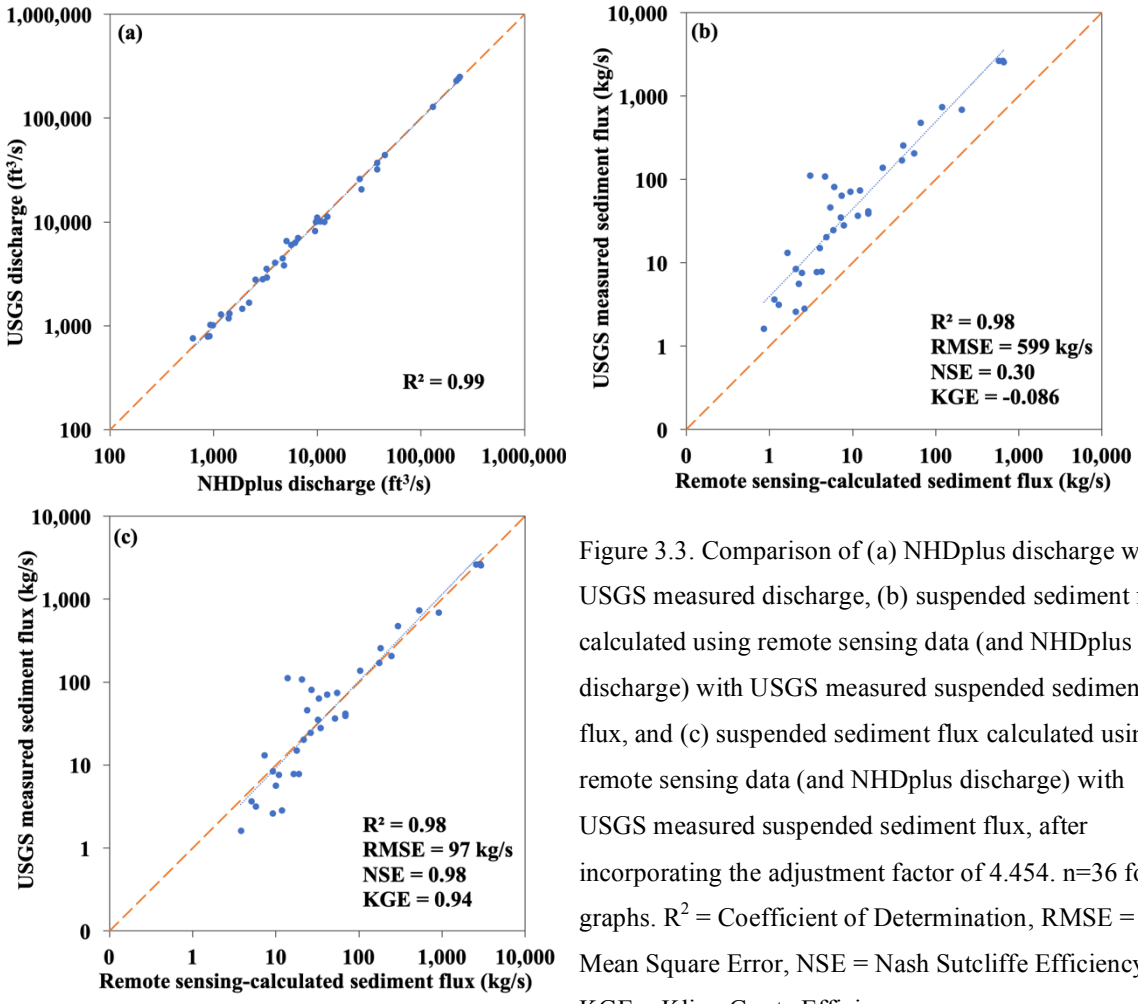

Figure 3.3. Comparison of (a) NHDplus discharge with USGS measured discharge, (b) suspended sediment flux calculated using remote sensing data (and NHDplus discharge) with USGS measured suspended sediment flux, and (c) suspended sediment flux calculated using remote sensing data (and NHDplus discharge) with USGS measured suspended sediment flux, after incorporating the adjustment factor of 4.454. n=36 for all graphs. R^2 = Coefficient of Determination, RMSE = Root Mean Square Error, NSE = Nash Sutcliffe Efficiency, KGE = Kling Gupta Efficiency.

A comparison between NHDplus discharge and USGS measured discharge shows that the discharge values correspond nearly perfectly to the in-situ measurements and, thus, can be considered as reliable (Figure 3.3a). This may also be attributed to the fact that NHDplus mean annual discharge is gauge adjusted based on the observed flow (Moore et al., 2019). NHDplus is, however, widely used in hydrological studies as a reliable source of mean annual discharge, so we are quite confident in these values throughout the CONUS. Based on these results, we can deduce that the source of underestimation of the remote sensing sediment flux can be attributed

to its derivation from surface sediment concentration (Dethier et al., 2020; Markert et al., 2018). It may also be attributed to remote sensing data missing high flow events which carry a high proportion of a river's total sediment load, due to the low temporal resolution of Landsat imagery and cloud cover during these events. We found that, a simple adjustment factor of 4.45 yields the strongest alignment with the 1:1 line, yielding the lowest sum of residuals and improved model performance statistics (RMSE, NSE, and KGE), so that sediment flux calculations are representative of the depth-averaged sediment flux in the in-situ observations (Figure 3.3c). This result shows that remote sensing-derived suspended sediment fluxes can be used to calculate *Te* with high accuracy using a simple adjustment factor. The efficiency of the uniform adjustment factor is surprising given the diversity of the gauge locations, the range of sediment flux values (3 orders of magnitude), and the known complexity in the fluvial sediment-depth relationship. The strong linear fit in figure 3.3c implies that average surface suspended sediment flux is uniformly 4.45 times smaller than depth-averaged flux across a wide range of rivers over the CONUS. This finding merits further investigation using a wider geographical range. A smarter adjustment factor may be warranted to reduce the relatively high scatter observed for smaller values of sediment flux.

3.2 Sediment Dynamics Along Longitudinal Profiles

The Missouri River is a good case study for examining the changes in sediment dynamics along longitudinal profiles due to obstruction by a diverse set of large dams (Figure 3.4). The largest of these dams in terms of reservoir capacity include the Garrison Dam forming Lake Sakakawea, Oahe Lake and Dam, and Fort Peck Lake and Dam, with reservoir storage capacities of 32.1 km^3, 29.1 km^3, and 23.6 km^3, respectively. Both the sediment concentration and flux

generally increase as the river flows downstream. The trends in sediment concentration and flux are generally similar. A rapid decrease in the sediment load (both concentration and flux) is observed within reservoirs (highlighted color sections in Figure 3.4b). This shows the deposition of sediment in the reservoir due to reduced flow velocity (Verstraeten and Poesen, 2000). Near the headwaters of the Missouri River, sediment flux increases downstream at a rate of 0.05 kg/s/km, and then a steep decrease in sediment is observed once it reaches the first set of relatively small cascading dams (collectively account for 3.1 km^3 storage capacity). The sediment load increases without obstructions from large dams for about 493 km downstream at a rate of 0.27 kg/s/km (180 to 675 km segment in Figure 3.4b). Once the river enters Fort Peck Lake, sediment load rapidly decreases at a rate of -0.52 kg/s/km due to deposition in the reservoir. Fort Peck Dam traps 94% of its incoming sediment flux as calculated by the remote sensing dataset. Sediment loads increase rapidly immediately after the Fort Peck dam due to the high sediment-yielding Milk River confluence (Figure 3.5).

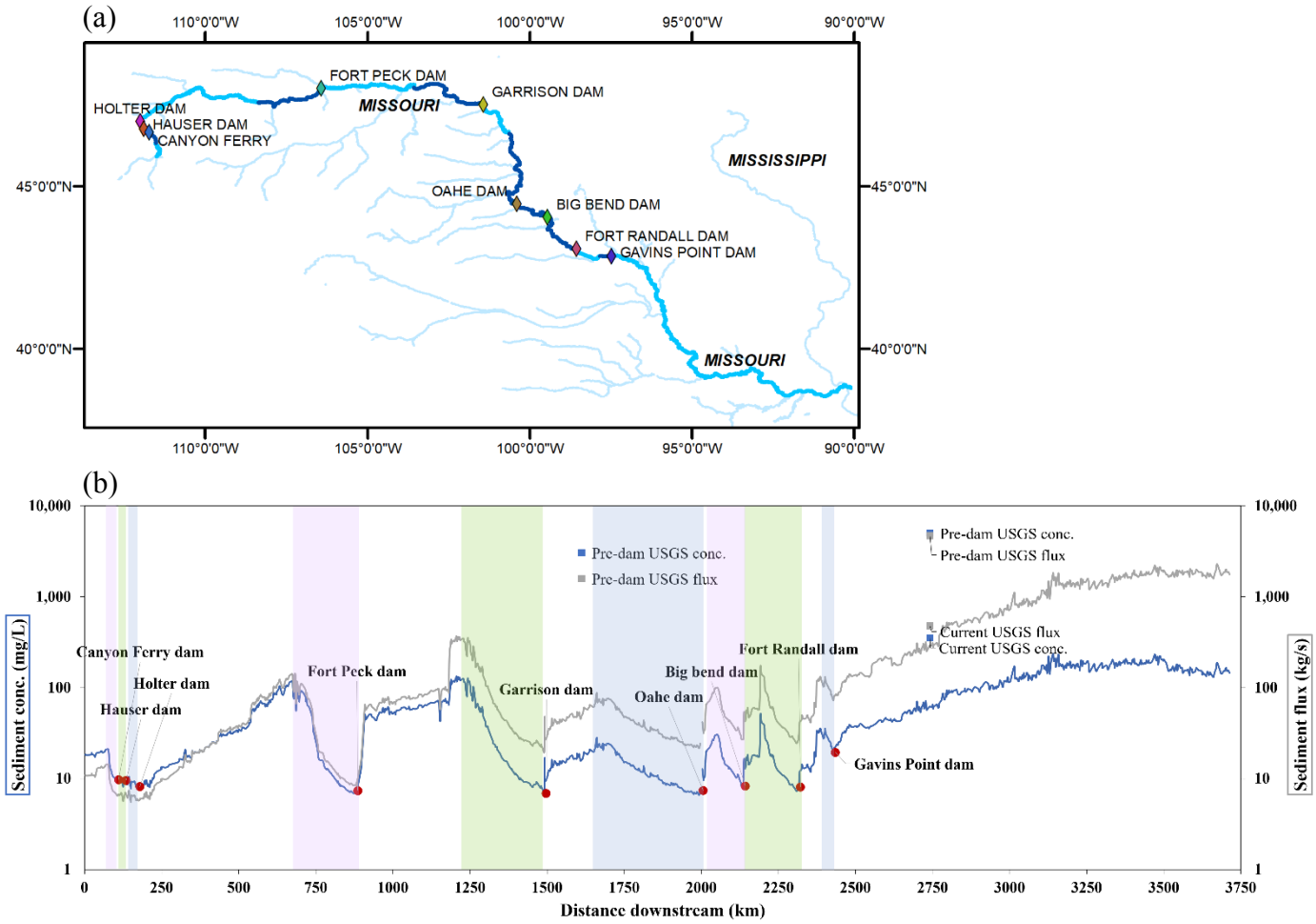

Figure 3.4. Longitudinal profile of sediment dynamics in the Missouri river. (a) Map of the Missouri River and its dams. (b) Trend in sediment concentration and flux along the Missouri River. The red dots show the dam locations, whereas the blue and grey lines show the sediment concentration (mg/L) and adjusted sediment flux (kg/s) obtained from the remote sensing data, respectively. Pre-dam construction and current observed long-term average sediment concentrations (blue squares) and fluxes (grey squares) were calculated from USGS gauge sites where data are available. The colored areas indicate the extent of reservoirs corresponding to the dams. Note that vertical axes are converted to log scale to enhance visualization.

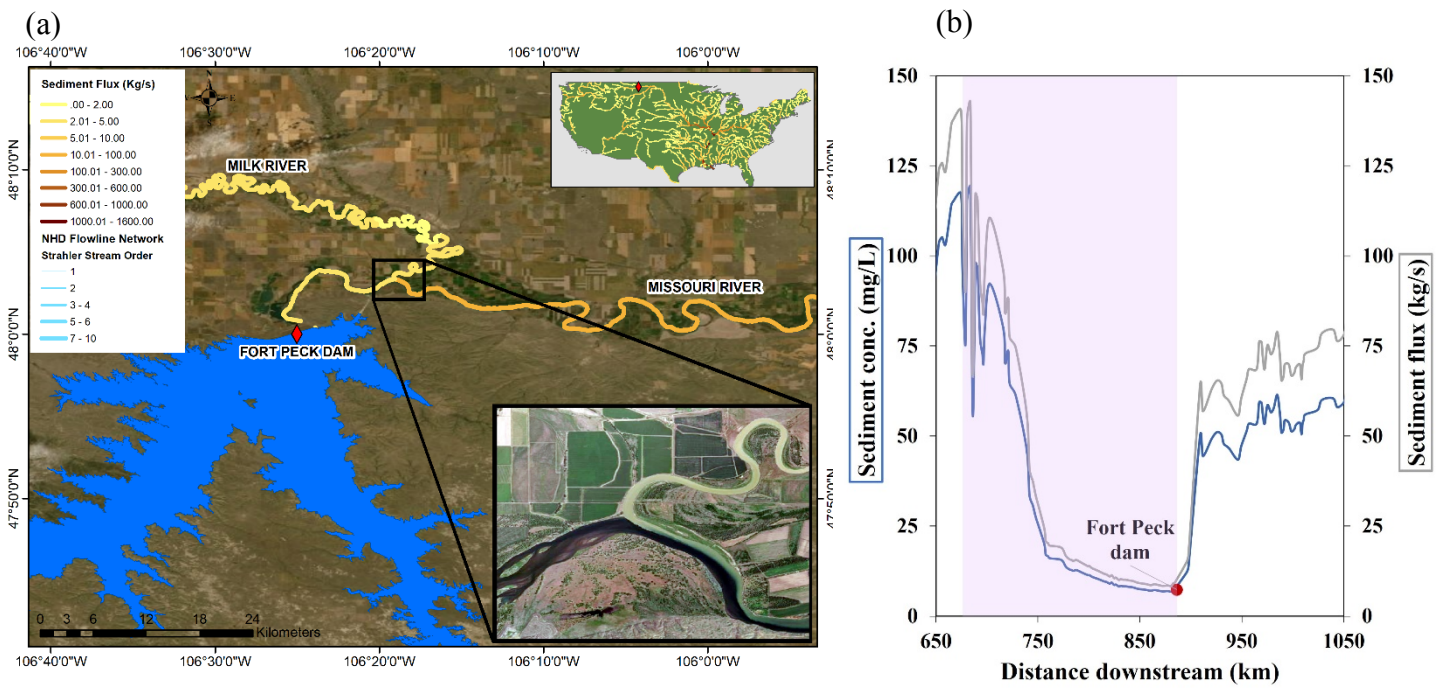

Figure 3.5. The Milk River joining the Missouri river immediately after the Fort Peck dam, contributing to a sudden increase in downstream sediment load. 5(b) shows the longitudinal sediment profile of the river segment with the colored bar showing the reservoir extent. Blue and grey lines show the sediment concentration (mg/L) and adjusted sediment flux (kg/s) obtained from the remote sensing data, respectively.

The next large dam along the Missouri profile, Garrison (km 1,500 in Figure 3.4b), traps 93.4% of its incoming sediment flux. The pattern of decrease in sediment within the reservoir length and a sudden increase in sediment after the dam can also be clearly observed at this location, as well as Oahe, Big Bend, and Fort Randall dams and reservoirs. The increase in sediment after the dam at Oahe, Big Bend, and Fort Randall dams are gradual increases within a short distance (as opposed to the sudden increase after Fort Peck) and can likely be attributed to both instream erosion and sediment influx from smaller tributaries. The spike in sediment flux and concentration at km 2,192 within Lake Francis Case (formed by the Fort Randall Dam) is due to the White River joining the Missouri river. The increase in sediment between Fort Randall

dam and Lewis and Clark Lake (formed by Gavins Point dam) at 2,374 km downstream point is due to the Niobrara River joining the Missouri River. Gavins Point dam also shows a similar pattern of sediment trapping and a gradual increase downstream. Along its most downstream segment (~2,400 – 3,750 km), the Missouri River flows without dam obstructions until it joins the Mississippi River, gaining sediment along the way, with considerable contribution from tributaries. The rate of increase in sediment flux along this segment of Missouri is 1.32 kg/s/km.

USGS gauge sediment concentration and flux data prior to dam construction were obtained for two locations along the Missouri River: Missouri River at Bismarck, ND at km 1,612 (USGS gauge number: 06342500) and Missouri River at Omaha, NE at km 2,741 (USGS gauge number: 06610000). The latter also provides post dam-construction measurements. For the Bismarck station, daily sediment data were available only for the year 1946, which was used to calculate the average sediment loads prior to dam construction. For the Omaha station, average prior-to-dam sediment concentration and flux were calculated using daily data for the period between 1939 – 1951, while contemporary sediment concentration and flux were calculated using daily data for the period between 1991 – 2019 (excluding 2004 – 2007 due to missing data). The contemporary sediment flux from USGS data at Omaha station (477 kg/s) compares reasonably well with the adjusted sediment flux from remote sensing data for this location (294 kg/s), considering the difference in the temporal range. The difference between the prior-to-dam and contemporary sediment fluxes observed at the gauge site is over an order of magnitude at the Omaha station (4694 kg/s to 477 kg/s) and two orders of magnitude at the Bismarck station (1587 kg/s to 49 kg/s).

The Colorado River (Figure 3.6) is well known for its near-zero sediment flux to the ocean due to the high degree of sediment trapping by dams and water extractions. Sediment load

increases at an average rate of 1.07 kg/s/km from the headwaters in Rocky Mountains National Park, CO, until km 620, downstream of which sediment load decrease, before entering the Glen Canyon reservoir (left-most highlighted section in Figure 3.6c). Glen Canyon Dam traps on average 95.8% of the incoming sediment load, resulting in a near-zero load downstream. Until the river enters Lake Mead (formed by the Hoover Dam), sediment flux generally increases at an average rate of 0.84 kg/s/km. The areas with missing (and highly fluctuating) remote sensing-captured SSC before the start of Lake Powell (formed by the Glen Canyon Dam), as well as in river reaches between Glen Canyon dam and Lake Mead, are the portions of the Colorado River that flow through the Canyonlands National Park, and the Grand Canyon, respectively. These more confined segments of the river pose challenges for remote sensing techniques due to (i) generally very narrow river widths, (ii) steep canyons creating hill shadows, (iii) in areas where rapids/white water areas are interspersed with slow water flows, rapids may be indicated as high SSC, and (iv) a number of small tributaries along this part of the river that deliver considerable amount of sediment to the Colorado River potentially contributing to the high variability.

The Hoover Dam traps 78.7% of the incoming sediment load, and the dams that follow such as Davis, Parker, Palo Verde diversion, etc. keep the sediment load from recovering. The Morelos diversion dam, which is the last dam on the Colorado River, diverts a large portion of its water for irrigating highly developed croplands in the Mexicali Valley, Mexico. The Colorado River has a very low water discharge from this point onwards (Figure 3.6b). Although the NHDplus river network and therefore sediment data ends at the Morelos diversion dam shortly before reaching the US-Mexico border, the river extends further until it reaches the ocean. This longitudinal river profile shows the dynamics leading to a very low sediment flux from the Colorado River to the ocean.

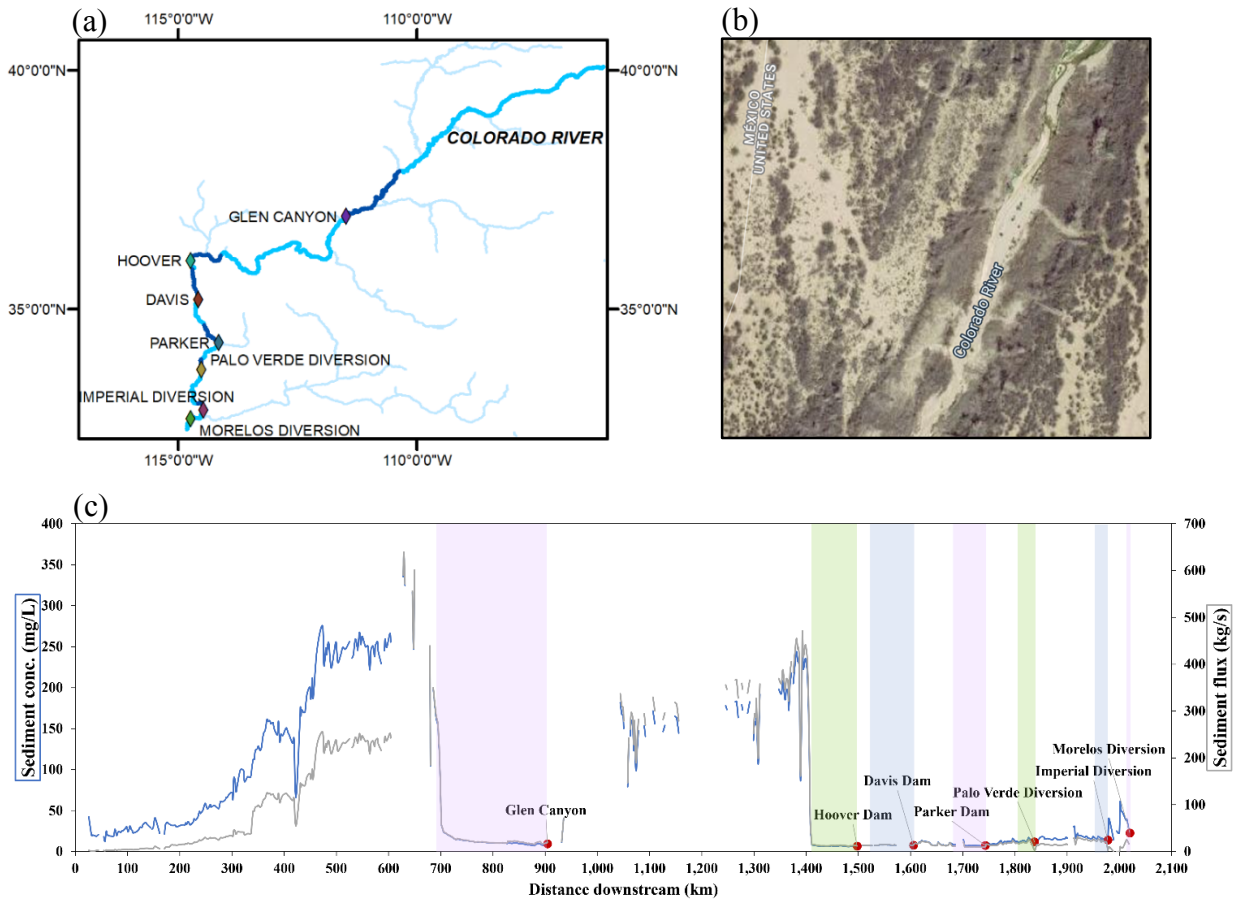

Figure 3.6. Longitudinal profile of sediment dynamics in the Colorado river. (a) Map of the Colorado River and its dams. (b) Colorado River after the Morelos Diversion Dam with very low discharge. (c) Mean sediment concentration and flux along the Colorado River. The red dots show the dam locations, whereas the blue and grey lines show the sediment concentration (mg/L) and adjusted sediment flux (kg/s) obtained from the remote sensing data, respectively. The colored areas indicate the extent of reservoirs corresponding to the dams.

Similar patterns in sediment trapping and downstream recovery are observed in other rivers (e.g., Figure 3.7(c) the Catawba and Wateree Rivers, Figure 3.7(d) the Tennessee River). In the Catawba and Wateree Rivers, clear decreases in sediment concentrations are observed at reservoir locations, however, this trend is not very prominent in sediment flux. This may be due to the gradual increase in discharge throughout the water course that alleviated the changes in sediment concentration until the Wylie dam (km 206). Sediment concentration and flux both

increase for about 28 km downstream of Wylie dam at a rate of 0.33 kg/s/km until the next set of cascading dams trap a large amount of sediment. Following these dams, a gain in sediment is observed until the Wateree River and Congaree River confluence, at a rate of 0.14 kg/s/km. In the Tennessee River (Figure 3.7d), although sediment concentration shows decreases at reservoir locations, sediment fluxes show a general increasing trend until the Kentucky Lake (km 846), despite multiple dam obstructions. The spikes in sediment within the lakes formed by the Wheeler dam and Kentucky dam are due to large tributaries. The spike immediately after Fort Loudoun Dam (km 80) is also owing to a tributary confluence.

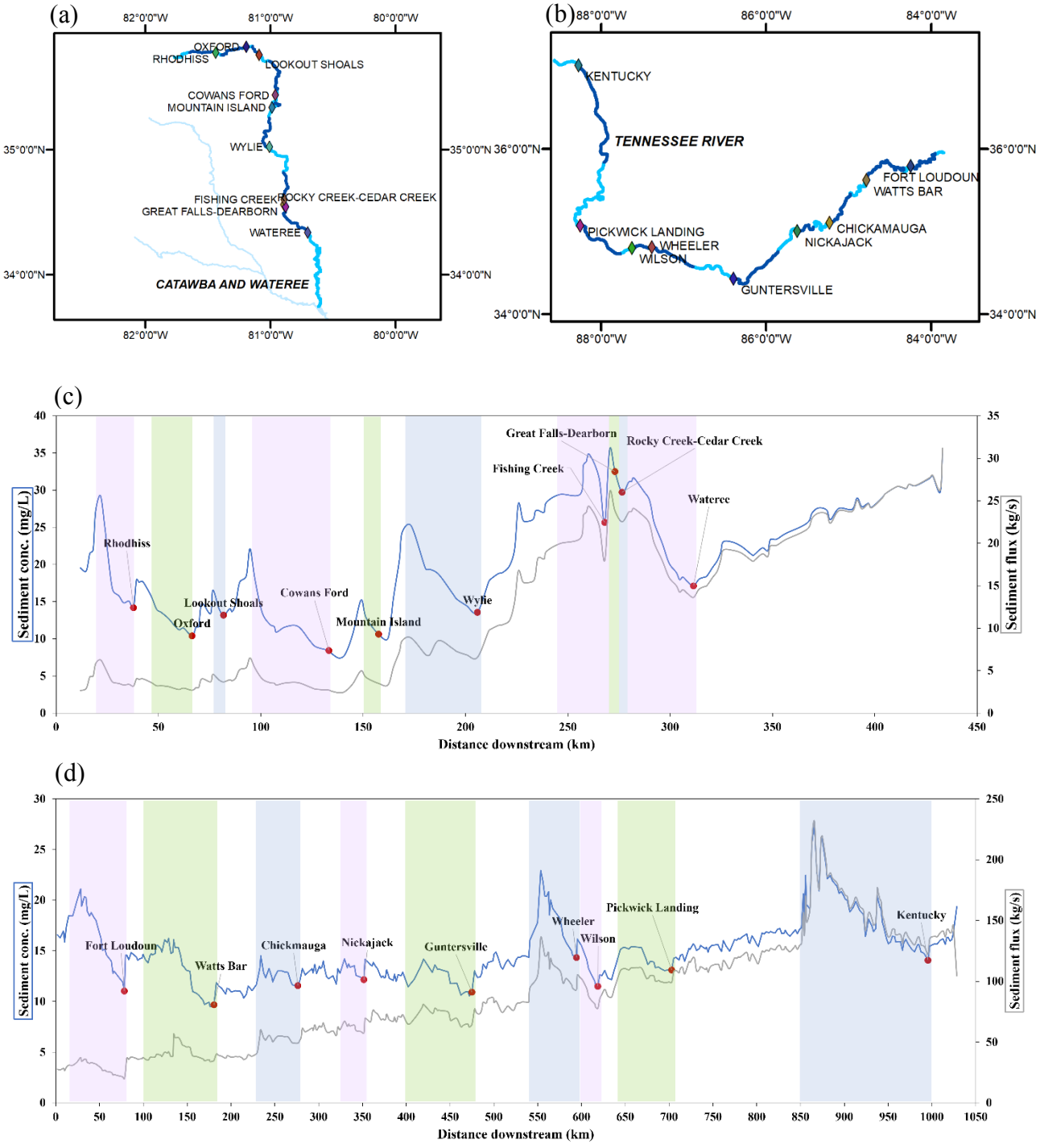

Figure 3.7. Longitudinal profile of sediment dynamics in the Catawba and Wateree and Tennessee Rivers. Map of (a) Catawba and Wateree and (b) Tennessee Rivers with their dams. Trend in sediment concentration and flux along the (c) Catawba and Wateree (d) Tennessee Rivers. The red dots show the dam locations, whereas the blue and grey lines show the sediment

concentration (mg/L) and adjusted sediment flux (kg/s) obtained from the remote sensing data, respectively. The colored areas indicate the extent of reservoirs corresponding to the dams.

The longitudinal river sediment profiles constructed using the remote sensing data also reveal how the effect of trapping gradually decays downstream of dams. Increases (or replenishment) of sediment downstream of large dams can be attributed to several mechanisms: (i) increased transport capacity of the river flow, leading to channel scour, incision, and bank erosion ("hungry rivers"; Kondolf et al., 2014a; Kondolf et al., 2014b; Kummu et al., 2010), which was shown to rapidly increase sediment loads downstream (Brandt, 2000; Williams and Wolman, 1984), (ii) large tributaries that drain sediment into the main river, (iii) eroded soil from the surrounding areas of the river reach catchment, and (iv) dams may have mechanisms to release sediment downstream. The relative proportions of downstream sediment recovery that can be attributed to these processes need to be quantified to better understand downstream sediment recovery processes. However, this remains challenging using our existing data, mainly due to lack of data on sediment flows in most major tributaries, limiting our ability to calculate the mass balance of sediment along river corridors.

3.3 CONUS Te Model

Reservoir *Te* calculated using remote sensing-derived adjusted sediment flux values (Eq. 1) for the 222 dams, range from 0.13% to 98.3% with a mean of 45.8%, median of 45.3% and a standard deviation of 27.3%. Figure 3.8 shows the spatial variability of the remote sensing-calculated *Te*. It can be observed that dams with the largest *Te* values are mostly located in the arid mid-west regions of the US, whereas dams in the Eastern and North-West parts of the country generally have lower *Te* values. This suggests that regional climate, particularly aridity,

may serve as a proxy for a combination of properties that are common for dams in arid regions. These properties may include sediment particle size, reservoir size and depth, and dam operations. Many of the dams in the arid mid-west have large reservoirs with limited or no ability to release sediment. Also, the sediments in this region tend to be coarser and are, therefore, more rapidly deposited due to higher settling velocity, once reaching the reservoir (Verstraeten and Poesen, 2000). Many of the dams on Eastern US rivers are not necessarily designed for storage (rather for navigation, hydropower generation etc.), and therefore, tend to be shallower and/or run-of-river dams. Also, suspended sediments in these regions tend to be finer, which decreases their ability to be trapped. Vörösmarty et al. (2003) also found that dams in arid regions tend to have larger *Te* values due to their highly variable discharge regimes, high demand for water for irrigation and community water uses, and the resulting necessity to store water.

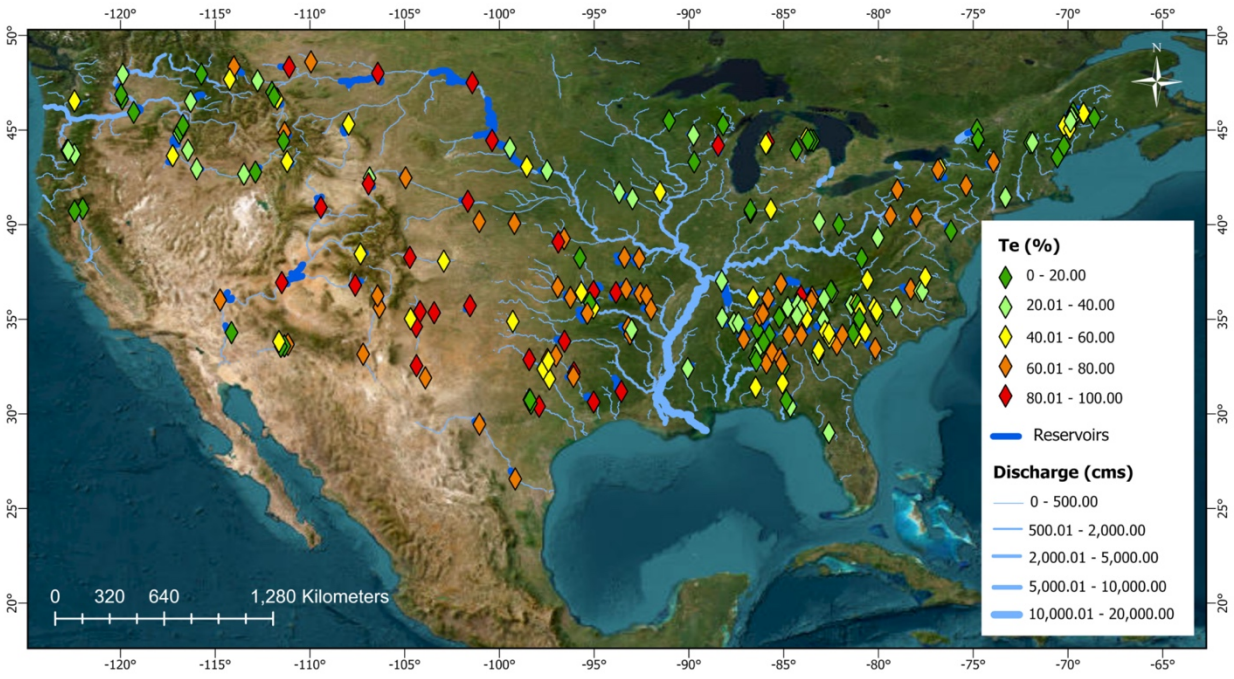

Figure 3.8. Trapping efficiency (Te; %) of the 222 dams calculated using observed remote sensing data.

Twenty two (22) explanatory variables were tested to predict reservoir *Te* using machine learning methods and multiple regression, based on the *Te* calculated for the 222 dams. The list of explanatory variables used is provided in Table 3.1. The multiple regression model yielded an R^2 of 0.72 (Adj. R^2 = 0.71) using four variables (log converted): incoming sediment flux, outgoing water discharge, reservoir length along the longest part, and reservoir storage. All these variables significantly contribute to the regression model ($p < 0.05$). This indicates that 72% of the variability in *Te* can be explained by these four variables with RMSE of 14.6% and a Nash Sutcliffe Efficiency (NSE) of 0.61. The resulting model equation is:

$$Te = -7.33 + 30.24\log(Q_{s\_in}) - 15.8\log(Q_{out}) + 18.01\log(L) + 14.56\ \log(S) \quad (2)$$

where Q_{s_in} is the adjusted incoming sediment flux (kg/s), Q_{out} is the outgoing discharge (m^3/s), L is the lake length along the longest part (km), and S is the reservoir storage capacity (km^3). The importance of the independent variables in the model in descending order based on the standard coefficients and contribution to change in the R^2, are Q_{s_in}, S, Q_{out}, and L. Figure 3.9 shows the performance of the multiple linear regression model (Eq. 2) in predicting *Te*.

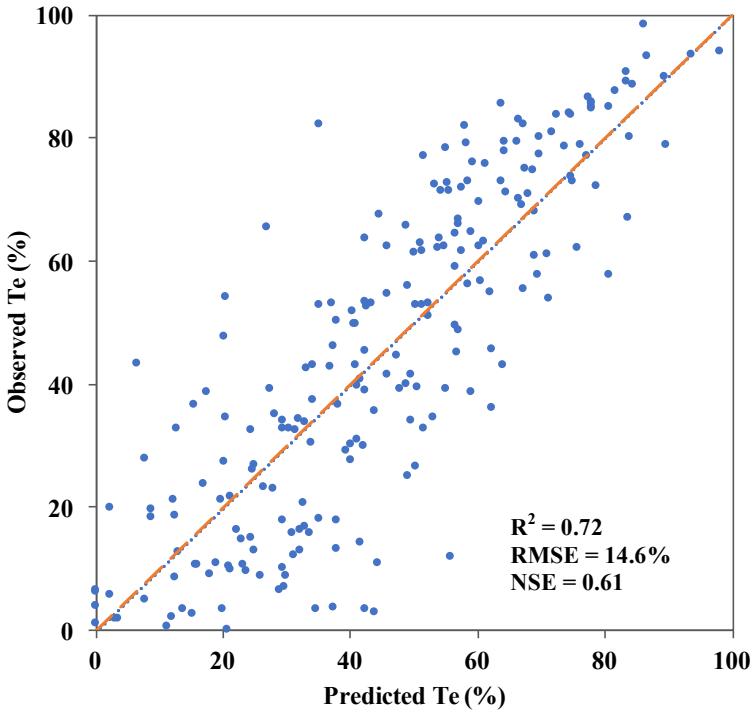

Figure 3.9. Evaluation of the Te predicted by the regression model (Eq. 2) and the Te calculated using remote sensing sediment data (n =222). The orange line is the 1:1 line. The trend line falls on the 1:1 line.

For comparison, we calculated *Te* for these US dams using the Brune (1953) formula for individual reservoirs, later adopted globally by Vörösmarty et al. (2003) and Syvitski et al., (2005). This is currently the most widely used approach to represent sediment trapping in large-scale sediment transport models. This method predicts *Te* for individual reservoirs as a function of local water residence time change, calculated as the effective reservoir capacity divided by local mean annual discharge. Figure 3.10 shows a comparison between *Te* calculated using Eq. 2 and the Brune (1953) formula for reservoirs with > 0.5 km^3 storage capacity (defined as large reservoirs by Vörösmarty et al. (2003)). Our *Te* model results in noticeably different values compared to the Brune (1953) approach. The most widely accepted idea about reservoir trapping

efficiencies yielded by previous studies is that *Te* is very large for large reservoirs and small for small reservoirs. Williams and Wolman (1984) suggested that *Te* of large reservoirs are commonly greater than 99%. Vörösmarty et al. (2003) indicate that the *Te* of large reservoirs is typically ~85%. Contrary to these findings, remote sensing sediment data across the CONUS shows that, large reservoirs can have a wide range of *Te* values.

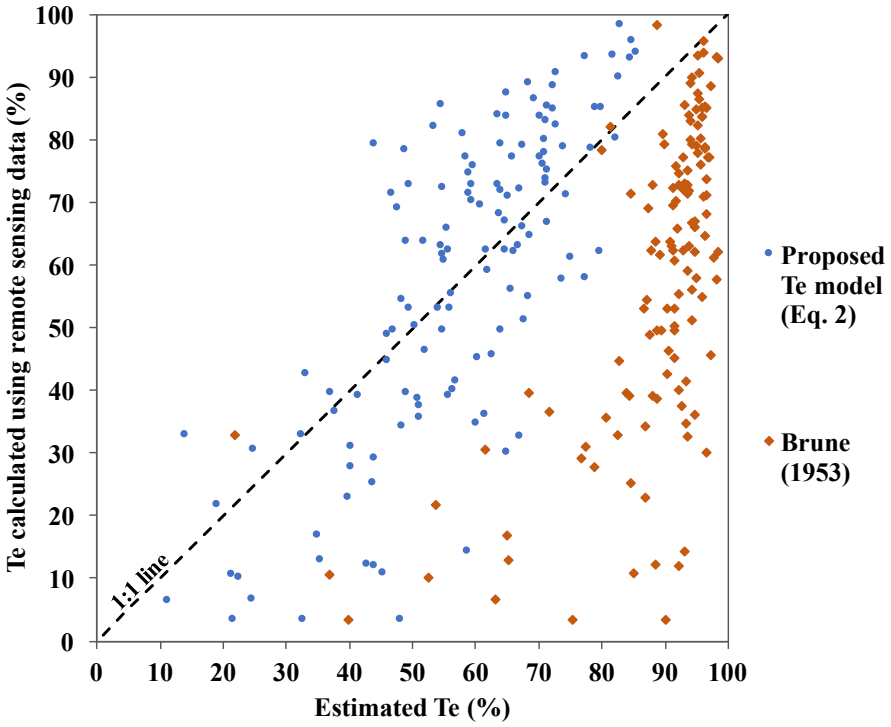

Figure 3.10. Comparison of Te calculated using the remote sensing data versus the proposed regression model (blue) and Brune (1953) method (red), for reservoirs with >0.5 km^3 storage capacity (n=65).

The new model (Eq. 2) provides new insights into the drivers of *Te*. The sediment flux entering the reservoir plays an important role in governing trapping within the reservoir and *Te* is higher for higher incoming sediment fluxes. This could be due to the availability of more materials for trapping, particularly if the proportion of larger particles which are more likely to

deposit within the reservoir, is higher. A study that looked at reservoir trapping for individual storm events found that, for similar detention times (length of time runoff from a storm event remains in the reservoir), high incoming sediment loads had higher *Te* (Rausch and Heinemann, 1975). Rausch and Schreiber (1981) also predicted *Te* for Callahan Reservoir by storm detention time, total storm runoff, and mean inflow sediment concentration. One criticism that conventional methods such as Brune (1953) receive is that they are developed for normally ponded reservoirs mostly located in temperate settings and do not yield accurate results for tropical rivers with highly variable inflows, desilting, or semi-dry reservoirs (Lewis et al., 2013; Verstraeten and Poesen, 2000). This may be because sediment trapping is highly influenced by the incoming sediment rates. The model proposed here addresses this issue by incorporating sediment inflow to the reservoir as a predictor variable.

The storage capacity of the dam impoundment is also included as a key variable indicating that larger reservoirs facilitate more trapping of sediment. Larger values of reservoir lengths provide sufficient time for sedimentation within the reservoir, leading to higher *Te* values. This parameter may be a proxy for sediment retention time of the reservoir which is widely used by methods such as Brune (1953) and Rausch and Heinemann (1975). If reservoir lengths cannot be calculated using established datasets such as NHDplus or GRanD reservoir polygons and river networks, it is advised to get the most representative reservoir length considering seasonality and reservoir operations.

Reservoir operating schemes and mechanisms, and timing of sediment release or flushing may be important variables that govern *Te* (Brandt, 2000; Kondolf et al., 2014a). However, incorporating these aspects into *Te* calculations is difficult due to data limitations, difficulty in predicting the timing of these mechanisms, and complexity in incorporating it into trapping

calculations. In this regard, the age of the dam as an explanatory variable may serve as a proxy, as newer dams tend to include sediment release mechanisms. However, dam age was found not to be a significant contributor to the model.

Reservoir storage and reservoir length parameters are widely available or can be extracted from existing datasets. Sediment fluxes into the reservoir and, in some cases, outgoing discharge are more challenging to obtain. To overcome the challenge of obtaining sediment data, a second model was developed using only widely available data to facilitate a wide range of applications:

$$Te = 60.78 - 21.93\log(Q_{out}) + 21.45\log(L) + 20.81\log(S) \quad (3)$$

Although this equation has a lower predictive accuracy compared to Eq. 2, it can also provide *Te* estimates with reasonable accuracy (R^2=0.61; Adj. R^2=0.60; RMSE = 17.1%).

A machine learning model development was also attempted. In machine learning techniques, large datasets help to learn 'hidden' patterns from the data and therefore have the potential to achieve higher accuracies than simple statistical methods (Lin et al., 2020). However, machine learning techniques are generally suitable for large datasets. The relatively small training dataset available in this study hindered the development of a robust machine learning model.

3.4 Global Te Model

We developed a third model for global-scale applications based on data from the commonly used Global Reservoir and Dam (GRanD) dataset (Lehner et al., 2011). In addition to

the remote sensing-derived *Te* of the 222 dams in the CONUS, 42 additional observed *Te* values outside the US were used to develop this model. The resulting model had an R^2=0.55 (Adj. R^2=0.54) and an RMSE of 19.2% using five explanatory variables:

$$Te = 34.74 - 20.9\log(Q_{out}) + 17.83\log(S) + 17.07\log(L) + 6.63\log(E) + 0.07H \quad (4)$$

where E is soil erosion from within the river reach catchment (tons per year per river reach) from Grill et al. (2019), and H is the dam height (m). Supplementary Figure S3.1 shows the performance of the global *Te* model (Eq. 4). Using this equation, *Te* was calculated for 6823 global dams in the GRanD database for which data were available for essential explanatory variables, and dam impoundments fall on the Grill et al. (2019) river network. For 70 GRanD dams that did not have reservoir polygons (e.g., individual dams that do not form reservoirs), a zero *Te* was assigned to indicate no sediment trapping for sediment modeling efforts. In addition, 54 dams primarily built for navigation were also assigned a zero *Te*. The resulting global *Te* dataset (Figure 3.11) had an average *Te* of 53.5% (Table 3.2).

Table 3.2: Descriptive statistics of Te values calculated using the global model.

	Number of Reservoirs	**Sum of reservoir capacities (km^3)***	**Mean *Te* (%)**	**Median *Te* (%)**	**Standard deviation *Te* (%)**
Global	**6823**	**6746 (1.0)**	**53.5**	**55.7**	**19.2**
Africa	624	1043.5 (1.67)	55.7	56.8	18.1
Asia	2203	2365.5 (1.07)	54.0	55.5	17.6
Australia and Oceania	234	95.5 (0.41)	52.2	55.8	22.5
Europe	1245	585.4 (0.47)	50.2	53.9	20.3
North America	2177	1734.5 (0.80)	53.7	56.0	20.1
South America	340	922 (2.7)	57.8	59.2	17.5

*the number within parenthesis is the mean reservoir capacity

Continental-scale analysis (Table 3.2) shows that the differences between continents in terms of average and median *Te* are small at this scale. South America, contrary to the relatively low *Te* values observed by Vörösmarty et al. (2003), has the highest average *Te*. This may be due to the recent constructions of large dams in the Amazon basin, specially in areas with high sediment yield (Latrubesse et al., 2017; Li et al., 2020), which were not included in Vörösmarty et al. (2003). Although the number of dams and the total reservoir storage capacity are lower in this continent, it has the highest mean reservoir capacity which can lead to larger *Te* values according to the proposed equation. Dams in Africa have the second highest average *Te* (55.7%) in agreement with Vörösmarty et al. (2003) likely due to (i) high proportion of dams in arid regions, (ii) the resulting need to have large reservoir capacities to stabilize highly variable river flows, and (iii) generally low river discharges (Vörösmarty et al., 2003). Although these conditions are similar to Australia and Oceania which has the smallest number of reservoirs and the lowest sum of storage capacities in GRanD, the continent resulted in a relatively lower average *Te* than expected. This is due to the large number of hydroelectric dams located in Tasmania and New Zealand with shorter water storage times and frequent water releases, which can reduce their *Te*. Asia and North America have the first and second largest number of dams in GRanD and the greatest sum of reservoir capacities, respectively, with a moderate continental average for *Te*. It is also important to note that these continental *Te* values are not representative of the overall *Te* of river basins, but are the averages of individual dam trapping efficiencies for each continent.

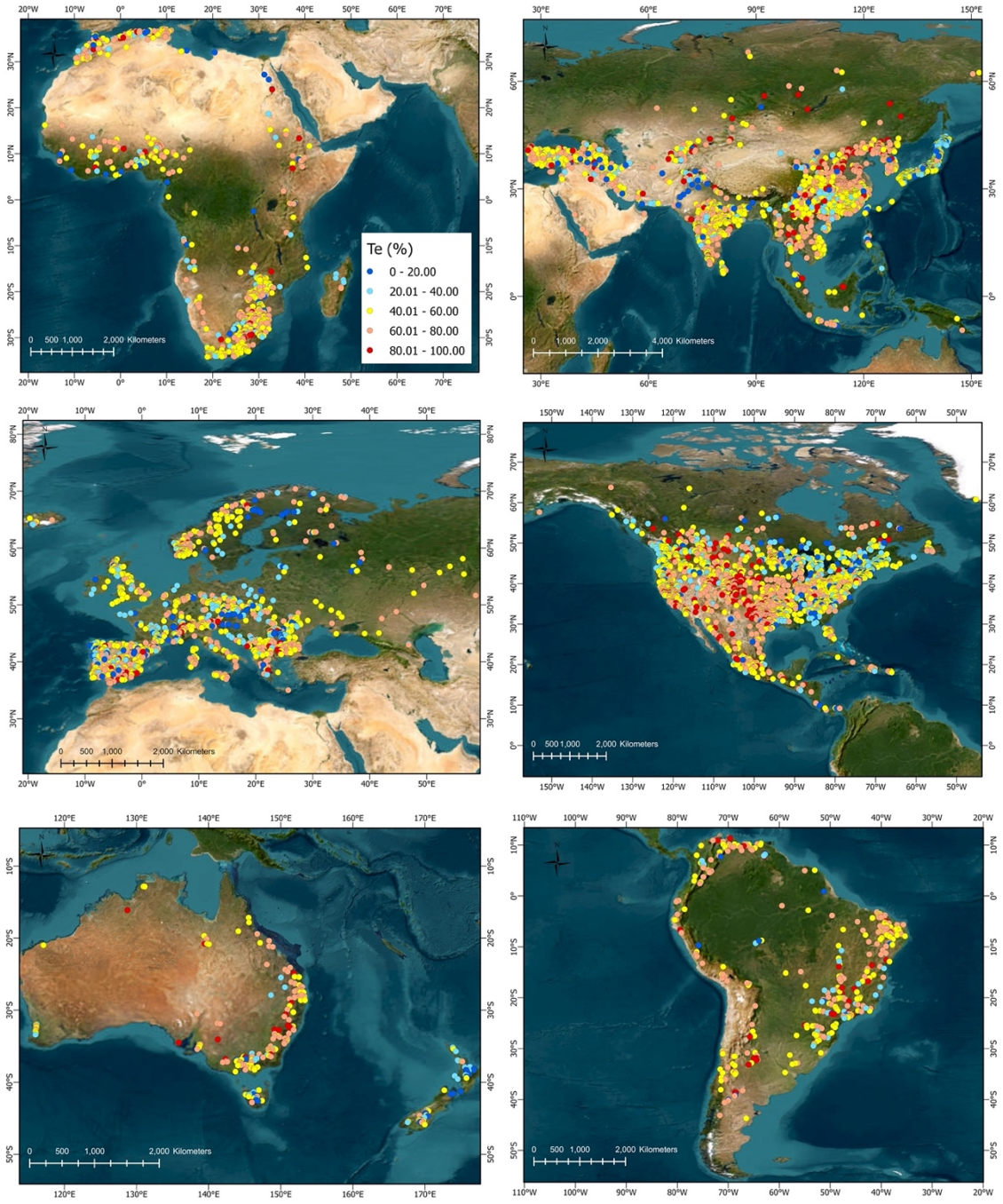

Figure 3.11. Global distribution of Reservoir Te (%) calculated using equation 4 for 6823 dams in the GRanD dataset.

In order to test the regional dependency of *Te*, we tested the explanatory variables to develop an equation only involving dam impoundments in China. *Te* for dams in China can be

predicted with a high accuracy (R^2=0.80; Adj. R^2=0.78; RMSE = 11.25%) using only three variables;

$$Te = 230.44 - 43.3\log(D) + 20.21\log(S) + 29.24\log(SA) \quad (5)$$

where D is drainage area (km^2), and SA is reservoir surface area (km^2). The negative relationship that upstream drainage area (D) has with *Te* in this model can be explained by the negative relationship between Q and *Te* in the global model as well as the CONUS model. In regional settings, Q and D tend to have a strong correlation. This may also be indicative of the fact that large rivers with large drainage areas can have smaller *Te* values in this region. However, it should be noted that all the observed *Te* values used to develop this equation are from the literature as opposed to the CONUS and global-scale analysis based on remote sensing data.

These different models for different regions indicate that *Te* may have a strong regional dependency and it may be more accurate to develop regional models (for regions smaller than continental scale) or calibrations for different settings. Some of the reasons for this regional dependency may include climate, river flow regimes, and dam type and operation. Our global *Te* model has a relatively lower predictive capability compared to the CONUS *Te* model, largely due to data limitations. The remote sensing SSC dataset used here for the CONUS is currently in the process of being expanded globally. Once this product is available, observed *Te* can be calculated for global dams, allowing us to develop more robust empirical models for predicting global *Te* and potentially use machine learning techniques.

4. Conclusion

Scarcity in sediment monitoring has limited the accuracy and universal applicability of reservoir sediment trapping parameterization in hydro-geomorphic models. Emerging remote sensing approaches now provide sediment concentration data at large spatial scales, offering unparalleled opportunities to improve our understanding of river sediment transport dynamics. Using such a dataset, we developed empirical models for calculating *Te*, based on dam, riverine, and basin attributes. The simplicity of the models will allow modelers to easily incorporate them into their fluvial sediment models, potentially considerably improving the models' ability to represent the effects of anthropogenic activities on sediment dynamics. The results demonstrate that remote sensing-based *Te* calculations can be particularly useful for large-scale hydrological models to represent the trapping efficiencies of reservoirs more realistically than currently available methods derived using theoretical approaches.

A comparison between USGS measured depth-averaged sediment fluxes and remote sensing-calculated surface sediment fluxes was conducted for 36 gauging stations. The results showed that, with an adjustment factor of 4.45, remote sensing-derived sediment strongly aligned with in-situ observations. In this study, we developed data-driven CONUS and global models to predict *Te* using remote sensing observations of long-term sediment data in the US. When compared with the *Te* calculated by previous methods, remote sensing data across the CONUS reveal that large reservoirs can have a wide range of *Te* values. This is contrary to the common assertion that *Te* is very large for large reservoirs and vice versa.

The development of regional and global models to predict *Te* revealed that regional models better predict *Te*, but global *Te* estimates are possible and can be used in global sediment

transport modeling. We found that reservoir characteristics, and fluvial sediment and water flux metrics are important controls of *Te* in both regional and global models.

Future work will include the implementation of the developed sediment trapping model within the WBMsed hydro-geomorphic modeling framework (Cohen et al., 2013, 2014). WBMsed is a spatially and temporally explicit global-scale model with a robust hydrological framework and well-established sediment modules. WBMsed *Te* module is currently based on the Vörösmarty et al. (2003) model. With forthcoming global remote sensing products of SSC, *Te* may also be dynamically assimilated directly for a large dataset of global dams. Improving the representation of sediment trapping in hydro-geomorphic models will aid in predicting current and future river sediment transport, quantifying the global sediment delivery into the ocean, studying ecological impacts associated with sediment in freshwater systems, and understanding anthropogenic influences on riverine fluxes.

Supplementary materials for chapter 3

Table S3.1. USGS gage observations (O-) used for validation of suspended sediment flux (Qs) and discharge (Q)

ID	USGS site #	Lat	Lon	Area (km^2)	USGS O-Qs time period	USGS O-Qs (kg/s)	USGS O-Q (m^3/s)	Remote sensing Qs (kg/s)	NHDplus Q (m^3/s)
1	01357500	42.79	-73.71	8,935	2003-2018	15.05	179.84	3.99	171.91
2	06486000	42.49	-96.41	814,811	1992-2019	257.31	909.59	40.53	1066.60
3	06610000	41.26	-95.92	836,049	1992-2019	476.65	1056.64	65.95	1065.09
4	06807000	40.68	-95.85	1,061,896	1992-2019	736.73	1259.21	118.54	1262.72
5	01331095	42.94	-73.65	9,772	1992-2001	2.61	198.59	2.05	183.99
6	05587455	38.95	-90.37	443,665	1990-2016	690.98	3665.79	204.44	3681.30
7	12340500	46.88	-113.93	15,594	1989-2016	3.65	79.48	1.14	83.65
8	07020500	37.90	-89.83	1,835,267	1988-2016	2659.89	6810.37	638.16	6483.72
9	04193500	41.50	-83.71	16,395	1988-2003	36.70	171.62	11.46	157.98
10	02489500	30.79	-89.82	17,024	1986-1993	39.20	284.70	15.35	330.61

11	05474000	40.75	-91.28	11,168	1985-2019	64.06	100.35	7.37	90.94
12	06452000	43.75	-99.56	25,680	1985-2019	111.70	21.61	3.08	17.83
13	05465500	41.18	-91.18	32,375	1985-2019	74.09	313.70	12.19	282.50
14	11303500	37.68	-121.27	35,066	1985-2019	7.79	108.86	3.68	134.60
15	08330000	35.09	-106.68	45,169	1985-2019	28.16	33.52	7.76	39.21
16	08332010	34.42	-106.80	49,806	1985-2019	24.67	28.87	5.86	27.66
17	08354900	34.26	-106.89	69,334	1985-2019	81.17	29.15	5.99	26.07
18	08358400	33.68	-107.00	71,743	1985-2019	71.14	22.33	9.30	24.72
19	11447650	38.46	-121.50	nan	1985-2019	41.72	587.21	15.39	749.23
20	05325000	44.17	-94.00	38,591	1985-2017	46.22	186.17	5.35	141.84
21	07010000	38.63	-90.18	1,805,223	1985-2017	2642.23	6522.81	572.56	6194.66
22	07022000	37.22	-89.46	1,847,181	1985-2017	2557.32	7081.22	658.07	6699.36
23	05586100	39.70	-90.65	69,264	1985-2011	170.20	740.62	39.04	722.86
24	05481650	41.68	-93.67	15,128	1985-2004	5.63	114.59	2.24	110.19
25	04198000	41.31	-83.16	3,240	1985-2002	7.62	36.61	2.44	33.25
26	05288500	45.13	-93.30	49,469	1985-1996	7.84	284.49	4.21	272.13
27	02116500	35.86	-80.39	5,905	1985-1994	20.40	82.78	4.81	91.75
28	09364500	36.72	-108.20	3,522	1985-1993	13.19	22.66	1.63	25.67
29	09217000	41.52	-109.45	36,260	1985-1992	3.16	41.63	1.28	53.22
30	01638500	39.27	-77.54	24,996	1985-1991	35.13	286.29	7.15	301.42
31	06115200	47.63	-108.69	105,281	1985-1991	138.49	231.88	23.02	268.70
32	06329500	47.68	-104.16	178,966	1985-1991	206.37	320.78	54.76	353.50
33	01567000	40.48	-77.13	8,687	1985-1990	2.83	127.17	2.63	130.88
34	05454500	41.66	-91.54	8,472	1985-1987	8.45	79.30	2.06	71.13
35	09368000	36.78	-108.68	33,411	1985-1986	108.66	47.48	4.61	61.73
36	12334550	46.83	-113.81	9,472	1986-2016	1.61	37.22	0.85	40.15

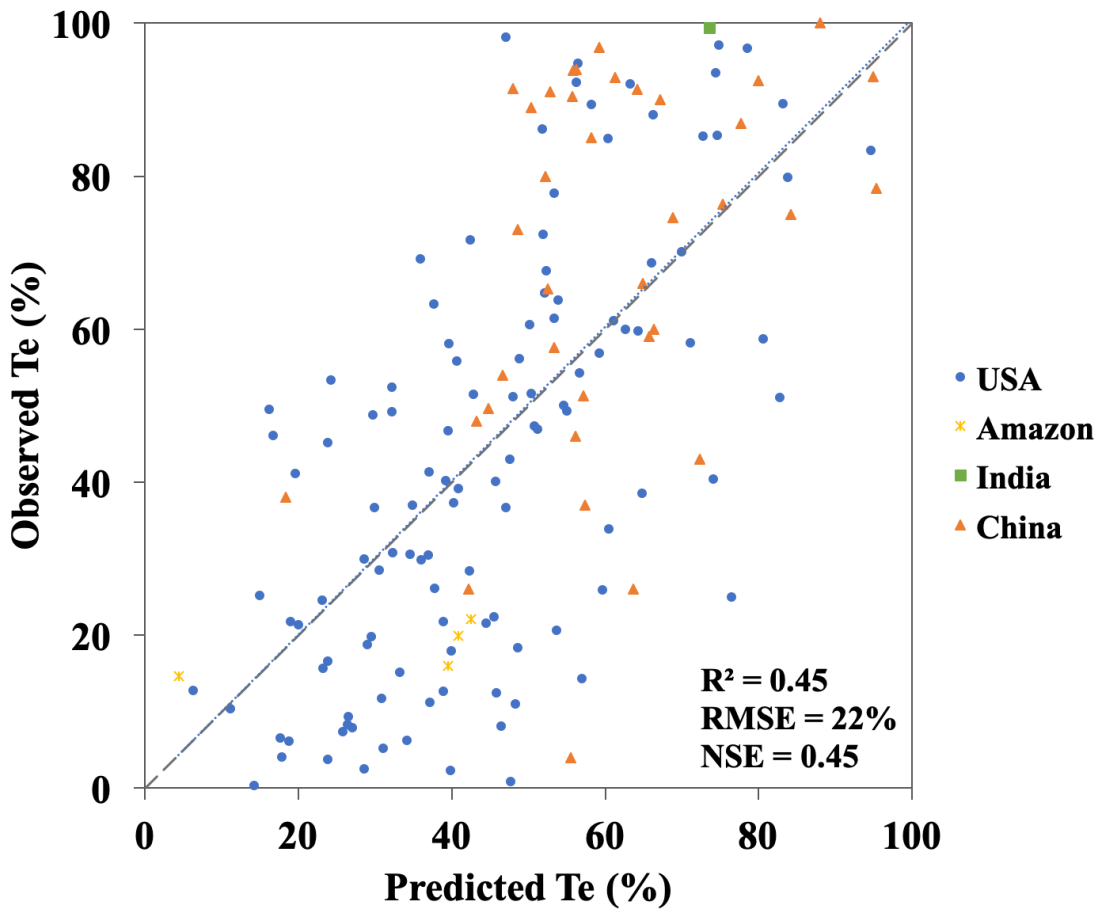

Figure S3.2. Evaluation of the global Te regression model (Eq. 4) and observed Te from remote sensing sediment data for dams in the US and Amazon, and from literature for dams in India and China (n =158). The grey line is the 1:1 line. The trend line falls on the 1:1 line.

5. References for Chapter 3

Best, J. and Darby, S.E. (2020). The Pace of Human-Induced Change in Large Rivers: Stresses, Resilience, and Vulnerability to Extreme Events. *One Earth*, *2*(6), pp.510-514.

Best, J. (2019). Anthropogenic stresses on the world's big rivers. *Nature Geoscience*, *12*(1), pp.7-21.

Biswas, A.K. and Tortajada, C. (2012). Impacts of the high Aswan Dam. In *Impacts of large dams: A global assessment* (pp. 379-395). Springer, Berlin, Heidelberg.

Blanchard, R.A., Ellison, C.A., Galloway, J.M., and Evans, D.A. (2011), Sediment concentrations, loads, and particle- size distributions in the Red River of the North and selected tributaries near Fargo, North Dakota, during the 2010 spring high-flow event: U.S. Geological Survey Scientific Investigations Report 2011–5064.

Borland, W.M. (1971). Reservoir sedimentation. In Shen, H.W., editor, River mechanics. Vol. II, Fort Collins, CO: Colorado State University, 29.1–29.38.

Brandt, S. A. (2000). Classification of geomorphological effects downstream of dams. *Catena*, *40*(4), 375-401.

Brismar, A. (2002). River systems as providers of goods and services: a basis for comparing desired and undesired effects of large dam projects. Environmental management, 29(5), pp.598-609.

Brown, C.B. (1943). Discussion of Sedimentation in reservoirs, by J. Witzig. Proceedings of the American Society of Civil Engineers 69, 1493–1500.

Brune, G.M. (1953). Trap efficiency of reservoirs. Eos, Transactions American Geophysical Union, 34(3), pp.407-418.

Chakrapani, G. J. (2005). Factors controlling variations in river sediment loads. Current science, 569-575.

Chen, C. (1975). Design of sediment retention basins. In Proceedings, national symposium on urban hydrology and sediment control, July, Lexington, KY: University of Kentucky, 285–98.

Churchill, M.A. (1948). Discussion of Analyses and use of reservoir sedimentation data by L.C. Gottschalk. In Proceedings of the federal inter- agency sedimentation conference, Denver, Colorado, Washington, DC: US Geological Survey, 139–40.

Cohen, S., Kettner, A.J., Syvitski, J.P. and Fekete, B.M. (2013). WBMsed, a distributed global-scale riverine sediment flux model: Model description and validation. *Computers & Geosciences*, *53*, pp.80-93.

Cohen, S., Kettner, A.J. and Syvitski, J.P. (2014). Global suspended sediment and water discharge dynamics between 1960 and 2010: Continental trends and intra-basin sensitivity. *global and planetary change*, *115*, pp.44-58.

Condé, R.D.C., Martinez, J.M., Pessotto, M.A., Villar, R., Cochonneau, G., Henry, R., Lopes, W. and Nogueira, M. (2019). Indirect assessment of sedimentation in hydropower dams using MODIS remote sensing images. Remote Sensing, 11(3), p.314.

Dethier, E.N., Renshaw, C.E. and Magilligan, F.J. (2020). Toward improved accuracy of remote sensing approaches for quantifying suspended sediment: Implications for suspended-sediment monitoring. Journal of Geophysical Research: Earth Surface, 125(7), p.e2019JF005033.

Dunn, F.E., Darby, S.E., Nicholls, R.J., Cohen, S., Zarfl, C. and Fekete, B.M. (2019). Projections of declining fluvial sediment delivery to major deltas worldwide in response to climate change and anthropogenic stress. *Environmental Research Letters*, *14*(8), p.084034.

Espinosa-Villegas, C. O., & Schnoor, J. L. (2009). Comparison of long-term observed sediment trap efficiency with empirical equations for Coralville Reservoir, Iowa. *Journal of Environmental Engineering*, *135*(7), 518-525.

ESRI, (2021). USA Detailed Water Bodies layer package for ArcGIS (downloaded from https://www.arcgis.com/home/item.html?id=84e780692f644e2d93cefc80ae1eba3a)

Gardner, J. R., Yang, X., Topp, S. N., Ross, M. R. V., Altenau, E. H., & Pavelsky, T. M. (2021). The color of rivers. Geophysical Research Letters, 48, e2020GL088946. https://doi.org/10.1029/2020GL088946.

Gardner, J., Pavelsky, T. M., Topp, S., Yang, X., Ross, M. R., & Cohen, S. (2023). Human activities change suspended sediment concentration along rivers. Environmental Research Letters, 18, 064032.

Gardner, J., Pavelsky, T., Yang, X., Topp, S., & Ross, M. (2022). River Sediment Database (RiverSed) (v1.0.0) [Dataset]. Zenodo. https://doi.org/10.5281/zenodo.4900563

Grill, G., Lehner, B., Thieme, M., Geenen, B., Tickner, D., Antonelli, F., Babu, S., Borrelli, P., Cheng, L., Crochetiere, H. and Macedo, H.E. (2019). Mapping the world's free-flowing rivers. *Nature*, *569*(7755), pp.215-221.

Haddeland, I., Heinke, J., Biemans, H., Eisner, S., Flörke, M., Hanasaki, N., Konzmann, M., Ludwig, F., Masaki, Y., Schewe, J. and Stacke, T. (2014). Global water resources affected by human interventions and climate change. Proceedings of the National Academy of Sciences,111(9), pp.3251-3256.

Heinemann, H.G. (1984). Reservoir trap efficiency. In Hadley, R.F. and Walling, D.E., editors, Erosion and sediment yield: some methods of measurement and modelling, Norwich: GeoBooks, 201–18.

Hu, B., Yang, Z., Wang, H., Sun, X., Bi, N. and Li, G. (2009). Sedimentation in the Three Gorges Dam and the future trend of Changjiang (Yangtze River) sediment flux to the sea. *Hydrology and Earth System Sciences*, *13*(11), pp.2253-2264.

Jothiprakash, V. and Vaibhav, G.A.R.G. (2008). Re-look to conventional techniques for trapping efficiency estimation of a reservoir. *International Journal of Sediment Research*, *23*(1), pp.76-84.

Kettner, A. J., & Syvitski, J. P. (2008). HydroTrend v. 3.0: A climate-driven hydrological transport model that simulates discharge and sediment load leaving a river system. *Computers & Geosciences*, *34*(10), 1170-1183.

Kondolf, G.M., Gao, Y., Annandale, G.W., Morris, G.L., Jiang, E., Zhang, J., Cao, Y., Carling, P., Fu, K., Guo, Q. and Hotchkiss, R. (2014a). Sustainable sediment management in reservoirs and regulated rivers: Experiences from five continents. *Earth's Future*, *2*(5), pp.256-280.

Kondolf, G.M., Rubin, Z.K. and Minear, J.T. (2014b). Dams on the Mekong: Cumulative sediment starvation. *Water Resources Research*, *50*(6), pp.5158-5169.

Kummu, M., Lu, X. X., Wang, J. J., & Varis, O. (2010). Basin-wide sediment trapping efficiency of emerging reservoirs along the Mekong. *Geomorphology*, *119*(3-4), 181-197.

Kummu, M., & Varis, O. (2007). Sediment-related impacts due to upstream reservoir trapping, the Lower Mekong River. *Geomorphology*, *85*(3-4), 275-293.

Laguionie, P., Crave, A. and Jigorel, A. (2007). Velocity and suspended sediment concentration profiles in rivers: in situ measurements and flux modelling. *WIT Transactions on Ecology and the Environment*, *104*, pp.335-343.

Latrubesse, E.M., Arima, E.Y., Dunne, T., Park, E., Baker, V.R., d'Horta, F.M., Wight, C., Wittmann, F., Zuanon, J., Baker, P.A. and Ribas, C.C. (2017). Damming the rivers of the Amazon basin. *Nature*, *546*(7658), pp.363-369.

Lehner, B., Liermann, C.R., Revenga, C., Vörösmarty, C., Fekete, B., Crouzet, P., Döll, P., Endejan, M., Frenken, K., Magome, J. and Nilsson, C. (2011). Global reservoir and dam (grand) database. *Technical Documentation, Version*, *1*, pp.1-14.

Lewis, S.E., Bainbridge, Z.T., Kuhnert, P.M., Sherman, B.S., Henderson, B., Dougall, C., Cooper, M. and Brodie, J.E. (2013). Calculating sediment trapping efficiencies for reservoirs in tropical settings: a case study from the Burdekin Falls Dam, NE Australia. *Water Resources Research*, *49*(2), pp.1017-1029.

Li, H.Y., Tan, Z., Ma, H., Zhu, Z., Abeshu, G.W., Zhu, S., Cohen, S., Zhou, T., Xu, D. and Leung, L.R. (2022). A new large-scale suspended sediment model and its application over the United States. Hydrology and Earth System Sciences, 26(3), pp.665-688.

Li, T., Wang, S., Liu, Y., Fu, B., & Gao, D. (2020). Reversal of the sediment load increase in the Amazon basin influenced by divergent trends of sediment transport from the Solimões and Madeira Rivers. Catena, 195, 104804.

Lin, P., Pan, M., Allen, G.H., de Frasson, R.P., Zeng, Z., Yamazaki, D. and Wood, E.F. (2020). Global estimates of reach-level bankfull river width leveraging big data geospatial analysis. *Geophysical Research Letters*, *47*(7), p.e2019GL086405.

Liu, S., Li, D., Liu, D., Zhang, X. and Wang, Z. (2022). Characteristics of sedimentation and sediment trapping efficiency in the Three Gorges Reservoir, China. Catena, 208, p.105715.

McKay, L., Bondelid, T., Dewald, T., Rea, A., Johnston, C. and Moore, R. (2015). NHDPlus version 2: user guide (data model version 2.1). *Horizon Systems*.

Markert, K.N., Schmidt, C.M., Griffin, R.E., Flores, A.I., Poortinga, A., Saah, D.S., Muench, R.E., Clinton, N.E., Chishtie, F., Kityuttachai, K. and Someth, P. (2018). Historical and operational monitoring of surface sediments in the lower mekong basin using landsat and google earth engine cloud computing. Remote Sensing, 10(6), p.909.

Moore, R.B., McKay, L.D., Rea, A.H., Bondelid, T.R., Price, C.V., Dewald, T.G., and Johnston, C.M. (2019). User's guide for the national hydrography dataset plus (NHDPlus) high resolution: U.S. Geological Survey Open-File Report 2019– 1096, 66 p., https://doi.org/10.3133/ofr20191096.

Mulligan, M., van Soesbergen, A. and Sáenz, L. (2020). GOODD, a global dataset of more than 38,000 georeferenced dams. *Scientific Data*, *7*(1), pp.1-8.

Narayanan, A. (2022). Sediment Response to Deforestation in the Amazon River Basin. Master's Thesis, University of Alabama, USA.

Overeem, I., Hudson, B.D., Syvitski, J.P., Mikkelsen, A.B., Hasholt, B., Van Den Broeke, M.R., Noël, B.P.Y. and Morlighem, M. (2017). Substantial export of suspended sediment to the global oceans from glacial erosion in Greenland. Nature Geoscience, 10(11), pp.859-863.

Peteuil, C. (2012). Sediment management of hydropower cascade: example of CNR run-of-river developments, French Rhone River, France. 5th International Yellow River Forum, China.

Rausch, D.L. and Heinemann, H.G. (1975). Controlling reservoir trap efficiency. *Transactions of the ASAE*, *18*(6), pp.1105-1108.

Rausch, D.L. and Schreiber, J.D. (1981). *Sediment and nutrient trap efficiency of a small flood-detention reservoir* (Vol. 10, No. 3, pp. 288-293). American Society of Agronomy, Crop Science Society of America, and Soil Science Society of America.

Renwick, W.H., Smith, S.V., Bartley, J.D. and Buddemeier, R.W. (2005). The role of impoundments in the sediment budget of the conterminous United States. Geomorphology, 71(1-2), pp.99-111.

Ross, M.R., Topp, S.N., Appling, A.P., Yang, X., Kuhn, C., Butman, D., Simard, M. and Pavelsky, T.M. (2019). AquaSat: A data set to enable remote sensing of water quality for inland waters. Water Resources Research, 55(11), pp.10012-10025.

Schmidt, J.C. and Wilcock, P.R. (2008). Metrics for assessing the downstream effects of dams. *Water Resources Research*, *44*(4).

Sharma, D.K., Sharma, S.K. and Suri, S. (2018). Sediment Management of Projects on Himalayan Rivers-A Case Study of Bhakra Dam and Beas Sutlej Link Project. *INCOLD Journal (A Half Yearly Technical Journal of Indian Committee on Large Dams)*, *7*(2), pp.3-8.

Syvitski, J. P. (2003). Supply and flux of sediment along hydrological pathways: research for the 21st century. *Global and Planetary Change*, *39*(1-2), 1-11.

Syvitski, J. P., Vörösmarty, C. J., Kettner, A. J., & Green, P. (2005). Impact of humans on the flux of terrestrial sediment to the global coastal ocean. *science*, *308*(5720), 376-380.

Syvitski, J., Ángel, J. R., Saito, Y., Overeem, I., Vörösmarty, C. J., Wang, H., & Olago, D. (2022). Earth's sediment cycle during the Anthropocene. Nature Reviews Earth & Environment, 3(3), 179-196.

Syvitski, J.P., Milliman, J.D. (2007). Geology, geography, and humans battle for dominance over the delivery of fluvial sediment to the coastal ocean. J. Geol.115 (1), pp.1–19.

Syvitski, J., Cohen, S., Miara, A. and Best, J. (2019). River temperature and the thermal-dynamic transport of sediment. Global and Planetary Change, 178, pp.168-183.

Tan, G., Chen, P., Deng, J., Xu, Q., Tang, R., Feng, Z., & Yi, R. (2019). Review and improvement of conventional models for reservoir sediment trapping efficiency. *Heliyon*, *5*(9), e02458.

USDA-SCS, (1983). National engineering hand- book (2nd edn) (Section 3: 'Sedimentation'; Chapter 8 'Sediment storage design criteria') Washington, DC: US Department of Agriculture.

Trabucco, A. and Zomer, R.J. (2019). Global aridity index and potential evapotranspiration (ET0) climate database v2. *CGIAR Consort Spat Inf*, *10*, p.m9.

Verstraeten, G. and Poesen, J. (2000). Estimating trap efficiency of small reservoirs and ponds: methods and implications for the assessment of sediment yield. *Progress in Physical Geography*, *24*(2), pp.219-251.

Vörösmarty, C.J., Meybeck, M., Fekete, B., Sharma, K., Green, P., Syvitski, J.P.M. (2003). Anthropogenic sediment retention: major global impact from registered river impoundments. Glob. Planet. Chang. 39 (1–2), pp.169–190.

Walling, D.E. (2012). The role of dams in the global sediment budget. *IAHS-AISH publication*, pp.3-11.

Wang, J., Walter, B.A., Yao, F., Song, C., Ding, M., Maroof, A.S., Zhu, J., Fan, C., McAlister, J.M., Sikder, S. and Sheng, Y. (2022). GeoDAR: georeferenced global dams and reservoirs dataset for bridging attributes and geolocations. Earth System Science Data, 14(4), pp.1869-1899.

Wei, X., Sauvage, S., Ouillon, S., Le, T. P. Q., Orange, D., Herrmann, M., & Sanchez-Perez, J. M. (2021). A modelling-based assessment of suspended sediment transport related to new damming in the Red River basin from 2000 to 2013. *Catena*, *197*, 104958.

Wohl, E. and Rathburn, S. (2003). Mitigation of sedimentation hazards downstream from reservoirs. *International Journal of Sediment Research*, *18*(2), pp.97-106.

Williams, G.P. and Wolman, M.G. (1984). *Downstream effects of dams on alluvial rivers* (Vol. 1286). US Government Printing Office.

Wu, Z., Zhao, D., Syvitski, J.P., Saito, Y., Zhou, J. and Wang, M. (2020). Anthropogenic impacts on the decreasing sediment loads of nine major rivers in China, 1954–2015. *Science of the Total Environment*, *739*, p.139653.

Yang, X., Pavelsky, T.M., Ross, M.R., Januchowski-Hartley, S.R., Dolan, W., Altenau, E.H., Belanger, M., Byron, D., Durand, M., Van Dusen, I. and Galit, H. (2022). Mapping flow-obstructing structures on global rivers. Water Resources Research, 58(1), p.e2021WR030386.

Zarfl, C., Lumsdon, A.E., Berlekamp, J., Tydecks, L., and Tockner, K. (2015). A global boom in hydropower dam construction. Aquat. Sci. 77, 161–171, https://doi.org/10. 1007/s00027-014-0377-0.

Ziegler, C.K. and Nisbet, B.S. (1995). Long-term simulation of fine-grained sediment transport in large reservoir. Journal of Hydraulic Engineering, 121(11), pp.773-781.

CHAPTER 4

SIMULATING ANTHROPOGENIC INFLUENCE ON FLUVIAL SEDIMENT DYNAMICS USING A GLOBAL RIVER SEDIMENT MODEL

Abstract

Riverine sediment is an important agent of material transport on the Earth, contributing to maintaining the connectivity between the planet's terrestrial realm, freshwater systems, and the ocean. Soil erosion and sediment transport through rivers are highly influenced by human activities such as land use changes and dam construction. In this study, we analyze the potential impact of land use change and sediment trapping on suspended sediment dynamics in large global rivers. We introduce a new sediment transport module within the WBMsed global scale hydro-geomorphic modeling framework, termed WBMsed-ELM. The new module includes a physically-based hillslope soil erosion and a mass-conserving sediment routing approach. These allow for more explicit representations of anthropogenic factors (i.e. sediment trapping behind dams and land use changes). The validation of model-predicted sediment fluxes against observed data shows that WBMsed-ELM has similar level of predictive skills as the original WBMsed model in capturing the spatial variability of long-term averaged global river sediment fluxes. Using this new model, we simulated the individual and combined impacts of croplands and dams on river sediment fluxes. Our predicted soil erosion in croplands is 11.9 billion tons per year for the year 2000, in agreement with the estimates in the literature. According to WBMsed-ELM, croplands alone have increased average global river sediment fluxes by 63.4% between 1960 and 2014. In contrast, dams have reduced the sediment load to the ocean by 19.1% only considering

large rivers. Comparison against longitudinal sediment dynamics from remote sensing show that the model does not represent well the sediment recovery downstream of dams. Due to this, our estimates of the global contemporary suspended sediment flux to the global ocean from large river outlets which is 0.12 billion tons per year, is much less than previous estimates. Considering the combined effect of land use changes and sediment trapping behind dams, WBMsed-ELM estimates that there is a net global increase of 6.4% in sediment delivery to the ocean, compared to pristine conditions.

1. Introduction

Sediment transported by river flows plays a key role in ecosystem functioning, biogeochemical cycling and geomorphological processes of the Earth (Vörösmarty et al., 2003; Walling and Fang, 2003). Sediment is responsible for creating landform features such as deltas and governing river channel morphology (Bamunawala et al., 2018; Ibáñez et al., 2019). As a major water quality indicator, it determines the turbidity of water flowing in rivers and can turn rivers into non-usable muddy water if in excess, also leading to an increase in flood risk due to sediment deposition (Battista et al., 2020; Lamb et al., 2020). Sediment contains and transports eroded soil from hillslopes to downstream areas, along with the nutrients and agricultural/industrial pollutants attached to them, acting as an important agent of nutrient and pollutant transport (Boardman et al., 2019; Walling, 2009). Especially, the significant contribution of particulate organic carbon to the Earth's terrestrial carbon budget is increasingly being recognized (Tan et al., 2017; Zhang et al., 2020). Alterations to the river sediment equilibrium may disrupt riverine, coastal, and marine ecosystem functioning as well as human water uses, and undermine the stability of man-made infrastructure (Battista et al., 2020;

Vercruysse et al., 2017). Therefore, evaluating and predicting these changes in river sediment fluxes is vital to understand the quality of available water resources on the planet and the functioning of earth surface processes (Haddeland et al., 2014; Tsuruta et al., 2018). While the processes governing each stage of the sediment transport continuum are fairly well understood – detachment of organic and inorganic matter from land surface through erosion, transport through runoff to a nearby stream, and transported downstream through suspension, deposition and resuspension in the water column toward the basin outlet – the combined interconnectivity of these stages is highly variable and complex in nature (Fryirs, 2013).

Human activities have substantially altered the natural sediment loads of global rivers in recent decades (Grill et al., 2019; Syvitski et al., 2022). For example, researchers have estimated that the fluvial sediment flux to the oceans decreased by about 26% between 1950 and 2000 due to the trapping of sediment by dams (Syvitski et al., 2005). On the other hand, agricultural expansion and deforestation have led to increased soil erosion and sediment supply from land through land clearing, soil disturbance, and irrigation (Garcia-Ruiz et al., 2015; Walling, 2009), while conservation agriculture and reduced tillage has shown to decrease sediment loads in the recent decades in countries such as the United States and Argentina (Li and Fang, 2016; Tan et al., 2021). Although a general scientific understanding about the relationships between natural sediment transport processes and anthropogenic influences exists, including them in predictive modeling frameworks is a challenging task (Cohen et al., 2014; Tsuruta et al., 2018). Such models can be used to elucidate the effect of anthropogenic modifications of the landscape, climate, and freshwater systems on riverine fluxes, study the influence of individual stressors, simulate future or theoretical change scenarios, quantify changes in ungagged locations, and predict spatial and temporal dynamics across the river systems from local to global scales

(Merritt et al., 2003). Although, the scientific literature has seen great advancements in numerical modeling of fluvial sediment at various scales over the past few decades, explicitly and accurately representing anthropogenic drivers in these models over large scales is still evolving (Fagundes et al., 2020). In this regard, progress has been made in recent years in enhancing and adopting existing complex physically-based models for application in large spatial scales (i.e. global) and improving the availability of the required input data (Li et al., 2022).

In this study, we developed a new global riverine sediment transport module within the WBMsed framework which features an explicit and process-based representation of soil erosion, along with sediment trapping behind dams. This allows us to investigate the effect of landscape processes and their anthropogenic modifications on global fluvial sediment fluxes. This new development utilized the capabilities of the WBMsed global-scale hydro-geomorphic model, which simulates spatially and temporally explicit water and sediment fluxes (Cohen et al., 2013, 2014). WBMsed is a suite of sediment modules (Cohen et al., 2022) within the WBMplus global daily water balance/transport model (Wisser et al., 2010), which constitutes a key element in the FrAMES hydrological–biogeochemical modeling framework (Wollheim et al., 2008). WBMsed's current suspended sediment module employs the BQART empirical model (Syvitski and Milliman, 2007) as its governing equation for calculating long-term average suspended sediment loads. The stochastic Psi equation (Morehead et al., 2003) is used to calculate daily sediment loads to capture the intra- and inter-annual variability observed in natural river systems (Morehead et al., 2003; Cohen et al., 2014). This model has been proven to be successful in predicting suspended sediment loads in global rivers and studying different mechanisms and drivers associated with these processes (e.g. Cohen et al., 2013, 2014; Syvitski et al., 2014, 2019;

Taylor et al., 2015). However, the empirical nature of the equations has its limitations and restricts our ability to understand the underlying physical processes in sediment transport and the mechanisms by which they are affected by various drivers of change. Although empirical models are simple to use and conceptually easy to understand, they can be ineffective for simulating environments outside those that were used to develop and calibrate them (De Vente et al., 2013; Tan et al., 2018). Also, the model currently does not explicitly route sediment along the river network, but rather predicts sediment load for each pixel, based on its upstream basin-averaged conditions.

The new sediment transport module, presented herein, includes (i) a hillslope soil erosion component to represent hillslope sediment supply to rivers, (ii) more explicit and improved representations of anthropogenic factors (i.e. dam construction and land use changes) that affect fluvial sediment dynamics, and (iii) process-based sediment yield representations and sediment routing in place of current empirical equations. However, it should be noted that no models are practically fully physically based (Pandey et al., 2016). Numerous empirical/conceptual procedures are included in the mathematical expressions used in these models to simulate different processes. The purpose of incorporating more physically based representations is to (i) get a more accurate representation of sediment erosion, deposition, and transport processes, (ii) be able to include spatially varying soil properties and surface characteristics to represent the complexity of the natural environment, and (iii) better understand the driving forces of changes.

Several review papers published recently have compared the capabilities and limitations of existing erosion and sediment transport models (De Vente et al., 2013; Merritt et al., 2003; Pandey et al., 2016; Papnicolaou et al., 2008; Zi et al., 2019). By comparing the performance of eight well-known sediment yield models, Tan et al. (2018), found that the Morgan model

(Morgan, 2001) performs best in predicting the spatial variability of sediment fluxes at large spatial scales because of its more realistic representation of erosion and sediment transport processes. In addition, several new models were developed in recent years to simulate global-scale sediment dynamics which intended to capture various aspects of sediment transport in much detail as possible. Some of these models include Hatono and Yoshimura (2020), MOSART-sediment by Li et al. (2022), improved Morgan model by Tan et al. (2018), sediment transport model developed by Tsutura et al. (2018). These models differ significantly in structures, spatial and temporal scales, input data requirements, and represented physical processes. In regards to soil erosion, Borrelli et al. (2017) and Borrelli et al. (2020) used the Revised Universal Soil Loss Equation (RUSLE; Renard et al., 1997) to model global soil erosion potential at a high-resolution for the present and future, respectively. After careful consideration of the available global scale hillslope erosion and sediment transport models, we adopted the soil erosion module developed for the Energy Exascale Earth System Model (E3SM) land model (ELM), named ELM soil erosion model (ELM-Erosion) by Tan et al. (2021), to simulate hillslope erosion and land-based sediment supply in the new sediment module.

ELM-Erosion implements the Morgan-Morgan-Finney model (Morgan & Duzant, 2008), which is capable of representing soil erosion and sediment transport processes in diverse environments (Tan et al., 2018, 2020). This model also shows a considerable improvement over the RUSLE model with a more realistic representation of the influence of topography on soil erosion. The model also has an explicit representation of land use changes including the effect of cropland management actions (e.g. conservation agriculture, crop residue management). In the implementation of ELM-Erosion within WBMsed (termed WBMsed-ELM), we introduced a new sediment routing scheme to explicitly transport the eroded sediment along the river network.

This routing scheme considers the impacts of dams on sediment trapping, which is calculated using a newly developed reservoir trapping efficiency parameter (Moragoda et al., *in press;* Chapter 3).

We conducted separate validations for the model simulated sediment fluxes using a variety of independent observation datasets. The model was then used to simulate suspended sediment dynamics in large global rivers for the period between 1960 – 2014 in response to human activities. The subsequent analyses explore the contribution of various factors (trapping behind dams and land use change) and their combinations that drive the trends in global sediment dynamics.

2. Methods

2.1 WBMsed-ELM Model Description

The ELM-Erosion model was introduced as a new sediment module within the WBMsed framework. The ELM-Erosion model description in Tan et al. (2021) was closely followed in this implementation with some adjustments and simplifications in some variable parameterizations, which are described in section 2.2.

ELM-Erosion calculates soil erosion as the sum of rainfall-driven erosion and runoff-driven erosion. It then calculates the sediment transport capacity of the overland flow. The amount of sediment flux reaching the river network is calculated as the lesser value between soil erosion and sediment transport capacity.

Soil detached by rainfall (F; kg m^{-2} s^{-1}) is calculated as

$$F = c_1 * K * P_{CA} * L * GC * (KE_{DT} + KE_{LD}) \quad (1)$$

where c_1 is a free adjustment parameter in ELM-Erosion calibrated based on soil texture, vegetation, and rain regimes, K is soil erodibility (kg J^{-1}), P_{CA} is conserved agriculture (CA) factor (P_{CA} = 2.7 if no cropland in a pixel is under CA and P_{CA} = 1 if 100% of cropland in a pixel is under CA), L is lithology erodibility index (highest for unconsolidated sediments and the lowest for acid plutonic rocks; Moosdorf et al., 2018), KE_{DT} is the kinetic energy (J m^{-2}) of the direct throughfall from both natural rainfall and anthropogenic irrigation and KE_{LD} is the kinetic energy (J m^{-2}) of the leaf drainage from natural rainfall calculated as

$$KE_{DT} = R * [(1 - CC) + CC * (1 - A)] * (11.87 + 8.73 * log_{10}(I)) \quad (2)$$

R is the total rainfall (mm), A is the fraction of the rainfall intercepted by the vegetation or canopy cover, CC is canopy cover fraction, and I is rainfall intensity (mm h^{-1});

$$KE_{LD} = R * CC * A * DR * (15.8 * PH^{0.5} - 5.87) \quad (3)$$

where DR is the fraction of leaf drainage and PH is the height of the plant canopy (m).

Runoff-driven erosion (H; kg m^{-2} s^{-1}) is calculated as

$$H = 19.1 * c_2 * Z * P_{CA} * L * I_g * GC * R_s * \sin\theta \quad (4)$$

where c_2 is a free adjustment parameter in ELM-Erosion calibrated based on soil texture, vegetation, and rain regimes, I_g is the BQART glacier erosion factor calculated as $I_g = 1 + 0.09 * A_g$ where A_g is the areal fraction (%) of glaciers in a grid cell, R_s is the surface runoff (mm), and θ is the slope angle. Z is soil detachability by runoff (kg mm^{-1}) which is calculated as $Z = 1/(0.5 * COH)$ where COH is the cohesion of the soil (Pa). The values of K and COH are assigned based on soil texture types, as described in Tan et al. (2018).

Sediment transport capacity of overland flow T_c (kg m^{-2} s^{-1}) is calculated as

$$T_c = 0.0191 * c_3 * SR * P_{CA} * L * I_g * R_s * \sin\theta^{\gamma} \quad (5)$$

where c_3 is a free basin-specific adjustment parameter in ELM-Erosion calibrated based on surface roughness, drainage density, and rain regimes, and SR is surface roughness factor.

We employed limited calibration to a small number of the aforedescribed variables. The original ELM-Erosion employs a power of 1.5 for R_s in Eq. 4 and a power of 2 for R_s in Eq. 5. In WBMsed-ELM each of these have been adjusted to 1, to reflect the model's greater runoff prediction range. Our validation procedure showed that the original exponent leads to overestimation of larger observed sediment flux values and underestimation of smaller observed sediment flux values. In addition, the exponent γ in Eq. 5 was 1.25 in ELM-Erosion following Pelletier (2012). We found that γ =1.0 produces a more realistic response in sediment flux to slope, specially in high slope areas.

The ground cover factor GC in equations 1 and 4 represents the reduction of erosion by plant residue and roots,

$$GC = e^{-b_C * \max(C_r, C_{LAI}) - b_R * B_R} \quad (6)$$

where C_r is surface cover fraction calculated from the plant residue, C_{LAI} is surface cover fraction calculated from leaf area index, b_C (b_{C1} and b_{C2} for rainfall-driven and runoff-driven) is plant functional type (pft)-specific parameters for the effectiveness of surface cover in reducing soil erosion, b_R(b_{R1} and b_{R2} for rainfall-driven and runoff-driven) is pft-specific parameters for the effectiveness of roots in reducing soil erosion, and B_R is root biomass density at the topsoil (kg m^{-3}).

The surface cover fraction C_r is calculated using plant residue biomass on the ground B_r (kg m^{-2}) as $C_r = 1 - e^{-\alpha * B_r}$, where α is a regression coefficient that is set as 6.680 for the residue of all pfts. The surface roughness factor SR in equation 5 is calculated as a function of Manning's coefficient n.

$$SR = \left(\frac{0.03}{n}\right)^{0.6} \tag{7}$$

where n is calculated as $n = 0.03 + 0.05 * \max(C_r, C_{LAI})$.

The WBMsed-ELM sediment routing scheme calculates sediment load in each pixel as the sum of sediment flux generated in that pixel and the sediment flux reaching to it from upstream. Sediment trapping behind dams is calculated using a newly developed global reservoir trapping efficiency (*Te*) model (Moragoda et al., 2023*;* Chapter 3). At dam locations, the *Te* value of the dam is applied to the incoming sediment flux, allowing only the outgoing sediment flux from the dam to flow downstream.

2.2 Model Data and Implementation

The WBMsed-ELM model simulations were conducted at 6 arc-min (0.1 degree) spatial resolution at daily time steps, for the period between 1960-2014. TerraClimate (Abatzoglou et al., 2018) was used as the climate forcing dataset. In Tan et al. (2021), the effects of LULC on soil erosion for the period between 1960- 2014 were simulated using LULC data from the Land Use Harmonized version 2 (LUH2) transient dataset (Hurtt et al., 2011) which was converted to 24 ELM plant functional types (pfts) including a bare ground pft, 14 natural vegetation pfts and 10 crop pfts. The 10 crop pfts include five rainfed crop pfts (e.g., corn, cereal, soybean and generic crop) and five irrigated crop pfts (e.g., corn, cereal, soybean and generic crop). The 14

natural pfts include needleleaf evergreen tree (temperate and boreal), needleleaf deciduous tree (boreal), broadleaf evergreen tree (tropical and temperate), broadleaf deciduous tree (tropical, temperate and boreal), broadleaf evergreen shrub, broadleaf deciduous shrub (temperate and boreal), C3 arctic grass, C3 grass, and C4 grass. We used a simplified representation of LULC in WBMsed-ELM by choosing the dominant pft class in each pixel for crop pfts and natural pfts, separately. The model then calculates rainfall-driven erosion (Eq. 1) and runoff-driven erosion (Eq. 4) for these two dominant land use classes separately, and computes weighted average rainfall-driven erosion and runoff-driven erosion based on the percentage cropland in each pixel. In the original ELM model, these two equations are calculated for all the pfts present in each pixel separately, and their weighted averages are computed based on the fraction of each pft in that pixel. In order to run the WBMsed-ELM model in 'pristine' mode, which excludes anthropogenic impacts, the dominant land use class was chosen only from the natural vegetation pfts, and all agricultural land uses were ignored. In addition, the pristine mode excludes the conserved agriculture factor (P_{CA}), irrigation water use, and dams. Equation input data for WBMsed-ELM and their spatial and temporal resolutions are given in Table 4.1.

Table 4.1. The list of input parameters of the soil erosion model

Parameter	**Description**	**Spatial Resolution (degree)**	**Temporal Resolution**	**Data source**
c_1, c_2, c_3	Free calibration parameters	0.5	Static	
P_{CA}	Conservation agriculture factor	0.5	Annual	E3SM – created using global CA map of Prestele et al. (2018) and for the United States (US), US county-level tillage data compiled by the Conservation Technology

				Information Center (CTIC, 2008)
L	Lithology erodibility index	0.1	Static	Global Lithological Map database v1.1 (GLiM, Hartmann & Moosdorf, 2012)
LAI	Leaf Area Index	1	Annual	E3SM land model
B_R	Root biomass density at the topsoil	0.5	Daily	E3SM land model
B_r	Plant residue biomass on the ground	0.5	Daily	E3SM land model
I	Rainfall intensity	0.5	Daily	E3SM land model
$QWDRIP$	Leaf drainage	0.5	Daily	E3SM land model
$QWTRGH$	Direct rain throughfall	0.5	Daily	E3SM land model
PH	Height of the plant canopy	0.1	Static	Simard et al. (2011)
A_g	Areal fraction of glaciers in a grid cell	0.5	Static	ICE5Gv102
R_s	Surface runoff			WBMplus which is the hydrological module of WBMsed
θ	Slope angle of the grid cell	0.5	Static	E3SM land model
Clay, Sand, Silt	Percentage clay, sand, and silt in soil in the top 20cm	0.1	Static	ISRIC-WISE v1.1
Land use	Dominant plant functional type (pft) class in each pixel (generated separately using the combination of natural and crop pfts, as well as natural pfts only)	0.1	Annual	E3SM - created using Land Use Harmonized version 2 (LUH2) transient data set (Hurtt et al., 2011)
CRP	Percentage of croplands in each pixel	0.5	Annual	E3SM land model
IWU	Irrigation Water Use	0.25	Static	Zhang et al. (2022)
Te	Sediment trapping efficiency by dams	0.1	Annual	Moragoda et al. (2023)

In order to test the influence of land use change, dams, their combined effect, we designed 3 experiments (Table 4.2). The Pristine experiment excludes croplands, conserved agriculture factor (P_{CA}), irrigation water use, and dams. The LULC experiment excludes dams,

but includes anthropogenic land use changes (i.e. croplands, irrigation, and P_{CA}). The *Te* experiment includes anthropogenic land use changes and sediment trapping by dams. The difference in the model predictions between LULC and Pristine, *Te* and LULC, *Te* and Pristine, is used to isolate the impacts of land use changes, dams, and anthropogenic factors (combined effect of land use and dams) on sediment flux, respectively.

Table 4.2. Summary of different model experiments to evaluate the influence of land use change, dams, their combined effect on sediment loads.

Experiment	Trapping efficiency	Agricultural land uses	Natural land uses
Pristine	No	No	Yes
LULC	No	Yes	Yes
Te	Yes	Yes	Yes

2.3 Validation of soil erosion and sediment flux

Separate evaluations were conducted for WBMsed-ELM soil erosion and final sediment flux values. Soil erosion simulations were compared against RUSLE (Borrelli et al., 2017) and the ELM simulations by Tan et al. (2021). Validation of sediment fluxes simulated by WBMsed-ELM was conducted using three datasets. The model's long-term average discharge and sediment flux predictions were compared against long-term average observations in 228 USGS sites which is a combination of the standard WBMsed validation dataset (Cohen et al., 2022) of 41 USGS sites where the discharge record is over 20 years in large rivers with discharge > 30 m^3/s and drainage areas > 10,000 km^2, and 187 USGS sites which comprises of both small and large rivers with a wide range of drainage areas and discharge values. The reason to conduct two

separate validations for the two USGS datasets is that the original WBMsed model is designed to predict sediment discharge in large rivers and could have substantial uncertainty for small rivers. Validation of global sites was conducted using values reported in 132 global basin outlets from the M&S05 database (Syvitski and Milliman, 2007), which is also a standard dataset used for the validation of WBMsed predictions (e.g. Cohen et al., 2014). Furthermore, the model predicted discharge and sediment fluxes were used to calculate sediment concentration and compared against 14 global Total Suspended Solid (TSS) observations in the Global Database on River Sediment Composition (GloRiSe; Müller et al, 2021). We also compared the WBMsed-ELM model predictions with the Gardner et al. (2022) dataset of remotely sensed fluvial sediment along the longitudinal profiles of two major rivers in the US.

3. Results

3.1 Global soil erosion predictions

WBMsed-ELM successfully reproduces the spatial variability of global soil erosion predicted by ELM-Erosion and the global RUSLE model developed by Borrelli et al. (2017) (Figure 4.1(a), (b) and (c)). The disparities in soil erosion predictions are mainly due to the land use simplification and the difference in the source of runoff input data used in WBMsed-ELM. To a lesser degree, the differences in a few other input data sources used in WBMsed-ELM (e.g. Leaf Area Index, irrigation water use, soil sand, silt and clay percentages, and plant canopy height) may also have contributed. We predict an average annual global soil erosion of 24.7 million ton/km^2/yr for the year 2001 whereas ELM-Erosion predicts 3.2 million ton/km^2/yr, and RUSLE-based modeling (Borrelli et al., 2017) estimated 76.7 million ton/km^2/yr. The near order

of magnitude difference in our model predictions compared to ELM-Erosion is due to the higher values of runoff predicted by the hydrological module of WBMsed-ELM.

(a)

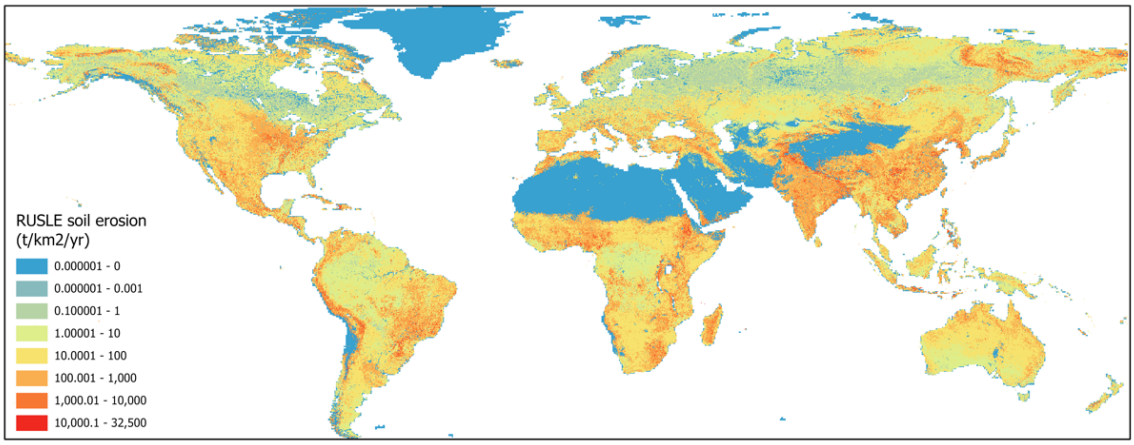

(b)

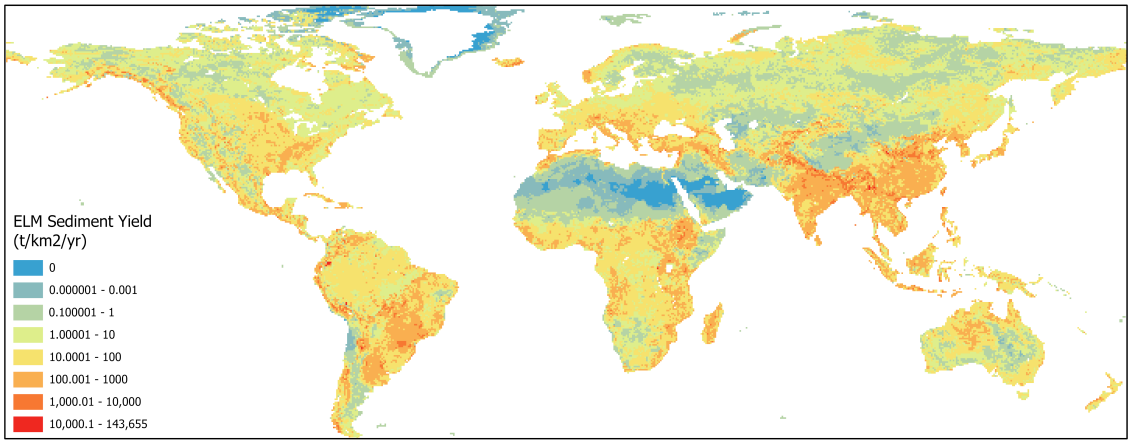

(c)

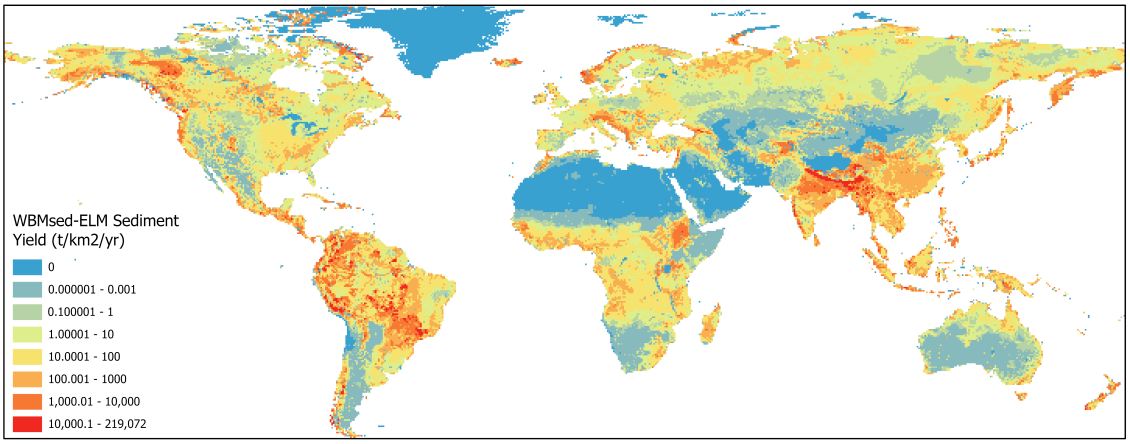

(d)

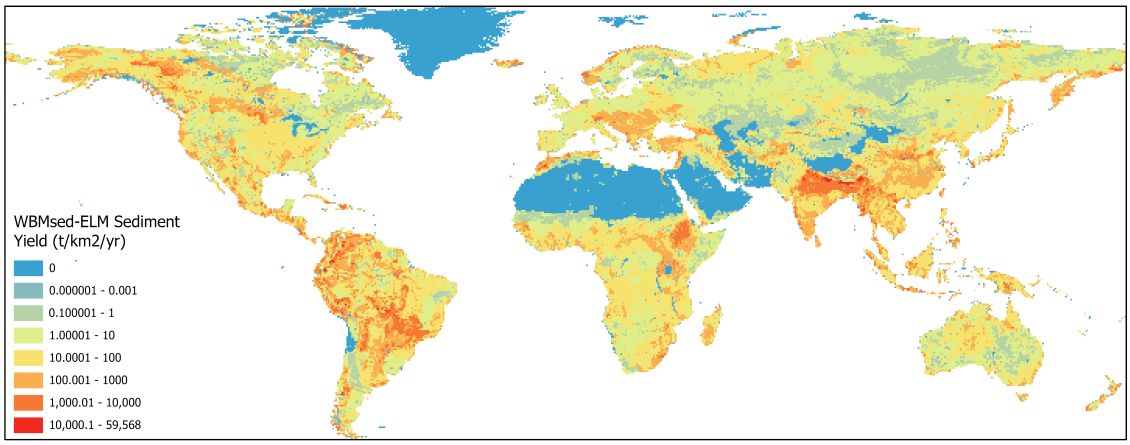

Figure 4.1. (a) RUSLE soil erosion from Borrelli et al. (2017), (b) ELM-Erosion sediment yield, (c) WBMsed-ELM sediment yield, (d) WBMsed-ELM sediment yield with original ELM runoff for 2001.

Figure 4.2 shows the difference in the spatial distribution of runoff between the two models. Considering the differences between Figure 4.1 (c) and (d), where the only main difference arises from runoff, it is clear that the differences in WBMsed-ELM predicted soil erosion mainly corresponds to the differences in the runoff input shown in figure 4.2. This is particularly evident in deserts and arid regions such as Gobi, Patagonian, Kalahari and Namib, central Asian deserts, Arabian desert, Thar desert, Australia, Eastern horn of Africa, and Mid-Western USA where runoff is generally much lower. The runoff used in ELM-Erosion, which comes from the hydrological simulations of E3SM, predicts higher runoff values for these areas. Lawrence et al. (2019) and Li et al. (2020) mention that E3SM, and Earth System Models in general, still have large uncertainties associated with runoff and streamflow simulations. In contrast, there is high degree of confidence in the accuracy of WBMplus hydrological predictions used in our model (Fekete et al., 2002; Cohen et al., 2022). Therefore, WBMplus runoff may have contributed to improving soil erosion predictions. However, comprehensive

validation datasets of observed soil erosion corresponding to the time period of simulations are not available to evaluate the model performance with these changes.

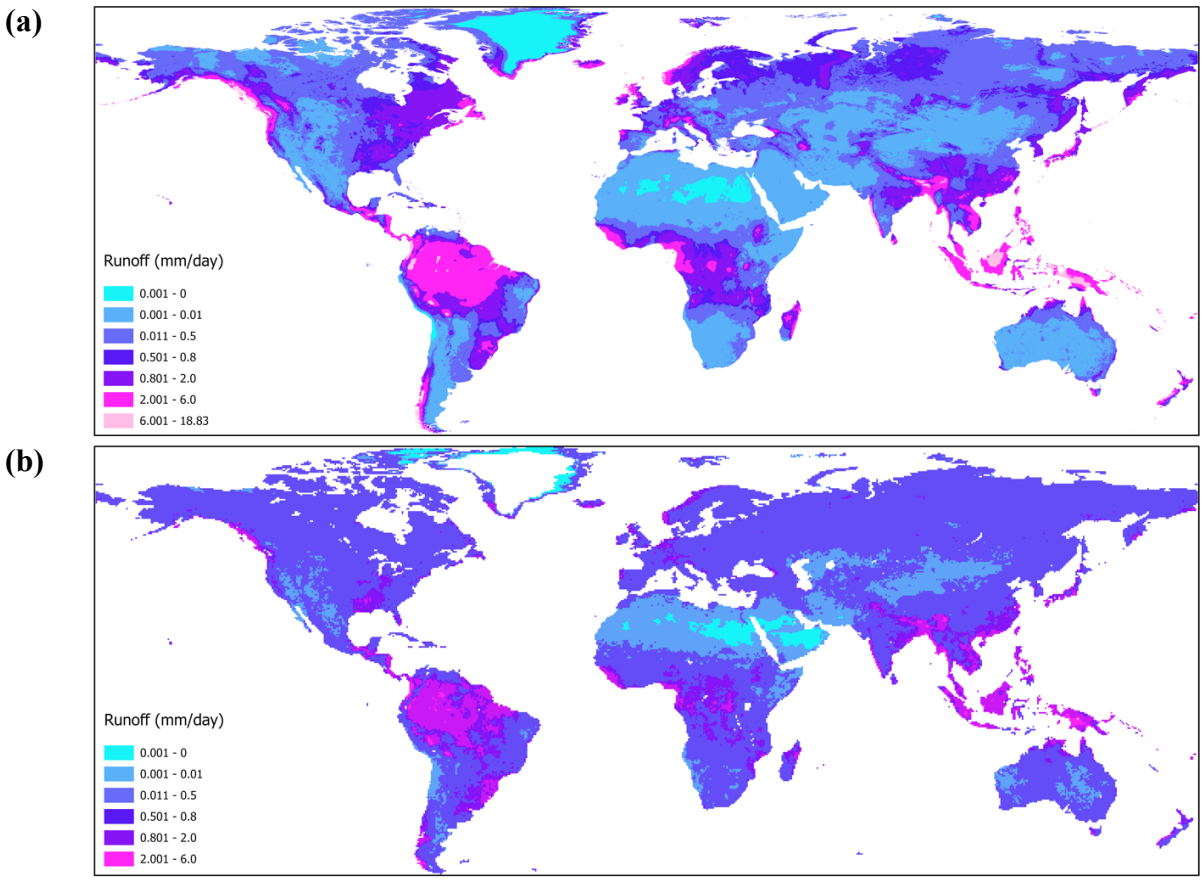

Figure 4.2. (a) Runoff input in WBMsed-ELM (b) Runoff in original ELM-Erosion.

The differences between Figure 4.1 (b) and (d), which shows the difference between the original ELM-Erosion and WBMsed-ELM using the same runoff input, could be mainly a result of the land use simplification used in WBMsed-ELM. This difference is more prominent in areas such as India, China, Australia, South-East Asia, some parts of Canada and Alaska, western Europe, Brazil, Argentina, some countries in central Asia, and the Amazon. Most of these regions consist of tropical and subtropical croplands where WBMsed-ELM generally underestimates soil erosion. Thus, the land use simplification in WBMsed-ELM may have

excluded the areas of more erosive croplands when choosing the dominant crop pft class. However, overestimations of soil erosion can be seen in Canada and Alaska and particularly the Amazon, where natural forests with dense vegetation are dominant. Although the reasons for this are less evident, it may be due to the influence of the calibration factor used by the runoff driven-erosion equation.

Both ELM-Erosion and WBMsed-ELM predict high soil erosion in (i) areas with high agricultural activity, including the plains in China, India, USA, and South America, (ii) areas with steep slopes such as Himalayas, Alps, and Andes mountain ranges, and (iii) areas with high runoff such as South-East Asia, Central America, some central African regions, some parts of Europe and Eastern and Western regions of North America. In contrast, lower soil erosion is predicted for arid areas with small amounts of runoff (e.g. Australia, Eastern horn of Africa, Mid-Western USA, and Mexico), and areas with dense vegetation which include tropical and boreal forests with the exception of Amazon. Soil erosion is negligible in desert areas such as the Sahara, central Asian deserts, Atacama, and Arabian desert.

3.2 Global river sediment flux predictions and validation

Figure 4.3 shows the results of the global river sediment fluxes simulated by WBMsed-ELM in the LULC experiment (no dam sediment trapping). The global map of river sediment fluxes mostly corresponds to the soil erosion predictions as expected. Consistent with observations (Milliman and Farnsworth, 2011; Syvitski and Milliman, 2007), the simulated global sediment flux toward the coastal regions is mainly contributed by large rivers in the tropics and subtropics, such as Amazon, Ganges-Brahmaputhra, Parana, Nile, Yangtze, Yellow, Mississippi, Indus, Mekong, Irrawaddy, and Congo (Cohen et al., 2014).

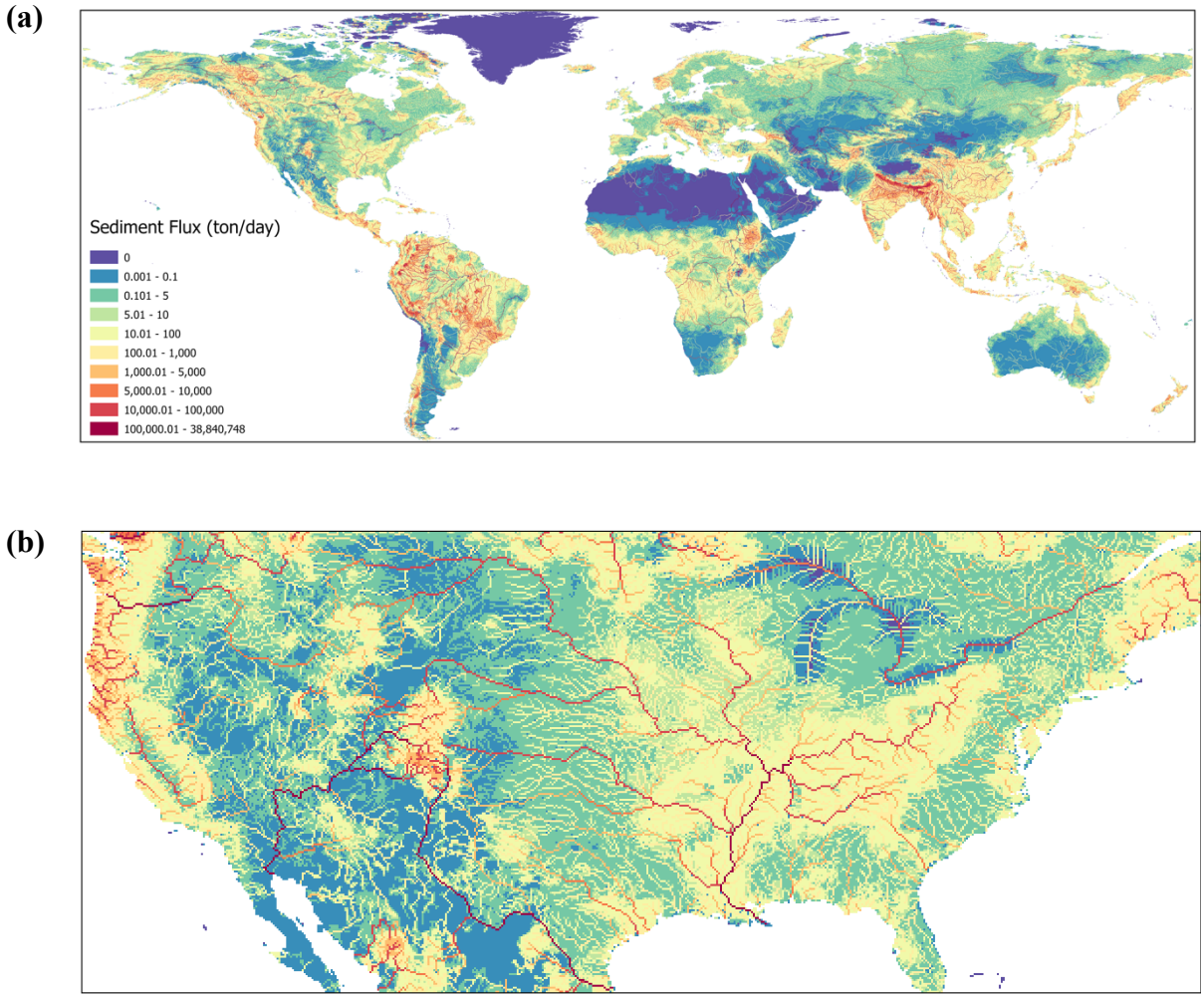

Figure 4.3. River sediment fluxes simulated by WBMsed-ELM in the LULC experiment (a) globally and, (b) for the Continental United States.

Figure 4.4 shows the validation conducted for WBMsed-ELM predicted water discharge and suspended sediment fluxes against observed data. The validation between the predicted and observed water discharge for 228 US sites (Figure 4.4a) and 132 global sites (Figure 4.4b) confirms the robustness of the WBMsed hydrological module in predicting the long-term average discharge globally as well as in the US. It is essential for the model to have accurate discharge predictions, as it is a major factor that drives sediment fluxes in rivers. The validation of model predicted sediment fluxes for the US against the WBMsed standard USGS measured

sediment fluxes (n=41) shown in Figure 4.4c and the validation statistics shown in Table 4.3 indicate that the pristine and LULC simulations compare well with the original WBMsed predictions and the model captures the spatial variability in sediment fluxes within the US reasonably well. This can also be seen with the global validation against the M&S05 dataset (Figure 4.4e). Both the original WBMsed and WBMsed-ELM predictions against the newly compiled USGS dataset show relatively lower prediction accuracy due to the fact that this dataset contains smaller rivers and variable time periods and number of observations. The original WBMsed can have substantial uncertainty for small rivers. Table 4.3 shows that our model (Pristine and LULC experiments) also has similar accuracy as the original WBMsed in predicting the sediment loads in these gauging stations. However, the *Te* experiment in general shows a poor performance compared to the other model setups and the original WBMsed. The reasons for this underperformance of the *Te* simulation is discussed in section 3.4.

It is important to note that WBMsed-ELM is a model configuration mainly aimed at explicitly simulating the major sediment transport processes and their driving factors such as various human activities (i.e. land use changes and dams) in global rivers. The process-based equations and their input data used in this model are still maturing for use at continental and global scales. On the other hand, the original WBMsed employs empirical equations which are developed based on their fit with global-scale observations, hence they tend to have superior correlation with observation datasets. However, this empiricism is a hurdle for the study of the processes and drivers affecting river sediment fluxes (Li et al., 2022). Therefore, it is reasonable for the newly developed WBMsed-ELM to have lower or comparable predictive accuracy than the original WBMsed. This new framework and the input datasets can be further improved and refined in the next steps to increase its accuracy. At this stage, we only opted to compare the

model's competence in capturing the spatial variability of long-term average predictions of sediment fluxes, which is the main purpose and capability of WBMsed. In the next steps, we hope to test the model performance in simulating the temporal variability in global river sediment fluxes.

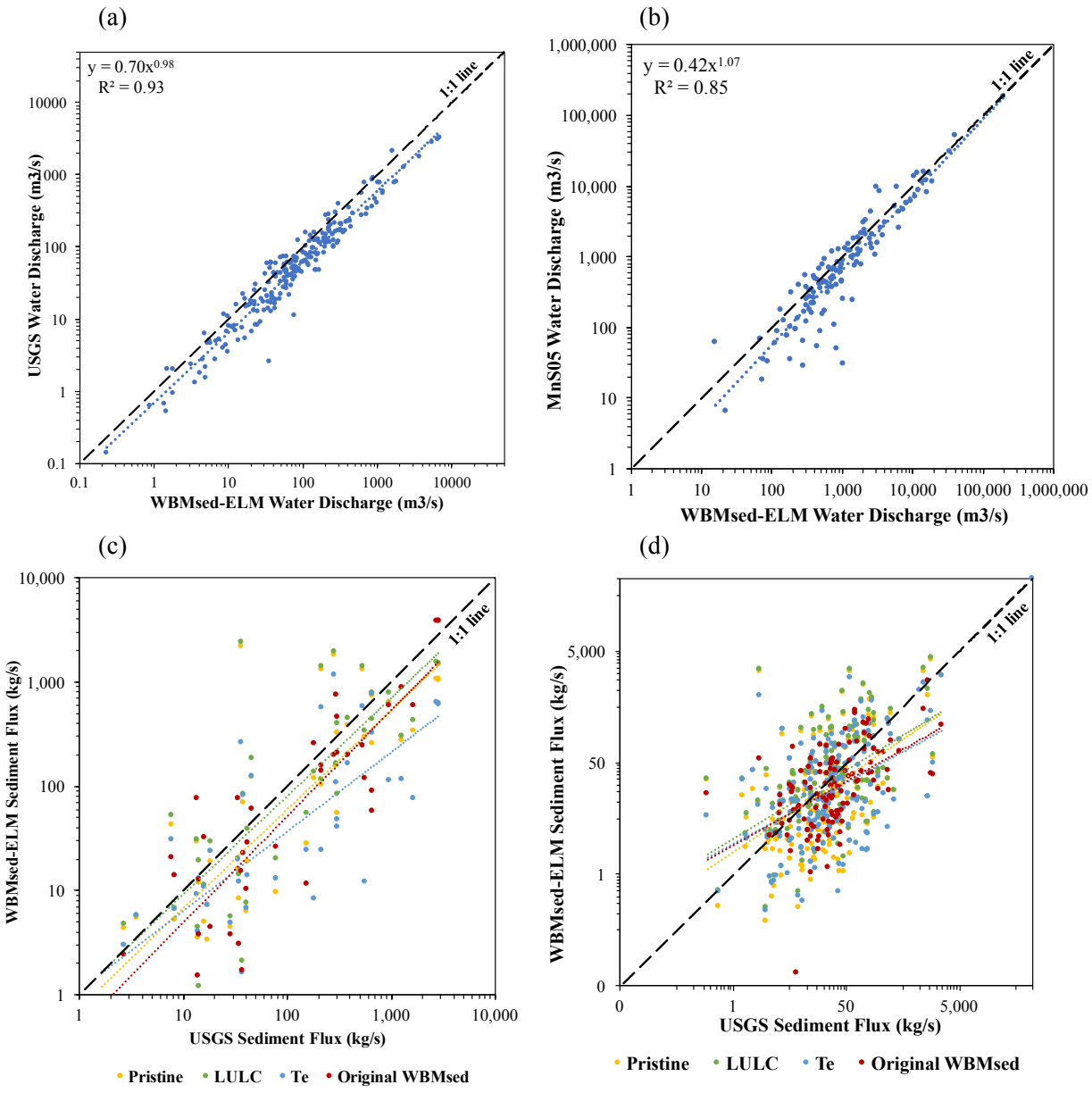

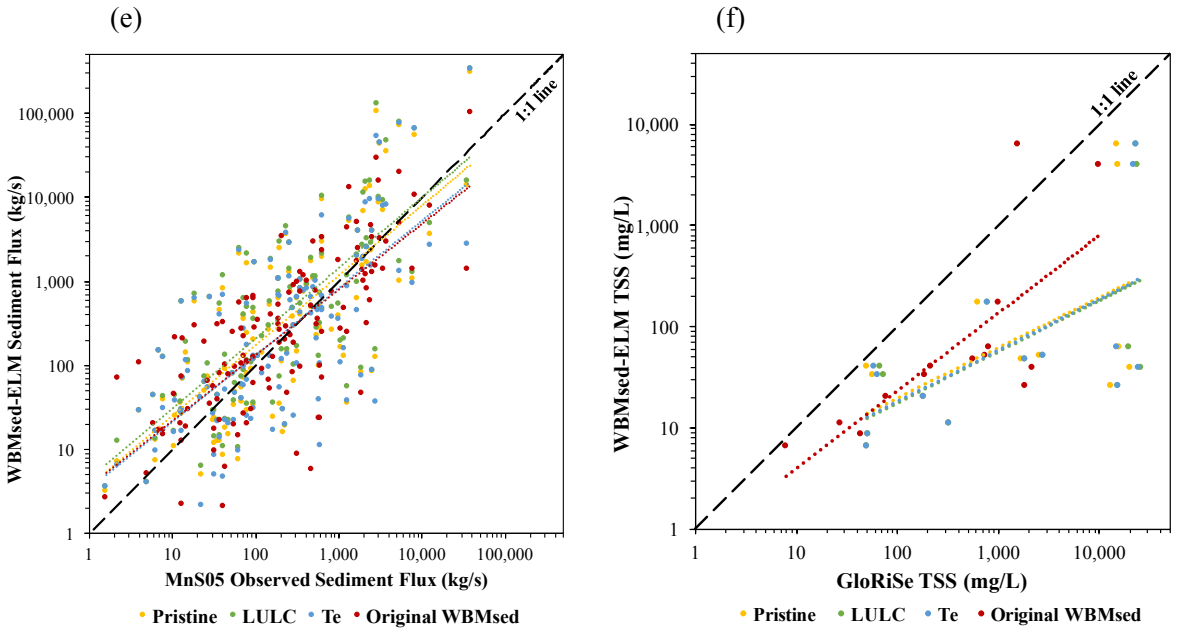

Figure 4.4. Comparison of long-term averaged WBMsed-ELM water discharge for (a) 228 US sites against USGS observed water discharge data (b) 132 global sites against M&S05 observed water discharge data (c) sediment loads for 41 US sites against the WBMsed standard USGS observed sediment dataset (d) sediment loads for 187 US sites against the new USGS observed sediment dataset (e) sediment loads for 132 global sites against M&S05 observed sediment data and, (f) sediment concentration for 14 global sites against the GloRiSe observed total suspended solids data.

Table 4.3. Coefficient of Determination (R^2) and Root Mean Square Error (RMSE) of the validation between WBMsed-ELM and observed sediment data shown in Figure 4.4.

	MnS92+ (n=132)		Standard USGS (n=41)		New USGS (n=187)		GloRiSe (n=14)	
	R^2	RMSE (kg/s)	R^2	RMSE (kg/s)	R^2	RMSE (kg/s)	R^2	RMSE (mg/L)
Pristine	0.56	26879	0.65	727	0.25	356	0.36	8894
LULC	0.57	30084	0.68	675	0.25	386	0.40	12261
Te	0.50	28035	0.58	718	0.21	262	0.39	11236
Original WBMsed	0.56	30163	0.72	370	0.26	317	0.55	2274

In order to test the sensitivity of the model simulated average global sediment flux to some of the important model input variables, we conducted a sensitivity analysis by excluding each variable from the model equations. The results in table 4.4 shows that the tested input variables have different levels of sensitivities and may lead to increases or decreases in average global sediment flux values. The model is more sensitive to variables such as slope and soil erodibility and they lead to a considerable decrease in average global sediment fluxes. On the contrary, the free parameter in the rainfall-driven erosion equation has much lower sensitivity to the model outputs.

Table 4.4. Sensitivity analysis of major variables in WBMsed-ELM model equations

		Average Global Sediment Flux (kg/s)			
Symbol	**Variable**	**Original WBMsed-ELM**	**Simulation excluding the variable**	**Difference**	**Percent difference**
L	Lithology	150.06	93.16	56.9	37.92
P_{CA}	Conservation Agriculture Factor	150.06	118.09	31.97	21.30
R_s	Runoff	150.06	244.24	-94.18	-62.76
θ	Slope	150.06	1564.2	-1414.14	-942.38
c_1	Free parameter in the rainfall-driven erosion equation	150.06	154.15	-4.0	-2.73
c_2	Free parameter in the runoff-driven erosion equation	150.06	138	12.06	8.04
c_3	Free parameter in the transport capacity equation	150.06	67.85	82.21	54.78
K	Soil Erodibility	150.06	328.81	-178.75	-119.12
I_g	BQART glacier erosion factor	150.06	140.32	9.74	6.49
C_{LAI}	Surface cover fraction calculated from Leaf Area Index	150.06	178.98	-28.92	-19.27

3.3 Human-induced land use change as a driver of river sediment flux

The difference between pristine and LULC experiments quantifies the impacts of croplands on sediment flux (Figure 4.5a). The global distribution of croplands across the world (Figure 4.5b) corresponds well with the areas that have experienced an increase in soil erosion and sediment loads from 1960-2014. In 2015, a total of 18.7 million km^2 of croplands were recorded in the world which accounts for about 12.6% of the global land area (Thenkabail et al., 2021). This is a 2% increase from the year 2000. Approximately 0.1 million km^2 of cropland are lost each year due to soil erosion, which threatens global food production (Pimentel and Burgess, 2013).

(a)

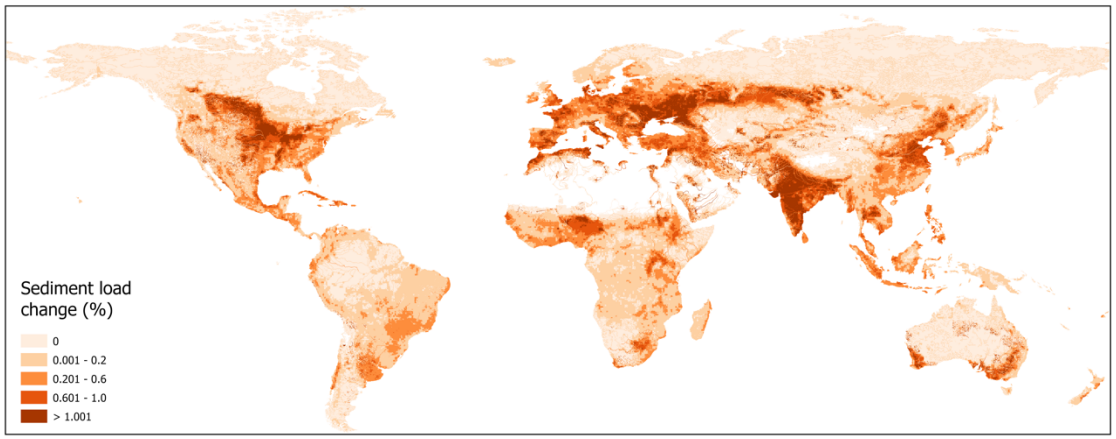

(b)

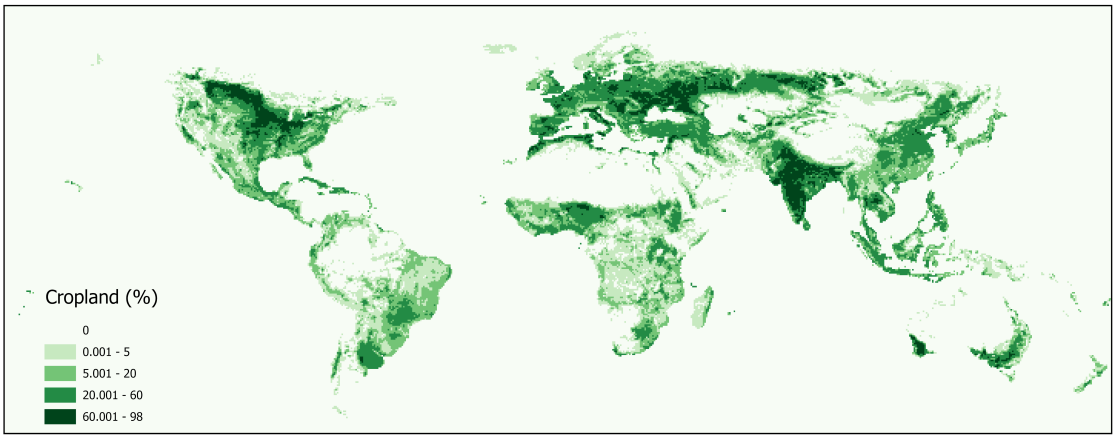

Figure 4.5. (a) agriculture-induced average sediment load increase from 1960-2014, (b) percentage of croplands in each pixel.

Our predicted soil erosion in croplands is 11.9 billion tons per year, for the year 2000, which is close to the estimate of ELM-Erosion (7.13 billion tons per year) and within the range of the estimate by Doetterl et al. (2012) which is 13.1 ± (6.6) billion tons per year for the same year. This shows that WBMsed-ELM successfully reproduces the original model despite its simplified land use representation. Increases in sediment fluxes due to agricultural activity are largest in countries such as India, USA, China, Russia, Ukraine, Brazil, Argentina, Canada, Nigeria, and Indonesia (Figure 4.5). These are also the top 10 leading countries in terms of percentage cropland area (Thenkabail et al., 2021). In addition, some parts of Africa, Australia, Europe, Central America, and Western Asia also experience high soil erosion and sediment loads owing to agricultural activity.

The Pristine and LULC experimental setups allow us to isolate and quantify the effect of human-induced land use changes on global river sediment fluxes during the study period. Our results indicate that croplands alone have increased average global river sediment fluxes by 1.4 billion tons per year between 1960 and 2014, which corresponds to an increase of 63.4%. This is nearly an order of magnitude less than the estimate by Van Oost et al. (2007) for global agricultural sediment fluxes from croplands (22 billion tons per year). Our estimates correspond to an annual average increase of 2.6 million tons per year, only attributable to increased soil erosion from croplands in the past half-century, without considering the influence of dams that has the contrasting effect and offset much of this increase before reaching the oceans.

3.4 Impacts of dams on river sediment fluxes

Figure 4.6 (a) and (b) show the longitudinal sediment profiles of Missouri and Colorado rivers, respectively, constructed using remote sensing sediment flux data (Gardner et al., 2022, 2023; Moragoda et al., 2023) and simulated sediment flux using the original WBMsed model configuration as well as WBMsed-ELM. The remote sensing observed sediment data show that sediment loads get replenished downstream after dams at a relatively rapid rate in most instances. This is reasonably well represented by original WBMsed, however, WBMsed-ELM has not been able to capture this phenomenon well. This difference is due to the different parameterization of *Te* between the two model configurations. WBMsed in its original version, calculate the effect of dams in a specific pixel as a (drainage area) weighted downstream fraction of all upstream dams, showing an increase in sediment that resembles downstream replenishment. In contrast, WBMsed-ELM explicitly routes sediment along the fluvial system and 'traps' sediment behind dams by reducing the amount transported downstream. The main reason for the pattern seen in WBMsed-ELM simulations is that we only implemented the *Te*, but the model currently lacks a representation of sediment replenishment downstream. A method to evaluate downstream sediment recovery that can be incorporated into sediment models is yet to be developed. Therefore, the lack of a sediment recovery representation has caused the model to underperform in the *Te* experiment, when simulating dam trapping efficiency in this explicit way.

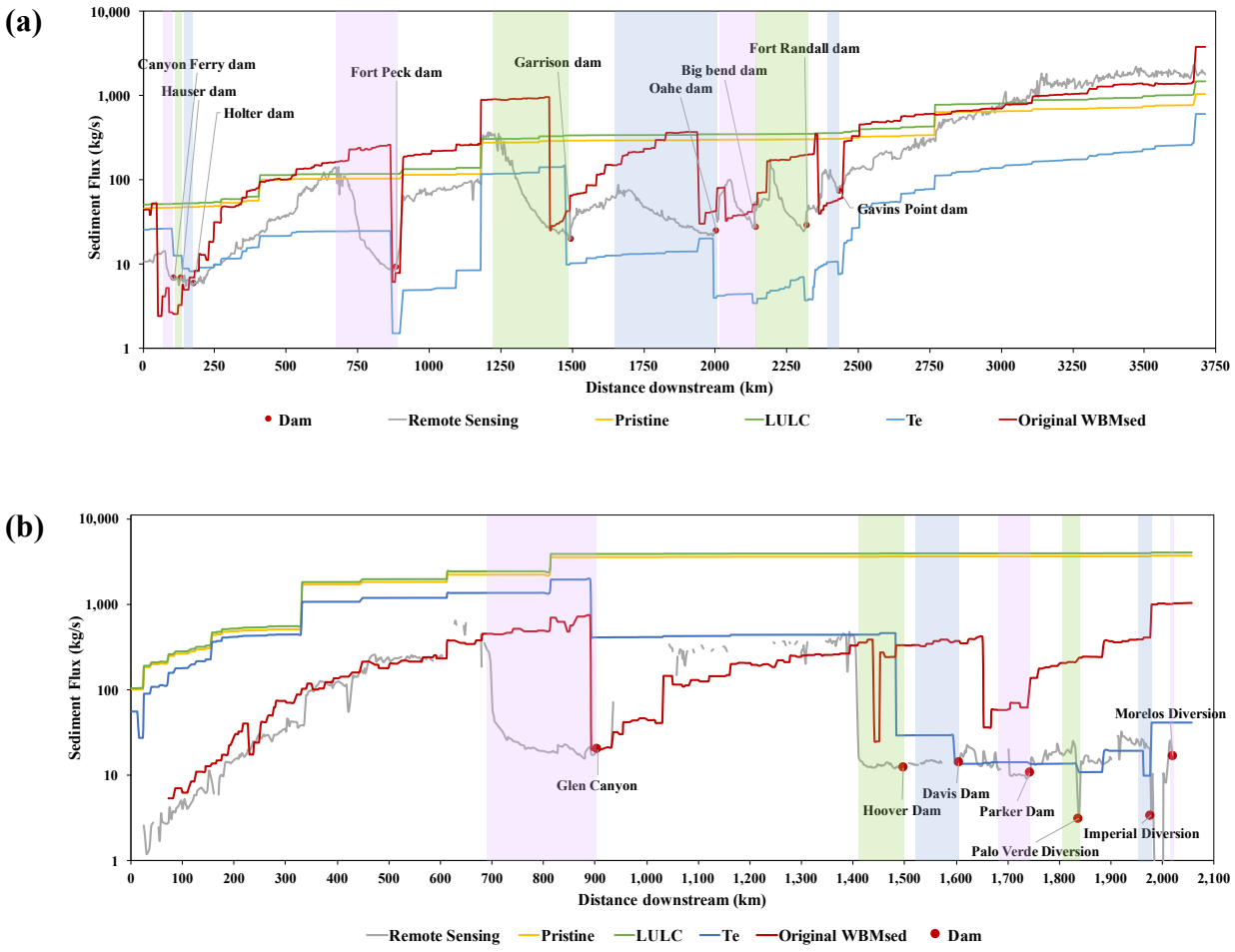

Figure 4.6. Longitudinal profiles of sediment flux in the (a) Missouri river, and (b) Colorado river. The colors of the line graphs represent the following data; Grey – remote sensing sediment flux (Gardner et al., 2022), Yellow – Pristine experiment, Green – LULC experiment, Blue – Te experiment, Red – Original WBMsed model. The vertical colored bars indicate the reservoir extents and red dots represent the corresponding dams.

It is also evident that WBMsed-ELM does not well represent the natural variability in sediment load as the river progresses downstream as shown by the remote sensing data and also simulated by the original WBMsed model. This is due to the fact that WBMsed-ELM currently is mainly driven by runoff instead of river discharge, as opposed to the original WBMsed. The lack of association with river discharge and in-stream sediment processes have made the model insensitive to the gradual increase in sediment loads observed in rivers. A routing scheme which

uses river discharge to govern downstream sediment transport in the model could resolve this issue in the future.

Declining sediment fluxes have been the observed global signal since the mid-20th century primarily owing to dams (Dethier et al., 2022), which is likely the major driving factor of changes in river sediment dynamics in the past several decades (Graf, 1999; Gupta et al., 2012). Despite the above discussed uncertainties, WBMsed-ELM is a useful tool to provide insights on the effect of dams and reservoirs on global river sediment fluxes. Figure 4.7 shows the average decline in sediment loads reaching the global ocean that can be attributed to dams and reservoirs during the study period, in 756 global river outlets with drainage areas greater than 10,000 km^2. River outlets with the largest declines are mostly located in North America, Europe, South and East Asia, and the Oceania. Our results indicate that dams have reduced the sediment load to the ocean by 19.1% only considering large rivers. Previous estimates made using only large rivers include Syvitski et al. (2005) which estimated a decrease of 20%, and Vörösmarty et al. (2003) a decrease of 30%.

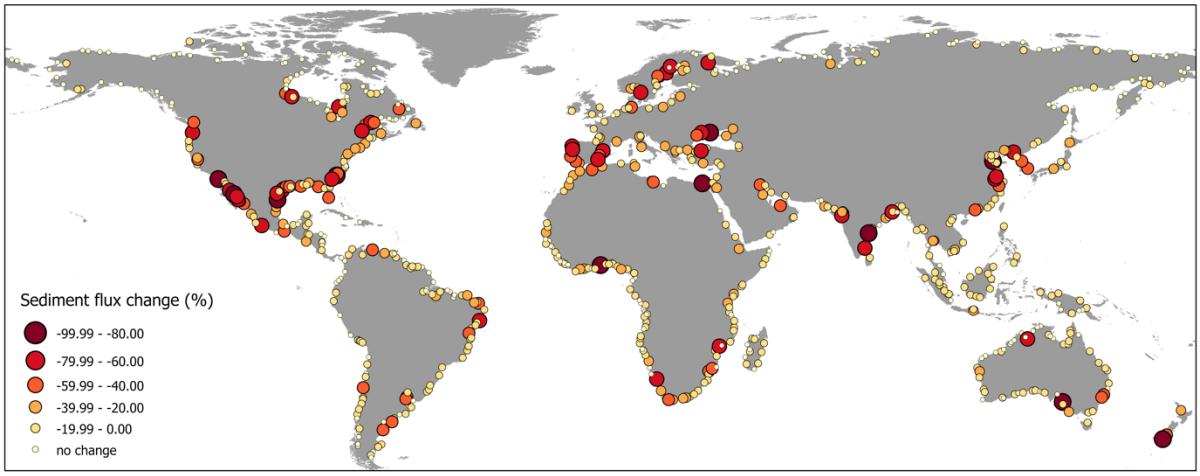

Figure 4.7. Sediment load reduction in 756 global river outlets (>10,000 km^2 drainage area) due to dams and reservoirs.

According to our estimates, the global contemporary suspended sediment flux to the global ocean from large river outlets is 0.12 billion tons per year. This is a considerable under-estimation from previous estimates such as Li et al. (2020) estimate of 12.9 billion tons per year, and Cohen et al. (2022) estimate of 15.1 billion tons per year for a similar number of outlets. We believe that this underestimation is due to the absence of downstream sediment recovery after dams in our model. However, our estimate of modern day sediment flux to the oceans without the presence of reservoirs (0.15 billion tons per year) is also much lower than previous estimates of 16.2 billion tons per year by Syvitski et al. (2005). Humans are simultaneously increasing the river sediment flux through agriculture-induced soil erosion and decreasing this flux through sediment retention behind dams. Considering the combined effect of land use changes and sediment trapping behind dams, WBMsed-ELM estimates that there is a net global increase of 6.4% in sediment delivery to the ocean, compared to pristine conditions. Syvitski et al. (2022) mentions that between 1950-2010, human activities such as land use changes have increased fluvial sediment delivery to the ocean by 215% while concurrently decreasing it by 49% mainly due to reservoir trapping.

4. Discussion

4.1 Model capabilities and accuracy

Our model simulation and validation shows that WBMsed-ELM is comparable to the original WBMsed in its ability to predict the spatial variability of sediment fluxes at the global scale. This is despite the still maturing physically-based equations to simulate major river sediment processes at a global scale, and input datasets with coarse resolutions and various levels of uncertainties. In order to achieve our goal of explicitly simulating soil erosion contribution to

river sediment loads in WBMsed, we chose ELM-Erosion by Tan et al. (2021) due to its process-based equations and equivalent predictive capability compared to the well-tested and widely used RUSLE model.

RUSLE is a relatively simple empirical model for predicting soil erosion, which has been successfully used in catchment-scale to global-scale studies (Borrelli et al., 2017). Several soil erosion and sediment load models also use empirical USLE, RUSLE or MUSLE (Modified-USLE) based approaches in them (e.g. PERFECT, CREAMS, AGNPS and SWAT). However, for this study, RUSLE was not an ideal model mainly due to its empirical and lumped nature. In addition, the comparison between ELM-Erosion and RUSLE has shown that ELM-Erosion has a more realistic relationship between soil erosion and topography (i.e. slope). For regions with high slope, the RUSLE model has a much stronger erosion response, which may not be realistic (Tan et al., 2021). On the other hand, ELM-Erosion employs separate equations for major suspended sediment processes (rainfall-driven erosion, runoff-driven erosion and sediment transport capacity) thus able to provide an estimate of sediment available for movement by the overland flow, whereas RUSLE provides potential soil erosion estimates which may be higher or lower than the transport capacity (Borrelli et al., 2021). In addition, WBMsed-ELM offers the opportunity to isolate the major human drivers of changes in global river sediment loads due to its ability to simulate soil erosion and sediment processes.

While WBMsed-ELM still needs to achieve better accuracy in terms of global river sediment flux predictions, it offers greater capabilities for WBMsed to explicitly simulate (i) hillslope soil erosion to represent upland sediment supply to rivers, (ii) more explicit and improved representations of anthropogenic factors (i.e. dam construction and land use changes) that affect fluvial sediment dynamics, and (iii) process-based soil erosion representations and

sediment routing in place of current empirical equations. With the current global context of ever increasing human influence on the natural Earth surface processes it is imperative to be able to isolate and quantify the impacts of each of the human drivers, which is a capability presented by WBMsed-ELM, with its more explicit and improved representation of dam sediment trapping and land use changes. In addition, the model configuration of WBMsed-ELM allows us to quantify the role played by different surface processes/mechanisms involved in global sediment dynamics and sediment delivery to coastal regions. This is much-needed information for management of the Earth's natural capital such as coastal wetlands that protect the land from accelerated sea level rise.

4.2 Limitations and future work

Evidently, the WBMsed-ELM model still has several uncertainties/limitations that may be contributing to inaccuracies in upland soil erosion and sediment flux predictions at the global scale. Most of these uncertainties are inherent to the original ELM-Erosion model structure and data requirements. ELM-Erosion uses a large number of input data layers to produce its outputs. Larger number of and more detailed input data could lead to larger uncertainties and biases in the predictions and often suffer from error accumulation and over-parameterization. Although the ELM-Erosion model is proven to be reasonably accurate, several of these data layers have large uncertainties especially at the global scale with relatively coarse resolutions (Tan et al., 2021). Therefore, the next steps of model refinements need to consider more simplified approaches for sediment flux simulations with considerably lower data requirements. One such uncertainty arises from the representation of land use classes in WBMsed-ELM, which is done through pfts following the original ELM-Erosion model. These pfts come from the ELM crop model and the

ELM-Erosion model has been calibrated using only 10 pfts classes. Therefore, various types of crops contributing to high or low erosion may be under-represented in the model. There are also uncertainties associated with pft predictions in ELM that may have propagated to WBMsed-ELM.

The model equations employed in WBMsed-ELM represent the sediment eroded from upland and carried by overland flow to rivers, which is known as wash load. Wash load mainly contains very fine particles which are usually in suspension and seldom deposit on the river bed (Lamb et al., 2020). However, total suspended sediment load of rivers consists of both wash load and suspended bed material load. Suspended bed material load mainly originates from the river bed material and interacts with the river bed usually after a period of suspension in the water column (Li et al., 2022). Research has shown that wash load is dominant in most locations. Li et al. (2022) and Sadeghi and Singh (2017) have found that the spatially averaged percentage of wash load in the total sediment load (including bed load) can be 62.2% and 79.1 ± (11.3) %, respectively. Cohen et al. (2022) showed that the original WBMsed model predicts the wash load to be 85% of the total suspended sediment load. Thus, future developments may need to include incorporating suitable equations to represent in-stream sediment processes.

The WBMsed-ELM sediment flux is currently driven by runoff and not discharge. This may have constrained the model's ability to simulate the natural variability in river sediment loads operated by discharge. Therefore, including in-stream sediment processes and/or incorporating discharge into the sediment routing scheme in WBMsed-ELM could overcome this challenge. As discussed in section 3.4, the downstream recovery of sediment after dams is currently lacking in the model. Future work needs to include a method to characterize this phenomenon to improve the model performance. In terms of model validation, the soil erosion

component in WBMsed-ELM with the changes that we incorporated, have not been tested against observation data. This is due to the lack of comprehensive validation datasets of observed soil erosion corresponding to the time period of simulations. Soil erosion validation could provide insights into the consequences of using WBMplus runoff, land use simplification, and other different input data sources in the WBMsed-ELM model. We also plan to evaluate the temporal variability in sediment flux predictions of WBMsed-ELM in addition to the long-term average predictions.

5. Conclusion

In this study, we developed a new soil erosion and sediment flux module within the WBMsed global scale hydro-geomorphic model which was named as WBMsed-ELM. This allows the model to simulate (i) hillslope erosion and land-based sediment supply to rivers, (ii) more explicit and improved representations of anthropogenic factors (i.e. dam construction and land use changes) that affect fluvial sediment dynamics, and (iii) process-based representations and sediment routing in place of current empirical equations. The goal of developing a more physically based sediment model was to (i) get a more accurate representation of river sediment processes, (ii) be able to include spatially varying soil properties and surface characteristics to represent the complexity of the natural environment, and (iii) better understand the driving forces of changes.

Using this new model, we simulated the individual and combined impacts of croplands and dams on river sediment fluxes. The validation of model-predicted sediment fluxes against observed data shows similar level of predictive skills with the original WBMsed model, despite the still maturing input datasets and physically-based equations in WBMsed-ELM at a global

scale. Our results indicate that croplands alone have increased average global river sediment fluxes by 1.4 billion tons per year between 1960 and 2014, which corresponds to an increase of 63.4%. Using 756 large river outlets across the globe (> 10,000 km^2 drainage area), WBMsed-ELM estimated that dams have reduced the average sediment load to the ocean by 19.1% during this period. However, the model's representation of the sediment trapping efficiency of dams needs a mechanism to recognize downstream sediment recovery processes, to generate more accurate predictions. Due to this, our estimates of the global contemporary suspended sediment flux to the global ocean from large river outlets which is 0.12 billion tons per year, is much less than previous estimates. Considering the combined effect of land use changes and sediment trapping behind dams, WBMsed-ELM estimates that there is a net global increase of 6.4% in sediment delivery to the ocean, compared to pristine conditions. Future work will include further simplifying the equations used in WBMsed-ELM to reduce the uncertainty associated with input data, incorporating suitable equations to represent in-stream sediment processes, incorporating discharge into the sediment routing scheme, and expanding the validation process. Overall, the WBMsed-ELM model offers several capabilities to explicitly simulate major river sediment processes and better represent individual and combined effects of anthropogenic stresses on global river sediment dynamics.

6. References for Chapter 4

Abatzoglou, J. T., Dobrowski, S. Z., Parks, S. A., & Hegewisch, K. C. (2018). TerraClimate, a high-resolution global dataset of monthly climate and climatic water balance from 1958–2015. Scientific data, 5(1), 1-12.

Bamunawala, J., Maskey, S., Duong, T. and van der Spek, A. (2018). Significance of Fluvial Sediment Supply in Coastline Modelling at Tidal Inlets. *Journal of Marine Science and Engineering*, *6*(3), p.79.

Battista, G., Molnar, P. and Burlando, P. (2020). Modelling impacts of spatially variable erosion drivers on suspended sediment dynamics. *Earth Surface Dynamics*, *8*(3), pp.619-635.

Boardman, J., Vandaele, K., Evans, R. and Foster, I.D. (2019). Off-site impacts of soil erosion and runoff: Why connectivity is more important than erosion rates. *Soil Use and Management*, *35*(2), pp.245-256.

Borrelli, P., Alewell, C., Alvarez, P., Anache, J. A. A., Baartman, J., Ballabio, C., et al. (2021). Soil erosion modelling: A global review and statistical analysis. Science of the Total Environment, 780, 146494. https://doi.org/10.1016/j.scitotenv.2021.146494

Borrelli, P., Robinson, D. A., Fleischer, L. R., Lugato, E., Ballabio, C., Alewell, C., et al. (2017). An assessment of the global impact of 21st century land use change on soil erosion. Nature Communications, 8, 2013. https://doi.org/10.1038/s41467-017-02142-7

Borrelli, P., Robinson, D. A., Panagos, P., Lugato, E., Yang, J. E., Alewell, C., et al. (2020). Land use and climate change impacts on global soil erosion by water (2015–2070). Proceedings of the National Academy of Sciences, 117, 21994–22001. https://doi.org/10.1073/pnas.2001403117

Cohen, S., Kettner, A. J., & Syvitski, J. P. (2014). Global suspended sediment and water discharge dynamics between 1960 and 2010: Continental trends and intra-basin sensitivity. Global and Planetary Change, 115, 44–58. https://doi.org/10.1016/j.gloplacha.2014.01.011

Cohen, S., Kettner, A. J., Syvitski, J. P., & Fekete, B. M. (2013). WBMsed, a distributed global-scale riverine sediment flux model: Model de- scription and validation. Computers & Geosciences, 53, 80–93. https://doi.org/10.1016/j.cageo.2011.08.011

Cohen, S., Syvitski, J., Ashley, T., Lammers, R., Fekete, B., & Li, H. Y. (2022). Spatial trends and drivers of bedload and suspended sediment fluxes in global rivers. Water Resources Research, 58(6), e2021WR031583.

CTIC. (2008). Crop residue management survey. Author. Retrieved from http://www.ctic.org/resourcedisplay/255/

Dethier, E. N., Renshaw, C. E., & Magilligan, F. J. (2022). Rapid changes to global river suspended sediment flux by humans. *Science*, *376*(6600), 1447-1452.

De Vente, J., Poesen, J., Verstraeten, G., Govers, G., Vanmaercke, M., Van Rompaey, A., Arabkhedri, M. and Boix-Fayos, C. (2013). Predicting soil erosion and sediment yield at regional scales: where do we stand?. Earth-Science Reviews, 127, pp.16-29.

Doetterl, S., Van Oost, K., & Six, J. (2012). Towards constraining the magnitude of global agricultural sediment and soil organic carbon fluxes. Earth Surface Processes and Landforms, 37(6), 642-655.

Fagundes de Oliveira, H., de Paiva, R.C.D., Fan, F.M., Buarque, D.C. and Fassoni-Andrade, A.C. (2020). Sediment modeling of a large-scale basin supported by remote sensing and in-situ observations. *Catena*, *190*, p.104535.

Fekete, B.M., Vörösmarty, C.J. and Grabs, W. (2002). High-resolution fields of global runoff combining observed river discharge and simulated water balances. Global Biogeochemical Cycles, 16(3), pp.15-1.

Fryirs, K. (2013). (Dis) Connectivity in catchment sediment cascades: a fresh look at the sediment delivery problem. *Earth Surface Processes and Landforms*, *38*(1), pp.30-46.

Garcia-Ruiz, J.M., Beguería, S., Nadal-Romero, E., González-Hidalgo, J.C., Lana-Renault, N. and Sanjuán, Y. (2015). A meta-analysis of soil erosion rates across the world. Geomorphology, 239, pp.160-173.

Gardner, J., Pavelsky, T. M., Topp, S., Yang, X., Ross, M. R., & Cohen, S. (2023). Human activities change suspended sediment concentration along rivers. Environmental Research Letters, 18, 064032.

Gardner, J., Pavelsky, T., Yang, X., Topp, S., & Ross, M. (2022). River Sediment Database (RiverSed) (v1.0.0) [Data set]. Zenodo. https://doi.org/10.5281/zenodo.4900563

Graf, W.L. (1999). Dam nation: A geographic census of American dams and their large-scale hydrologic impacts. Water resources research, 35(4), pp.1305-1311.

Grill, G., Lehner, B., Thieme, M., Geenen, B., Tickner, D., Antonelli, F., Babu, S., Borrelli, P., Cheng, L., Crochetiere, H. and Macedo, H.E. (2019). Mapping the world's free-flowing rivers. Nature, 569(7755), pp.215-221.

Gupta, H., Kao, S. J., & Dai, M. (2012). The role of mega dams in reducing sediment fluxes: A case study of large Asian rivers. Journal of Hydrology, 464, 447-458.

Haddeland, I., Heinke, J., Biemans, H., Eisner, S., Flörke, M., Hanasaki, N., Konzmann, M., Ludwig, F., Masaki, Y., Schewe, J. and Stacke, T. (2014). Global water resources

affected by human interventions and climate change. Proceedings of the National Academy of Sciences,111(9), pp.3251-3256.

Hartmann, J., & Moosdorf, N. (2012). The new global lithological map database GLiM: A representation of rock properties at the Earth surface. Geochemistry, Geophysics, Geosystems, 13, Q12004. https://doi.org/10.1029/2012gc004370

Hatono, M., & Yoshimura, K. (2020). Development of a global sediment dynamics model. Progress in Earth and Planetary Science, 7, 1-15.

Hurtt, G. C., Chini, L. P., Frolking, S., Betts, R. A., Feddema, J., Fischer, G., et al. (2011). Harmonization of land-use scenarios for the period 1500–2100: 600 years of global gridded annual land-use transitions, wood harvest, and resulting secondary lands. Climatic Change, 109, 117. https://doi.org/10.1007/s10584-011-0153-2

Ibáñez, C., Alcaraz, C., Caiola, N., Prado, P., Trobajo, R., Benito, X., Day, J.W., Reyes, E. and Syvitski, J.P.M. (2019). Basin-scale land use impacts on world deltas: Human vs natural forcings. *Global and planetary change*, *173*, pp.24-32.

Lamb, M.P., de Leeuw, J., Fischer, W.W., Moodie, A.J., Venditti, J.G., Nittrouer, J.A., Haught, D. and Parker, G. (2020). Mud in rivers transported as flocculated and suspended bed material. *Nature Geoscience*, *13*(8), pp.566-570.

Lawrence, D.M., Fisher, R.A., Koven, C.D., Oleson, K.W., Swenson, S.C., Bonan, G., Collier, N., Ghimire, B., van Kampenhout, L., Kennedy, D. and Kluzek, E. (2019). The Community Land Model version 5: Description of new features, benchmarking, and impact of forcing uncertainty. Journal of Advances in Modeling Earth Systems, 11(12), pp.4245-4287.

Li, Z., & Fang, H. (2016). Impacts of climate change on water erosion: A review. Earth-Science Reviews, 163, 94-117.

Li, H.Y., Tan, Z., Ma, H., Zhu, Z., Abeshu, G.W., Zhu, S., Cohen, S., Zhou, T., Xu, D. and Leung, L.R. (2022). A new large-scale suspended sediment model and its application over the United States. Hydrology and Earth System Sciences, 26(3), pp.665-688.

Li, L., Ni, J., Chang, F., Yue, Y., Frolova, N., Magritsky, D., Borthwick, A.G., Ciais, P., Wang, Y., Zheng, C. and Walling, D.E. (2020). Global trends in water and sediment fluxes of the world's large rivers. *Science Bulletin*, *65*(1), pp.62-69.

Merritt, W.S., Letcher, R.A. and Jakeman, A.J. (2003). A review of erosion and sediment transport models. *Environmental modelling & software*, *18*(8-9), pp.761-799.

Milliman, J. D., & Farnsworth, K. L. (2011). River discharge to the coastal ocean: A global synthesis. Cambridge University Press.

Moosdorf, N., Cohen, S., & von Hagke, C. (2018). A global erodibility index to represent sediment production potential of different rock types. Applied Geography, 101, 36–44. https://doi.org/10.1016/j.apgeog.2018.10.010

Moragoda, N., Cohen, S., Gardner, J., Muñoz, D., Narayanan, A., Moftakhari, H., & Pavelsky, T. M. (2023). Modeling and analysis of sediment trapping efficiency of large dams using remote sensing. Water Resources Research, 59, e2022WR033296. https://doi.org/10.1029/2022WR033296

Morehead, M.D., Syvitski, J.P., Hutton, E.W.H., Peckham, S.D. (2003). Modeling the temporal variability in the flux of sediment from ungauged river basins. Global and Planetary Change 39 (1–2), 95–110.

Morgan, R. P. C. (2001). A simple approach to soil loss prediction: A revised Morgan-Morgan-Finney model. Catena, 44(4), 305–322. https:// doi.org/10.1016/S0341-8162(00)00171-5

Morgan, R. P. C., & Duzant, J. H. (2008). Modified MMF (Morgan–Morgan–Finney) model for evaluating effects of crops and vegetation cover on soil erosion. Earth Surface Processes and Landforms, 33, 90–106. https://doi.org/10.1002/esp.1530

Müller, G., Middelburg, J. J., and Sluijs, A. (2021). Introducing GloRiSe – a global database on river sediment composition, Earth Syst. Sci. Data, 13, 3565–3575, https://doi.org/10.5194/essd-13-3565-2021.

Pandey, A., Himanshu, S.K., Mishra, S.K. and Singh, V.P. (2016). Physically based soil erosion and sediment yield models revisited. *Catena*, *147*, pp.595-620.

Papanicolaou, A. T. N., Elhakeem, M., Krallis, G., Prakash, S., & Edinger, J. (2008). Sediment transport modeling review—current and future developments. Journal of hydraulic engineering, 134(1), 1-14.

Pelletier, J. D. (2012). A spatially distributed model for the long-term suspended sediment discharge and delivery ratio of drainage basins. Journal of Geophysical Research, 117, F02028. https://doi.org/10.1029/2011jf002129.

Pimentel, D., & Burgess, M. (2013). Soil erosion threatens food production. Agriculture, 3(3), 443-463.

Prestele, R., Hirsch, A. L., Davin, E. L., Seneviratne, S. I., & Verburg, P. H. (2018). A spatially explicit representation of conservation agriculture for application in global change studies. Global Change Biology, 24, 4038–4053. https://doi.org/10.1111/gcb.14307

Renard, K., Foster, G., Weesies, G., McCool, D. & Yoder, D. (1997). Predicting Soil Erosion by Water: a Guide to Conservation Planning with the Revised Universal Soil Loss Equation (RUSLE) (USDA-ARS, Washington).

Sadeghi, S. H., & Singh, V. P. (2017). Dynamics of suspended sediment concentration, flow discharge and sediment particle size interdependency to identify sediment source. Journal of Hydrology, 554, 100-110.

Simard, M., Pinto, N., Fisher, J. B., & Baccini, A. (2011). Mapping forest canopy height globally with spaceborne lidar. Journal of Geophysical Research: Biogeosciences, 116(G4).

Syvitski, J., Ángel, J. R., Saito, Y., Overeem, I., Vörösmarty, C. J., Wang, H., & Olago, D. (2022). Earth's sediment cycle during the Anthropocene. Nature Reviews Earth & Environment, 3(3), 179-196.

Syvitski, J. P. M., & Milliman, J. D. (2007). Geology, geography, and humans battle for dominance over the delivery of fluvial sediment to the coastal ocean. The Journal of Geology, 115, 1–19. https://doi.org/10.1086/509246

Syvitski, J. P., Vörösmarty, C. J., Kettner, A. J., & Green, P. (2005). Impact of humans on the flux of terrestrial sediment to the global coastal ocean. science, 308(5720), 376-380.

Syvitski, J., Cohen, S., Miara, A., & Best, J. (2019). River temperature and the thermal-dynamic transport of sediment. Global and Planetary Change, 178, 168-183.

Syvitski, J. P., Cohen, S., Kettner, A. J., & Brakenridge, G. R. (2014). How important and different are tropical rivers?—An overview. Geomorphology, 227, 5-17.

Tan, Z., Leung, L. R., Li, H. Y., & Cohen, S. (2021). Representing global soil erosion and sediment flux in Earth System Models. Journal of Advances in Modeling Earth Systems, 14(1), e2021MS002756.

Tan, Z., Leung, L. R., Li, H.-Y., Tesfa, T., Zhu, Q., & Huang, M. (2020). A substantial role of soil erosion in the land carbon sink and its future changes. Global Change Biology, 26, 2642–2655. https://doi.org/10.1111/gcb.14982

Tan, Z., Leung, L.R., Li, H., Tesfa, T., Vanmaercke, M., Poesen, J., Zhang, X., Lu, H. and Hartmann, J. (2017). A Global data analysis for representing sediment and particulate organic carbon yield in Earth System Models. *Water Resources Research*, *53*(12), pp.10674-10700.

Tan, Z., Leung, L. R., Li, H. Y., & Tesfa, T. (2018). Modeling sediment yield in land surface and Earth system models: Model comparison, development, and evaluation. Journal of Advances in Modeling Earth Systems, 10(9), 2192-2213.

Taylor, P.G., Wieder, W.R., Weintraub, S., Cohen, S., Cleveland, C.C. and Townsend, A.R. (2015). Organic forms dominate hydrologic nitrogen export from a lowland tropical watershed. Ecology, 96(5), pp.1229-1241.

Thenkabail, P.S., Teluguntla, P.G., Xiong, J., Oliphant, A., Congalton, R.G., Ozdogan, M., Gumma, M.K., Tilton, J.C., Giri, C., Milesi, C. and Phalke, A. (2021). Global cropland-extent product at 30-m resolution (GCEP30) derived from Landsat satellite time-series data for the year 2015 using multiple machine-learning algorithms on Google Earth Engine cloud (No. 1868). US Geological Survey.

Tsuruta, K., Hassan, M.A., Donner, S.D. and Alila, Y. (2018). Development and application of a large-scale, physically based, distributed suspended sediment transport model on the Fraser River Basin, British Columbia, Canada. *Journal of Geophysical Research: Earth Surface*, *123*(10), pp.2481-2508.

Van Oost, K., Quine, T.A., Govers, G., De Gryze, S., Six, J., Harden, J.W., Ritchie, J.C., McCarty, G.W., Heckrath, G., Kosmas, C. and Giraldez, J.V. (2007). The impact of agricultural soil erosion on the global carbon cycle. Science, 318(5850), pp.626-629.

Vercruysse, K., Grabowski, R.C. and Rickson, R.J. (2017). Suspended sediment transport dynamics in rivers: multi-scale drivers of temporal variation. Earth-science reviews, 166, pp.38-52.

Vörösmarty, C.J., Meybeck, M., Fekete, B., Sharma, K., Green, P., Syvitski, J.P.M. (2003). Anthropogenic sediment retention: major global impact from registered river impoundments. Glob. Planet. Chang. 39 (1–2), pp.169–190.

Walling, D. E. and Fang, D. (2003). Recent trends in the suspended sediment loads of the world's rivers. Global Planet. Change, 39, pp.111–126.

Walling, D.E. (2009). The impact of global change on erosion and sediment transport by rivers: current progress and future challenges. UNESCO.

Wisser, D., Fekete, B.M., Vörösmarty, C.J., Schumann, A.H. (2010). Reconstructing 20th century global hydrography: a contribution to the Global Terrestrial Network–Hydrology (GTN–H). Hydrology and Earth System Sciences 14 (1), 1–24.

Wollheim, W.M., Vörösmarty, C.J., Bouwman, A.F., Green, P., Harrison, J., Linder, E., Peterson, B.J., Seitzinger, S.P., Syvitski, J.P.M. (2008). Global N removal by freshwater aquatic systems using a spatially distributed, within-basin approach. Global Biogeochemical Cycles 22, GB2026. doi:10.1029/ 2007GB002963.

Zhang, H., Lauerwald, R., Regnier, P., Ciais, P., Yuan, W., Naipal, V., Guenet, B., Van Oost, K. and Camino-Serrano, M. (2020). Simulating erosion-induced soil and carbon delivery from uplands to rivers in a global land surface model. *Journal of advances in modeling earth systems*, *12*(11), p.e2020MS002121.

Zhang, K., Li, X., Zheng, D., Zhang, L., & Zhu, G. (2022). Estimation of Global Irrigation Water Use by the Integration of Multiple Satellite Observations. Water Resources Research, 58(3), e2021WR030031. https://doi.org/10.1029/2021WR030031.

Zi, T., Kumar, M., & Albertson, J. (2019). Intercomparing varied erosion, deposition and transport process representations for simulating sediment yield. Scientific reports, 9(1), 1-13.

CHAPTER 5

OVERALL CONCLUSION

River sediment plays a fundamental role in the functioning of ecosystems, biogeochemical cycles, and geomorphological processes on Earth. Anthropogenic activities such as land use changes, water diversions, and dam construction have significantly modified natural sediment transport processes in rivers. Robust numerical models of sediment transport can be highly valuable in understanding the impacts of these human-induced stresses on global river fluxes.

In this dissertation, I investigated the effects of key anthropogenic modifications of the landscape and fluvial systems on sediment flux dynamics in large global rivers. Through a detailed review of the literature and an extensive meta-analysis, I found that dry soil has the lowest resistance to erosion and thus has a high erodibility, and erosion resistance increases (erodibility decreases) with increasing antecedent moisture content until a certain threshold. An exemplar relation that could be used to represent the variation in erosion resistance with soil moisture content was developed for use in hydro-geomorphic models in Chapter 2.

In order to better parameterize a key anthropogenic driver of river sediment transport in hydro-geomorphic models, a new reservoir trapping efficiency (*Te*) parameter was introduced in Chapter 3. The parameter was developed using a novel high-resolution and spatially continuous remote sensing fluvial sediment product. I developed data-driven CONUS and global models to predict *Te* in large-scale hydro-geomorphic models using remote sensing observations of long-term sediment data in the US. Contrary to the previous estimates in literature, the results of this

study showed that, large reservoirs can have a wide range of *Te* values. The global *Te* model developed in this chapter estimated an average global trapping efficiency of 53.5% using 6823 large global dams.

To enable the analysis of the key anthropogenic drivers affecting fluvial sediment dynamics, I developed a new soil erosion and sediment flux module within the WBMsed global-scale hydro-geomorphic model (Chapter 4). This new model termed WBMsed-ELM includes (i) hillslope erosion and land-based sediment supply to rivers, (ii) more explicit and improved representations of anthropogenic factors (i.e. dam construction and land use changes) that affect fluvial sediment dynamics, and (iii) process-based representations and sediment routing in place of current empirical equations. The validation of model-predicted sediment fluxes against observed data shows a similar level of predictive skills with the original WBMsed model, despite the still maturing input datasets and physically-based equations in WBMsed-ELM at the global scale. The model can benefit from a mechanism to represent downstream sediment recovery when simulating the impacts of dams. The WBMsed-ELM model offers several capabilities to explicitly simulate major river sediment processes and better represent individual and combined effects of anthropogenic stresses on global river sediment dynamics. The results presented in this chapter show that croplands alone have increased average global river sediment fluxes by 1.4 billion tons per year between 1960 and 2014, which corresponds to an increase of 63.4%. Using 756 large river outlets across the globe (> 10,000 km^2 drainage area), WBMsed-ELM estimated that dams on the contrary have reduced the average sediment load to the ocean by 19.1% during this period. Considering the combined effect of land use changes and sediment trapping behind dams during the study period, a net global increase of 6.4% is estimated in the sediment load to the global ocean, compared to pristine conditions.

Overall, this dissertation provides a comprehensive global outlook on key human factors influencing river sediment processes, and presents a robust modeling framework that enables the prediction and analysis of sediment fluxes on a global scale in a more explicit and process-based manner. The outcomes of this research are envisioned to help guide informed decision making and sustainable management of large global rivers, by improving the prediction of the imperative global picture. This will help strike a healthy balance between the well-being of the world's precious riverine ecosystem and ever-growing demographic and socio-economic demands.

REFERENCES

Bamunawala, J., Maskey, S., Duong, T. and van der Spek, A. (2018). Significance of Fluvial Sediment Supply in Coastline Modelling at Tidal Inlets. *Journal of Marine Science and Engineering*, *6*(3), p.79.

Battista, G., Molnar, P. and Burlando, P. (2020). Modelling impacts of spatially variable erosion drivers on suspended sediment dynamics. *Earth Surface Dynamics*, *8*(3), pp.619-635.

Best, J. and Darby, S.E. (2020). The Pace of Human-Induced Change in Large Rivers: Stresses, Resilience, and Vulnerability to Extreme Events. *One Earth*, *2*(6), pp.510-514.

Best, J. (2019). Anthropogenic stresses on the world's big rivers. *Nature Geoscience*, *12*(1), pp.7-21.

Boardman, J., Vandaele, K., Evans, R. and Foster, I.D. (2019). Off-site impacts of soil erosion and runoff: Why connectivity is more important than erosion rates. *Soil Use and Management*, *35*(2), pp.245-256.

Bryan, R.B. (2000). Soil erodibility and processes of water erosion on hillslope. Geomorphology, 32(3-4), pp.385-415.

Cohen, S., Kettner, A.J. and Syvitski, J.P. (2014). Global suspended sediment and water discharge dynamics between 1960 and 2010: Continental trends and intra-basin sensitivity. *global and planetary change*, *115*, pp.44-58.

Darby, S.E., Hackney, C.R., Leyland, J., Kummu, M., Lauri, H., Parsons, D.R., Best, J.L., Nicholas, A.P. and Aalto, R. (2016). Fluvial sediment supply to a mega-delta reduced by shifting tropical-cyclone activity. Nature, 539(7628), pp.276-279.

Dunn, F.E., Darby, S.E., Nicholls, R.J., Cohen, S., Zarfl, C. and Fekete, B.M. (2019). Projections of declining fluvial sediment delivery to major deltas worldwide in response to climate change and anthropogenic stress. *Environmental Research Letters*, *14*(8), p.084034.

Fagundes de Oliveira, H., de Paiva, R.C.D., Fan, F.M., Buarque, D.C. and Fassoni-Andrade, A.C. (2020). Sediment modeling of a large-scale basin supported by remote sensing and in-situ observations. *Catena*, *190*, p.104535.

Grissinger, E. H. (1966). Resistance of selected clay systems to erosion by water. Water Resources Research, 2(1), 131–138. https://doi.org/10.1029/WR002i001p00131

Haddeland, I., Heinke, J., Biemans, H., Eisner, S., Flörke, M., Hanasaki, N., Konzmann, M., Ludwig, F., Masaki, Y., Schewe, J. and Stacke, T. (2014). Global water resources affected by human interventions and climate change. Proceedings of the National Academy of Sciences,111(9), pp.3251-3256.

Hatono, M., & Yoshimura, K. (2020). Development of a global sediment dynamics model. Progress in Earth and Planetary Science, 7, 1-15.

Ibáñez, C., Alcaraz, C., Caiola, N., Prado, P., Trobajo, R., Benito, X., Day, J.W., Reyes, E. and Syvitski, J.P.M. (2019). Basin-scale land use impacts on world deltas: Human vs natural forcings. *Global and planetary change*, *173*, pp.24-32.

Knapen, A., Poesen, J., Govers, G., Gyssels, G., & Nachtergaele, J. (2007). Resistance of soils to concentrated flow erosion: A review. Earth-Science Reviews, 80(1–2), 75–109. https://doi.org/10.1016/j.earscirev.2006.08.001

Kondolf, G.M., Gao, Y., Annandale, G.W., Morris, G.L., Jiang, E., Zhang, J., Cao, Y., Carling, P., Fu, K., Guo, Q. and Hotchkiss, R. (2014). Sustainable sediment management in reservoirs and regulated rivers: Experiences from five continents. *Earth's Future*, *2*(5), pp.256-280.

Lamb, M.P., de Leeuw, J., Fischer, W.W., Moodie, A.J., Venditti, J.G., Nittrouer, J.A., Haught, D. and Parker, G. (2020). Mud in rivers transported as flocculated and suspended bed material. *Nature Geoscience*, *13*(8), pp.566-570.

Latrubesse, E.M., Arima, E.Y., Dunne, T., Park, E., Baker, V.R., d'Horta, F.M., Wight, C., Wittmann, F., Zuanon, J., Baker, P.A. and Ribas, C.C. (2017). Damming the rivers of the Amazon basin. *Nature*, *546*(7658), pp.363-369.

Lehner, B., Liermann, C.R., Revenga, C., Vörösmarty, C., Fekete, B., Crouzet, P., Döll, P., Endejan, M., Frenken, K., Magome, J. and Nilsson, C. (2011a). High-resolution mapping of the world's reservoirs and dams for sustainable river-flow management. *Frontiers in Ecology and the Environment*, *9*(9), pp.494-502.

Lewis, S.E., Bainbridge, Z.T., Kuhnert, P.M., Sherman, B.S., Henderson, B., Dougall, C., Cooper, M. and Brodie, J.E. (2013). Calculating sediment trapping efficiencies for reservoirs in tropical settings: a case study from the Burdekin Falls Dam, NE Australia. *Water Resources Research*, *49*(2), pp.1017-1029.

Li, L., Ni, J., Chang, F., Yue, Y., Frolova, N., Magritsky, D., Borthwick, A.G., Ciais, P., Wang, Y., Zheng, C. and Walling, D.E. (2020). Global trends in water and sediment fluxes of the world's large rivers. *Science Bulletin*, *65*(1), pp.62-69.

Li, H.Y., Tan, Z., Ma, H., Zhu, Z., Abeshu, G.W., Zhu, S., Cohen, S., Zhou, T., Xu, D. and Leung, L.R. (2022). A new large-scale suspended sediment model and its application over the United States. Hydrology and Earth System Sciences, 26(3), pp.665-688.

Merritt, W.S., Letcher, R.A. and Jakeman, A.J. (2003). A review of erosion and sediment transport models. *Environmental modelling & software*, *18*(8-9), pp.761-799.

Moragoda, N., Cohen, S., Gardner, J., Muñoz, D., Narayanan, A., Moftakhari, H., & Pavelsky, T. M. (2023). Modeling and analysis of sediment trapping efficiency of large dams using remote sensing. Water Resources Research, 59, e2022WR033296. https://doi.org/10.1029/2022WR033296

Moragoda, N., Kumar, M. and S. Cohen, (2022). Representing the role of soil moisture on erosion resistance in sediment models: Challenges and opportunities. Earth-Science Reviews, p.104032. DOI: https://doi.org/10.1016/j.earscirev.2022.104032

Mulligan, M., van Soesbergen, A. and Sáenz, L. (2020). GOODD, a global dataset of more than 38,000 georeferenced dams. *Scientific Data*, *7*(1), pp.1-8.

Syvitski, J.P. and Kettner, A. (2011). Sediment flux and the Anthropocene. *Philosophical Transactions of the Royal Society A: Mathematical, Physical and Engineering Sciences*, *369*(1938), pp.957-975.

Syvitski, J.P., Kettner, A.J., Overeem, I., Hutton, E.W., Hannon, M.T., Brakenridge, G.R., Day, J., Vörösmarty, C., Saito, Y., Giosan, L. and Nicholls, R.J. (2009). Sinking deltas due to human activities. *Nature Geoscience*, *2*(10), pp.681-686.

Syvitski, J.P., Milliman, J.D. (2007). Geology, geography, and humans battle for dominance over the delivery of fluvial sediment to the coastal ocean. J. Geol.115 (1), pp.1–19.

Tan, Z., Leung, L.R., Li, H., Tesfa, T., Vanmaercke, M., Poesen, J., Zhang, X., Lu, H. and Hartmann, J. (2017). A Global data analysis for representing sediment and particulate organic carbon yield in Earth System Models. *Water Resources Research*, *53*(12), pp.10674-10700.

Tan, Z., Leung, L.R., Li, H.Y. and Tesfa, T. (2018). Modeling sediment yield in land surface and earth system models: Model comparison, development, and evaluation. *Journal of Advances in Modeling Earth Systems*, *10*(9), pp.2192-2213.

Tsuruta, K., Hassan, M.A., Donner, S.D. and Alila, Y. (2018). Development and application of a large-scale, physically based, distributed suspended sediment transport model on the Fraser River Basin, British Columbia, Canada. *Journal of Geophysical Research: Earth Surface*, *123*(10), pp.2481-2508.

Vercruysse, K., Grabowski, R.C. and Rickson, R.J. (2017). Suspended sediment transport dynamics in rivers: multi-scale drivers of temporal variation. Earth-science reviews, 166, pp.38-52.

Vörösmarty, C.J., Meybeck, M., Fekete, B., Sharma, K., Green, P., Syvitski, J.P.M. (2003). Anthropogenic sediment retention: major global impact from registered river impoundments. Glob. Planet. Chang. 39 (1–2), pp.169–190.

Wada, Y., de Graaf, I.E. and van Beek, L.P. (2016). High-resolution modeling of human and climate impacts on global water resources. *Journal of Advances in Modeling Earth Systems*, *8*(2), pp.735-763.

Walling, D. E. and Fang, D. (2003). Recent trends in the suspended sediment loads of the world's rivers. Global Planet. Change, 39, pp.111–126.

Walling, D.E. (2009). *The impact of global change on erosion and sediment transport by rivers: current progress and future challenges*. UNESCO.

Zarfl, C., Lumsdon, A.E., Berlekamp, J., Tydecks, L., and Tockner, K. (2015). A global boom in hydropower dam construction. Aquat. Sci. 77, 161–171, https://doi.org/10. 1007/s00027-014-0377-0.

Zhang, H., Lauerwald, R., Regnier, P., Ciais, P., Yuan, W., Naipal, V., Guenet, B., Van Oost, K. and Camino-Serrano, M. (2020). Simulating erosion-induced soil and carbon delivery from uplands to rivers in a global land surface model. *Journal of advances in modeling earth systems*, *12*(11), p.e2020MS002121.